

Analysing Neuronal Network Architectures: From Weight Distributions to Structure and Back

THÈSE N° 5302 (2012)

PRÉSENTÉE LE 14 MARS 2012

À LA FACULTÉ INFORMATIQUE ET COMMUNICATIONS
LABORATOIRE DE CALCUL NEUROMIMÉTIQUE (IC/SV)
PROGRAMME DOCTORAL EN NEUROSCIENCES

ÉCOLE POLYTECHNIQUE FÉDÉRALE DE LAUSANNE

POUR L'OBTENTION DU GRADE DE DOCTEUR ÈS SCIENCES

PAR

Christian TOMM

acceptée sur proposition du jury:

Prof. H. Lashuel, président du jury
Prof. W. Gerstner, directeur de thèse
Prof. G. Einevoll, rapporteur
Prof. C. Petersen, rapporteur
Prof. S. Rotter, rapporteur



ÉCOLE POLYTECHNIQUE
FÉDÉRALE DE LAUSANNE

Suisse
2012

Acknowledgements

I would like to thank Prof. Wulfram Gerstner for giving me the opportunity to undertake my studies in such a stimulating and positive environment. I thank also Prof. Carl Petersen for his interest and support and my collaborators Sandrine Lefort and Michael Avermann.

I also wish to thank all my colleagues at the Laboratory of Computational Neuroscience for their discussions and ideas. I am especially indebted to Tim Vogels, who provided me with much support and advice.

Above all, I thank my wife and family for their support and love throughout my whole PhD.

Abstract

The connections cortical neurons form are different in each individual human or animal. Although there are known and determined large scale connections between areas of the brain that are common across individuals, the local connectivity on smaller scales varies between individuals. Connections between neurons in a single cortical column are seemingly random and were thus modeled in theoretical studies using the principle of sparse random networks.

In this thesis I investigate how the simplifications of sparse random networks affect the behaviour and plausibility of the network. First, I focus on the global weight distribution in random sparse networks and test the impact of various weight distributions on network excitability.

Random sparse networks also commonly assume an independent distribution of connections in the network. Experimental results indicate that this assumption is not true in biological neuronal networks. In the second part of this thesis it is shown how changes in degree distributions of the network can be employed to improve the similarity of random networks to biological observations.

A third aspect studied in this work is the impact of connection strengths on a local level. Network responses to larger stimuli in *in vitro* experiments are not reproducible by classical sparse random networks. It is shown how changes in the distributions of local connection strengths can be used to improve the network response behaviour with respect to these experimental findings.

Finally, these network adjustments are combined and the adjusted networks are tested on further data of *in vivo* recordings. The adjusted networks show a biologically more plausible behaviour than the random sparse network topologies in all tested scenarios.

Keywords

Computational Neuroscience, Neuronal Networks, Fine-Scale Structure, Weight Distribution, Degree Distribution

Zusammenfassung

Verbindungen zwischen Neuronen im Cortex von Mensch und Tier sind von Individuum zu Individuum verschieden. Obwohl Verbindungen zwischen Gehirnarealen in unterschiedlichen Individuen ähnlich vorhanden sind, variieren ihre lokalen Verbindungen auf kleineren Skalen. Neuronale Verbindungen in einer einzelnen corticalen Säule sind annähernd zufällig und wurden daher in theoretischen Arbeiten mit dünnbesetzten Zufallsnetzwerken simuliert.

In dieser Dissertation untersuche ich, in welcher Weise die Vereinfachungen der Annahme von dünnbesetzten Zufallsnetzwerken das Verhalten und die Plausibilität dieser Netzwerke beeinflusst. Hierzu betrachte ich zunächst die globale Gewichtsverteilung in dünnbesetzten Zufallsnetzwerken und teste den Einfluss verschiedener Gewichtsverteilungen auf die Erregbarkeit der Netzwerke.

Dünnbesetzte Zufallsnetzwerke nehmen üblicherweise unabhängig verteilte Verbindungen im Netzwerk an. Experimentelle Ergebnisse weisen jedoch darauf hin, dass diese Annahme in biologischen Netzwerken nicht zutrifft. Diese Dissertation zeigt, wie Veränderungen in den Gradverteilungen des Netzwerks genutzt werden können, um die Ähnlichkeit zu biologischen Netzwerken zu verbessern.

Ein dritter Aspekt der in dieser Arbeit untersucht wird, ist der Einfluss der Gewichtsverteilung auf lokalem Niveau. Netzwerkantworten auf größere Stimulationen in *in vitro* Experimenten können nicht von klassischen dünnbesetzten Zufallsnetzwerken reproduziert werden. Es wird gezeigt, wie Änderungen in lokalen Gewichtsverteilungen genutzt werden können, um die Netzwerkantworten bezüglich dieser Experimente zu verbessern.

Schlussendlich werden all diese Veränderungen kombiniert und die so verbesserten Netzwerke im Vergleich zu weiteren Daten von *in vivo* Experimenten getestet. Die verbesserten Netzwerke zeigen hierbei ein biologisch plausibleres Verhalten als klassische, dünnbesetzte Zufallsnetzwerke in allen getesteten Szenarios.

Schlüsselworte

Computational Neuroscience, Neuronale Netzwerke, Feinstruktur, Gewichtsverteilung, Gradverteilung

Contents

| | |
|---|------------|
| Acknowledgements | iii |
| Abstract (English/Deutsch) | iv |
| List of Figures | ix |
| List of Tables | xii |
| 1 Introduction | 1 |
| 1.1 Random Network Architectures | 3 |
| 1.1.1 Network Construction | 3 |
| 1.1.2 Weight Distributions | 4 |
| 1.1.3 Types of Network Populations | 5 |
| 1.1.4 Network Simulations | 5 |
| 1.1.5 Neuron Models | 5 |
| 1.1.6 Roles of Random Networks | 6 |
| 1.2 Biological Background | 8 |
| 1.2.1 Barrel Cortex | 8 |
| 1.2.2 Pairwise Connectivity Measurements | 10 |
| 1.2.3 Network Connectivity Measurements | 13 |
| 1.3 Non-random Network Architectures | 20 |
| 1.4 Visualising High Dimensional Parameter Spaces | 23 |
| 1.5 Optimisation Techniques | 25 |
| 1.5.1 Particle Swarm Optimisation | 25 |
| 1.5.2 Strength Pareto Evolution Algorithm (SPEA-2) | 25 |
| 2 Random Layered Networks | 27 |
| 2.1 Experimental Basis | 28 |
| 2.1.1 Connectivity Data | 28 |
| 2.1.2 Single Cell Data | 30 |
| 2.2 Network Model | 31 |
| 2.2.1 Weight Distributions | 32 |
| 2.2.2 Network Stimulation | 34 |
| 2.2.3 Threshold for Further Excitation | 35 |
| 2.3 Results | 36 |
| 2.3.1 Impact of Different Weight Distributions Network Excitability | 36 |
| 2.3.2 Layer Specific Differences | 39 |
| 2.4 Summary | 40 |

Contents

| | | |
|----------|---|-----------|
| 3 | Modifying Local Connectivity | 43 |
| 3.1 | Experimental Basis | 44 |
| 3.1.1 | Probabilities of Shared Input | 44 |
| 3.2 | Network Model | 45 |
| 3.2.1 | Network Populations | 45 |
| 3.2.2 | Connectivity | 46 |
| 3.3 | Changing Network Structure | 46 |
| 3.3.1 | Modifying Degree Distributions | 47 |
| 3.3.2 | Quantification of Network Similarity | 49 |
| 3.3.3 | Parameter Significance | 50 |
| 3.4 | Results | 50 |
| 3.4.1 | Significant Parameters | 51 |
| 3.4.2 | Effects of Degree Distributions on Shared Input | 54 |
| 3.4.3 | Covariation Effects of Multiple Parameters | 56 |
| 3.4.4 | Small-World Networks | 57 |
| 3.4.5 | Scale-Free Networks | 58 |
| 3.4.6 | Network Motifs | 58 |
| 3.5 | Summary | 59 |
| 4 | Modifying Local Weight Distributions | 61 |
| 4.1 | Experimental Basis | 62 |
| 4.1.1 | Channelrhodopsin Evoked Responses | 62 |
| 4.1.2 | Connectivity | 62 |
| 4.2 | Network Model | 62 |
| 4.2.1 | Neuron Model | 63 |
| 4.2.2 | Connectivity | 63 |
| 4.2.3 | Stimulation in the Model Networks | 63 |
| 4.2.4 | Quantification of Model Networks | 64 |
| 4.2.5 | Parameter Significance | 65 |
| 4.3 | Changing Local Weight Distributions | 65 |
| 4.4 | Results | 67 |
| 4.4.1 | Results for a Uniform Random Network | 68 |
| 4.4.2 | Significant Parameters | 70 |
| 4.4.3 | Particle Swarm Optimisation | 72 |
| 4.4.4 | Effects of Parameters on Individual Populations | 72 |
| 4.4.5 | Results for an Adjusted Random Network | 73 |
| 4.5 | Summary | 74 |
| 5 | Combining Architectural Changes | 77 |
| 5.1 | Response Properties and Structured Networks | 78 |
| 5.2 | Combined Approach | 79 |
| 5.3 | Fitting Response Distributions in a Structurally Adjusted Network | 81 |
| 5.4 | Effects of Inhibitory Activity in Network Simulations | 87 |
| 5.4.1 | Inhibitory Reversal Potential | 87 |
| 5.4.2 | Stimulus Size | 89 |
| 5.5 | Summary | 90 |

| | | |
|----------|---|------------|
| 6 | Effects of Architecture on the Functional Behaviour of Networks | 93 |
| 6.1 | Simplified <i>in-vivo</i> Simulations | 93 |
| 6.1.1 | Results | 94 |
| 6.1.2 | Summary | 97 |
| 6.2 | Temporal Inputs to Multiple Barrels | 98 |
| 6.2.1 | Experimental Basis | 99 |
| 6.2.2 | Modeling Basis | 99 |
| 6.2.3 | Extension of the Previous Layer 2/3 Model to a Spatial Scale | 101 |
| 6.2.4 | Results | 102 |
| 6.2.5 | Summary | 105 |
| 6.3 | The Adjusted Network Architecture in <i>in vivo</i> Scenarios | 105 |
| 7 | Limitations and Perspectives | 107 |
| 7.1 | Other Architectural Changes | 107 |
| 7.1.1 | Scale-Free Networks | 107 |
| 7.1.2 | Small-World Networks | 108 |
| 7.1.3 | Distance Dependent Probability | 108 |
| 7.2 | Plasticity | 109 |
| 7.2.1 | Global Weight Distributions | 110 |
| 7.2.2 | Degree Distributions | 110 |
| 7.2.3 | Local Weight Distributions | 110 |
| 7.2.4 | Plasticity as a Mechanism for Shaping Network Architectures | 110 |
| 7.3 | Active Networks | 111 |
| 8 | Conclusions | 113 |
| A | Source Code for the Generation of Structured Weight Lists | 115 |
| | Bibliography | 116 |

List of Figures

| | | |
|-----|---|----|
| 1.1 | Synaptic pathway in the rodent barrel cortex | 8 |
| 1.2 | Relationship between response interaction and cell location in relation to the barrel structure in the superficial layers | 10 |
| 1.3 | Whole-cell <i>in vitro</i> recordings of the mouse C2 barrel column | 12 |
| 1.4 | Connected pairs of excitatory neurons share input | 14 |
| 1.5 | Channelrhodopsin stimulation in layer 2/3 of mouse barrel cortex | 16 |
| 1.6 | Probability of spiking in response to a channelrhodopsin stimulus <i>in vivo</i> . . . | 18 |
| 1.7 | Example of dimensional stacking | 24 |
| 2.1 | Distribution of synaptic strengths | 30 |
| 2.2 | Network responses for a layered network | 35 |
| 2.3 | Threshold for further excitation | 37 |
| 2.4 | Comparison of different global weight distributions | 38 |
| 2.5 | Schematic of possible network interactions | 41 |
| 3.1 | Diagram of the idea of changing degree distributions | 49 |
| 3.2 | Dimensional stacking for the parameter space spanned by varying the structural parameters | 51 |
| 3.3 | Shared input networks consisting of five neurons | 54 |
| 3.4 | Network structure and Small-World-ness | 57 |
| 4.1 | Diagram of the idea of introducing weight correlations | 66 |
| 4.2 | A ChR2 like stimulus in a uniform random three population network model . . | 68 |
| 4.3 | Dimensional stacking for the parameter space spanned by varying the excitatory weight correlations | 71 |
| 4.4 | Dimensional stackings for each population for the parameter space spanned by varying the excitatory weight correlations | 72 |
| 4.5 | A ChR2 like stimulus in a three population network model with adapted excitatory local weight distributions | 74 |
| 5.1 | Response distributions for optimal structure | 78 |
| 5.2 | Spiking in inhibitory network populations | 81 |
| 5.3 | Parameter space for the connections of excitatory and fast-spiking neurons . . | 83 |
| 5.4 | Parameter space for the non-fast-spiking population | 84 |
| 5.5 | Response distributions for an all adjusted network | 86 |
| 5.6 | Single neuron responses on different membrane potentials show disynaptic inhibition | 88 |

List of Figures

| | | |
|-----|--|-----|
| 5.7 | Random network responses for different stimulation sizes | 89 |
| 6.1 | Evoked spikes in simulations of up- and downstates in a uniform random network | 95 |
| 6.2 | Evoked spikes in simulations of up- and downstates in an adjusted network . . | 97 |
| 6.3 | Summary of <i>in vivo</i> fraction of firing neurons after stimulation | 98 |
| 6.4 | Results for temporal stimulation of two whiskers in a simplified model | 100 |
| 6.5 | Spatially extended layer 2/3 network with layer 4 inputs | 101 |
| 6.6 | Facilitation of responses to temporal stimulations of two adjacent whiskers . . | 103 |
| 6.7 | Activity distributions for multiple network setups | 104 |
| 6.8 | Differences in activity distributions for adjusted and unconnected networks . . | 105 |

List of Tables

| | | |
|-----|---|----|
| 2.1 | Excitatory synaptic connectivity and uEPSP amplitudes in the mouse C2 barrel column. | 29 |
| 2.2 | Intrinsic electrophysiological properties of excitatory neurons in the mouse C2 barrel column | 31 |
| 3.1 | Synaptic connectivity and uEPSP amplitudes in layer 2/3 of the mouse C2 barrel cortex | 47 |
| 3.2 | Constraining parameters on the structural fitting technique | 53 |
| 3.3 | Shared input probabilities | 53 |
| 4.1 | Constraining parameters on the weight domain fitting technique | 73 |
| 5.1 | Constraining parameters on the combined fitting technique | 85 |
| 5.2 | Optimal parameter found by SPEA-2 optimisation | 87 |

1 Introduction

Random networks are used widely in theoretical studies of neuronal networks. The main assumption of these networks is that the probability of there being a connection between any two neurons is independent of other, existing connections in the network. However, more and more experimental results indicate that biological neuronal networks are not in this sense random, and, in addition, that the connection strengths between neurons show a wide distribution.

In this thesis, I explore the impact of classical assumptions on network structure and behaviour. In Chapter 2, the assumption that connection strengths can be assumed to be the same for all connections in a network model is investigated. The impact of multiple weight distributions is tested by measuring the network excitability. The results indicate that weight distribution shape has a strong impact on network excitability.

The effects of using more complex connectivity patterns in network construction are investigated in Chapter 3. A network of excitatory and two types of inhibitory neurons is constructed and the similarity of this network structure to biological observations is quantified. The structure of the network is then varied and it is shown that moving away from a random network architecture by altering the local connectivity it is possible to better agree with biological findings. Specifically, the degree distributions of the network are altered to fit network models to biological data that cannot be explained by the classical random network model.

Chapter 1. Introduction

It is not only experimental data on connectivity that challenge the classical random network model; in addition experimental paradigms in which multiple cells are stimulated at the same time cannot be reproduced by classical random networks. This is described in Chapter 4. I show how this shortcoming can be explained and how specific changes in local weight distributions can be used to improve the model network response.

The two approaches to improving network connectivity structure and local weight distributions are combined in Chapter 5. Both approaches are used to construct plausible networks that can reproduce the response characteristics of biological neural networks as well as the connectivity structure observed in experiments. The problems with this approach are due to the high dimensional parameter space that needs to be investigated. These problems are discussed and solutions presented to reduce the computational complexity of the problem.

After constructing network models that are more biologically plausible than classical networks, the properties of these networks are investigated in more complex scenarios. In Chapter 6, the differences between classical and adjusted network models are tested in a simplified simulation of *in vivo* up- and downstates. Furthermore, the role of network architecture in temporal sensory input is investigated.

Finally, shortcomings and perspectives for future work are discussed in Chapter 7. Following this, a summary of the results presented in this thesis is given.

In this introduction, the concept, construction and role in previous studies of random networks is described. Following this, the experimental basis of network connectivity measurements are discussed. These results lead to an interest on non-random network structures, which are discussed in the following part. Finally, an overview of visualisation and optimisation techniques used throughout this thesis is given.

1.1 Random Network Architectures

In this section, the concept of random networks is introduced. I show how these networks can be constructed and what parameters are used. An overview of selected studies that used random networks is given to highlight their role in theoretical work.

1.1.1 Network Construction

The main assumption of the random sparse architecture is that neurons are uniformly connected. This means that the probability of each neuron being a pre- or postsynaptic neuron does not depend on the position of the neuron in the network. The reason for the choice of fixed probabilities is that this fixed scheme does not introduce any more parameters that would need to be restrained by biological data. The only structural parameter that is needed for the construction of such a network is the connection probability p . It is also possible to express the connection probability as the average number of inputs to a single cell:

$$p = K/N \tag{1.1}$$

where K is the desired number of inputs per cell and N the size of the network.

The selection of the connections to be formed in the network can be done in many ways. The prevalent one is to go through all combinations of pairs of neurons and decide if they should form a connection or not, based on the connection probability p . This approach leads to quite diverse networks since the number of connections formed is not fixed, but is distributed binomially around $p \times n \times m$ with n and m being the population size of the pre- and postsynaptic population. This has the drawback, that all the algorithm must go through all possible connections and with big populations this can be rather costly in terms of computational power.

Another approach is to directly draw $p \times n \times m$ pairs of pre- and postsynaptic neurons from a discrete uniform distribution. This approach constructs the same number of connection

each time and is not as complex as the first approach. However, with increasing connection probability, the chance of choosing the same pre- and postsynaptic neuron pair twice is not negligible. Thus, this algorithm needs a doublet checking in addition, to avoid multiple connections. This can be done via a lookup table which stores if a connection was already formed. In the case of an already existing connection either the pre- or the postsynaptic neuron is redrawn until a new pair is found. If no such pair exist (or after a sufficient number of trials), the other neuron is redrawn and the process is repeated until a new connection is found. It is this algorithm that is used throughout this thesis (also see Appendix A).

1.1.2 Weight Distributions

After choosing a pre- and postsynaptic neuron pair, a synaptic weight is assigned to each connection to control the postsynaptic effect of a connection. A common approach of assigning synaptic weights to the constructed connections is to assume a uniform connection strength (Van Vreeswijk and Sompolinsky, 1996; Brunel, 2000), i.e. that each connection is assigned the same strength.

In contrast, it is also possible to assume specific distributions of synaptic weights which are sampled for each connection. For example, Vogels and Abbott, 2005 used a general weak set of synapses and a specific strengthened set for signal propagation. This could be seen as approximating a skewed or bimodal distribution.

In biological experiments it has been shown that the distribution of synaptic weights is highly skewed. Many connections have a rather small weight, while very few connections can be found that have a strong weight (Markram et al., 1997; Lefort et al., 2009; Avermann et al., 2011). The impact of different types of weight distributions on the excitability of a model network is the focus of Chapter 2.3.1.

1.1.3 Types of Network Populations

The term ‘population’ in network models usually refers to groups of neurons with distinct properties. Here ‘population’ is used to refer to different layers of the cortex (Chapters 2 and 6.2), where each layer is thought to comprise the same type of cells with the same connectivity properties.

The term ‘population’ is also used for different classes of excitatory and inhibitory cells (from Chapter 3 onward). Again, the connectivity properties are constant for each cell type pair.

1.1.4 Network Simulations

All simulations are written in pyNN (Davison et al., 2009). This is a simulator independent language that allows one to program simulations without explicitly using a specific simulator. The resulting programs can be used with a variety of simulators. The work presented here was executed using the NEST simulator (Gewaltig and Diesmann, 2007) as the backend.

The NEST simulator is specifically aimed towards an efficient simulation of large scale networks with realistic connectivity. Thus, it was chosen as the simulator used in this work. For an overview of different network simulators see Brette et al., 2007.

1.1.5 Neuron Models

Two different types of neuron model are used throughout this work. For the first part (Chapter 2), leaky integrate-and-fire neurons with exponential postsynaptic currents (Gerstner and Kistler, 2002) are used. This neuron type integrates synaptic inputs over time and emits a spike when the voltage crosses a given threshold. In addition, the membrane potential decays over time to a resting membrane potential, hence the term leaky integrate-and-fire neuron. The synaptic inputs are modeled via a current step that exponentially decays in time. One of the main advantages of this model is that it can be simulated very fast and it allows the simulation of larger networks.

Chapter 1. Introduction

In later parts from Chapter 3 on, the adaptive exponential integrate-and-fire neuron model (Gerstner and Brette, 2009) is used. This model is an extension of the standard leaky integrate-and-fire model. In addition to a fixed threshold, this model uses an exponential term to simulate spike initiation which allows for a better agreement with biological observations. It also incorporates subthreshold and spike-triggered adaptation which can be used to model a variety of different spiking patterns (Naud et al., 2008).

One other difference in the neuron model in Chapters 4 and following is that it is based on synaptic conductances instead of the current based synapses of the former model. This allows for accurate modeling of synaptic reversal potentials. In Chapter 6.1, these reversal potentials will be used to simulate neuronal responses on different depolarisation levels.

1.1.6 Roles of Random Networks

Random sparse networks have been the architecture of choice for many theoretical studies for a long time (Van Vreeswijk and Sompolinsky, 1996; Amit and Brunel, 1997a; Brunel, 2000; Vogels and Abbott, 2005; Morrison et al., 2007; Hertz, 2010; Renart et al., 2010). For example, in Van Vreeswijk and Sompolinsky, 1996, random sparse networks are used to investigate the irregular spiking activity observed in experimental data. To this end, random networks with excitatory and inhibitory neurons are constructed so that all neurons receive on average K excitatory and inhibitory connections as well as K external inputs. The strengths of these connections are sufficiently strong so that \sqrt{K} inputs evoke spikes in postsynaptic cells. The same synaptic strength is used for all synapses. They are able to show that for a sparse network with strong synapses, the network can reproduce irregular spiking activity and show chaotic behaviour that persists even when the network is driven with non-fluctuating external stimulation. This is due to a balance between excitation and inhibition. The inhibitory activity cancels the excitatory activity in a way that yields strongly irregular patterns of activity. The same basic random network is used by Renart et al., 2010 to show that highly shared input does not necessarily cause correlated spiking in the network. It seems intuitive that shared input should cause correlated activity. However, in a network with balanced excitation and inhibition

as described above, correlated excitatory and inhibitory activity can lead to cancellation of correlations. Thus, the resulting average correlations are low even for highly shared input.

Vogels and Abbott, 2005 also use a random network with fixed connection probabilities. The network is constructed using excitatory and inhibitory neurons at a ratio of 4:1 respectively. Two synaptic strengths are used, one for excitatory and one for inhibitory connections. The goal here is to investigate how signals can be propagated in a random network. A pool of neurons is defined as the first layer of a propagation chain. Subsequent layers are grouped by choosing neurons that receive at least three connections from the previous layer. Without modifications, this chain cannot propagate a signal to be fed into the first layer. The authors show that through selectively strengthening the synapses along the chain, it is possible to achieve propagation of an asynchronous signal.

It is also possible to analytically determine the behaviour of random sparse networks (Amit and Brunel, 1997b; Brunel and Hakim, 1999; Brunel, 2000). In Amit and Brunel, 1997b, the average firing rates of random sparse networks of excitatory and inhibitory neurons are calculated analytically using self-consistent analysis. The concept of self-consistent analysis relies on the assumption that neurons interacting in a closed network, each receiving input from other neurons that have similar firing statistics to itself. This assumption allows one to calculate neuronal activity analytically. Brunel, 2000 used a generalisation of this technique on random sparse networks of excitatory and inhibitory neurons and showed that the resulting spiking network activity can be separated into four cases. Network activity can either be synchronous or asynchronous on a global level and single neurons in the network can show either regular firing or irregular firing. The specific parameter ranges for these four states were determined analytically and thus provide a complete characteristic of network behaviour for different parameters. For a review of network activity dynamics, see Vogels et al., 2005.

Sparse random networks have been used to model many different biological observations and provide insight into how biological neuronal networks may work.

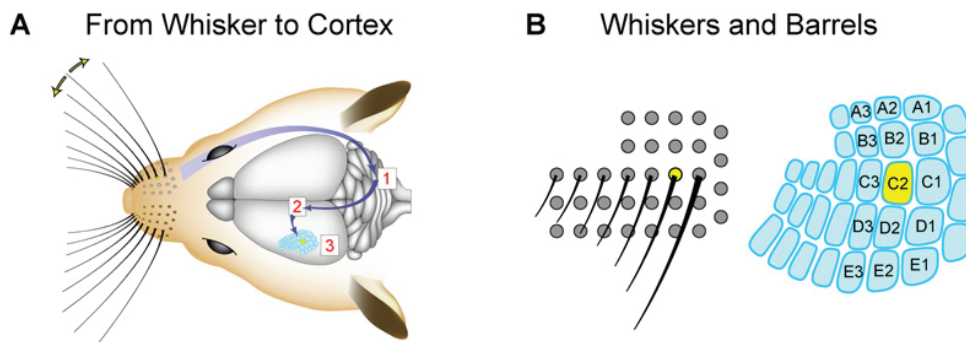


Figure 1.1: **Synaptic Pathway in the Rodent Barrel Cortex**

A Deflections of a single whisker on the snout of rodents evokes direct responses in the Trigeminal nucleus (1). These neurons project to the thalamus (2) and these in turn have direct projections to neurons in the somatosensory cortex (3) *B* Somatotopic organisation of the barrel field. Each whisker (left) is represented at one particular location in the barrel field of the somatosensory cortex (right). The yellow marker indicates the position of the C2 whisker and the C2 barrel. (Modified from Petersen, 2007)

1.2 Biological Background

In this section, the cortical region of barrel cortex where most of the data used in this thesis is taken is introduced. Further, it is described how pairwise connectivity is measured, and some of the problems when investigating network connectivity with pairwise recordings are indicated. Finally, the use of other experimental techniques to elucidate network connectivity is described, with particular focus on two optical techniques, namely glutamate uncaging and channelrhodopsin stimulation.

1.2.1 Barrel Cortex

The modeling approach presented here is based on data from the barrel cortex. This region of the brain specific to rodents is responsible for processing tactile information from the whiskers, hairs on the snout of the animal (Petersen, 2007). Figure 1.1 shows the synaptic pathway to the barrel cortex. In Figure 1.1 A the head of the animal is shown with its whiskers on the snout. A whisker deflection evokes activity in the trigeminal nucleus which is then transmitted via one synapse into different parts of the thalamus, constituting multiple pathways. These pathways

converge on a single barrel in the somatosensory cortex. Figure 1.1 B shows the somatotopic organisation of the barrel field. Each whisker is related to one specific barrel in the cortex. These barrels are about $300\mu\text{m}$ in diameter in the mouse brain (Lefort et al., 2009).

The somatotopic organisation is a remarkable feature that makes modeling this area interesting. Because of the highly localised representation, models of a relatively small scale may be sufficient to analyse the information processing. One particular example of the effect of such a localised representation is given in the temporal integration of sensory information. Stimulating a single whisker leads to an increased firing probability for neurons in the corresponding barrel column (Shimegi et al., 2000; Petersen et al., 2003). This is mostly due to the somatotopic organisation of the whisker pathway. One important question following this observation is how does the activity of single neurons change when multiple whiskers are stimulated?

In Shimegi et al., 2000 two adjacent whiskers are stimulated with varying interstimulus intervals (ISI). During these stimulations, the spiking activity of neurons in the region of the corresponding barrel columns is recorded. This recorded activity is compared to the linear sum of activity evoked by stimulating each of the two whiskers in solitude.

The facilitation index (FI) quantifies this comparison. A facilitation index equal to one indicates no difference, while responses larger than expected have a facilitation index greater than one. A summary of this experiment is shown in Figure 1.2. The recorded cells are binned into three categories. This categorisation is depicted in the right part of Figure 1.2. The left part of Figure 1.2 shows the facilitation index of the three classes for multiple trials with different interstimulus intervals.

The middle population shows strong facilitation for small interstimulus intervals in either direction and shows slight suppression for larger interstimulus intervals. The neurons inside one barrel (caudal and rostral) show normal activation when their principal whisker is stimulated first with long interstimulus intervals (negative ISI for caudal, positive ISI for rostral). In the reverse case a strong suppression is seen, meaning that neurons respond less than expected

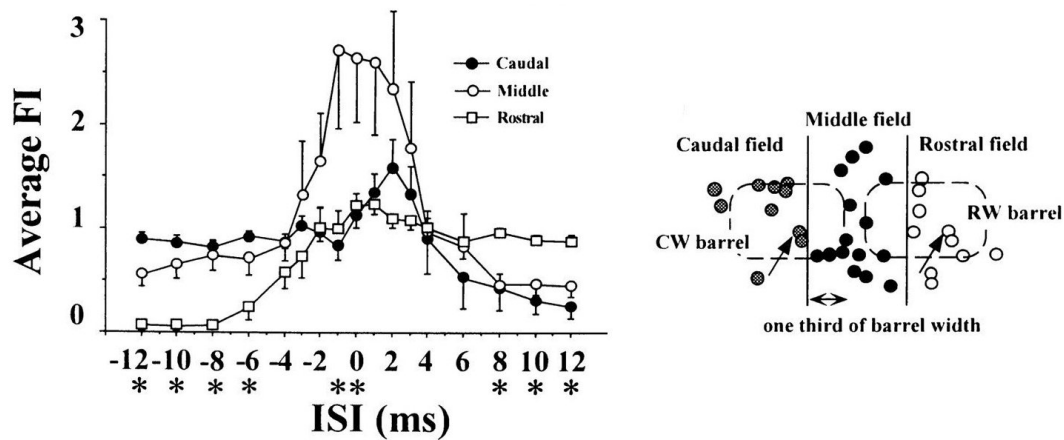


Figure 1.2: **Relationship between response interaction and cell location in relation to the barrel structure in the superficial layers**

Left Average facilitation index (FI) for each group of neurons for varying interstimulus intervals (ISI) *Right* Locations of recorded cells in layer 2/3. Overlaid is the position of the corresponding layer 4 barrel in dashed lines. Each recorded cell is classified either ‘caudal’, ‘middle’ or ‘rostral’. ‘Middle’ neurons are located adjacent to one-third of each barrel and in the septal region between barrels. ‘Caudal’ and ‘rostral’ neurons were located in the lateral two-thirds of each barrel. (Modified from Shimegi et al., 2000)

from the single stimulation trials if the stimulation of the adjacent whisker comes first.

Surprisingly, for the caudal population there is facilitation greater than one if the rostral whisker is activated 1-3 ms before the caudal whisker. It is hypothesised that the strong facilitatory effect in the middle group comes from the temporal overlay of excitatory inputs from both stimulated whiskers. The suppression seen in the rostral and caudal groups may come from different excitatory and inhibitory connectivity profiles. This data is used in Chapter 6.2.

1.2.2 Pairwise Connectivity Measurements

To collect data on network connectivity it is necessary to record from multiple neurons at the same time. The most direct approach is to use intracellular recordings in an *in vitro* setup.

This allows the stimulation of single cells to evoke action potentials and at the same time measure the membrane potential in other cells to infer the connectivity.

An example of this approach from Lefort et al., 2009 is shown in Figure 1.3. Here intrinsic imaging (Grinvald et al., 1986) is used to locate the C2 barrel before performing the intracellular recordings. The connectivity of a single barrel is investigated (Figure 1.3 A,B), and the resulting section of the brain is shown in Figure 1.3 C, left. In the middle, six electrodes for intracellular recording were lowered into the tissue and six different cells were recorded. The morphology of those cells is shown in Figure 1.3 C right and D. By stimulating each cell and recording the responses of the other cells, it is possible to infer a specific connectivity between the six patched neurons (Figure 1.3 E). The single traces of the stimulation are shown in Figure 1.3 F

Since the direct membrane potential traces are measured in the intracellular recordings, it is possible to recover the synaptic strength of each connection. Throughout my work, I use the unitary postsynaptic potential (uPSP) as measured in these experiments as the value of synaptic strength or synaptic weight. I also assume that two given cells have at most one connection. This is not necessarily the case in biological networks, as two cells can have multiple synaptic contacts (Feldmeyer et al., 1999). The evoked response of a presynaptic spike can thus be composed of multiple synapses. The synaptic strength on a single synapse level, however, is difficult to obtain and thus the unitary postsynaptic potential is used as an approximation of the real synaptic weight.

This approach is used by multiple studies for a long time (Markram et al., 1997; Feldmeyer et al., 1999; Holmgren et al., 2003; Feldmeyer et al., 2006; Thomson and Lamy, 2007; Helmstaedter et al., 2008; Lefort et al., 2009). Although this technique provides a lot of insight into connectivity in different areas and cell types, it has major drawbacks when trying to investigate network connectivity on a higher order, since the connections tested are only based on pairwise measurements.

Only when examining more than two neurons simultaneously, the investigation of higher order connectivity becomes possible, although it is still difficult since connectivity in the

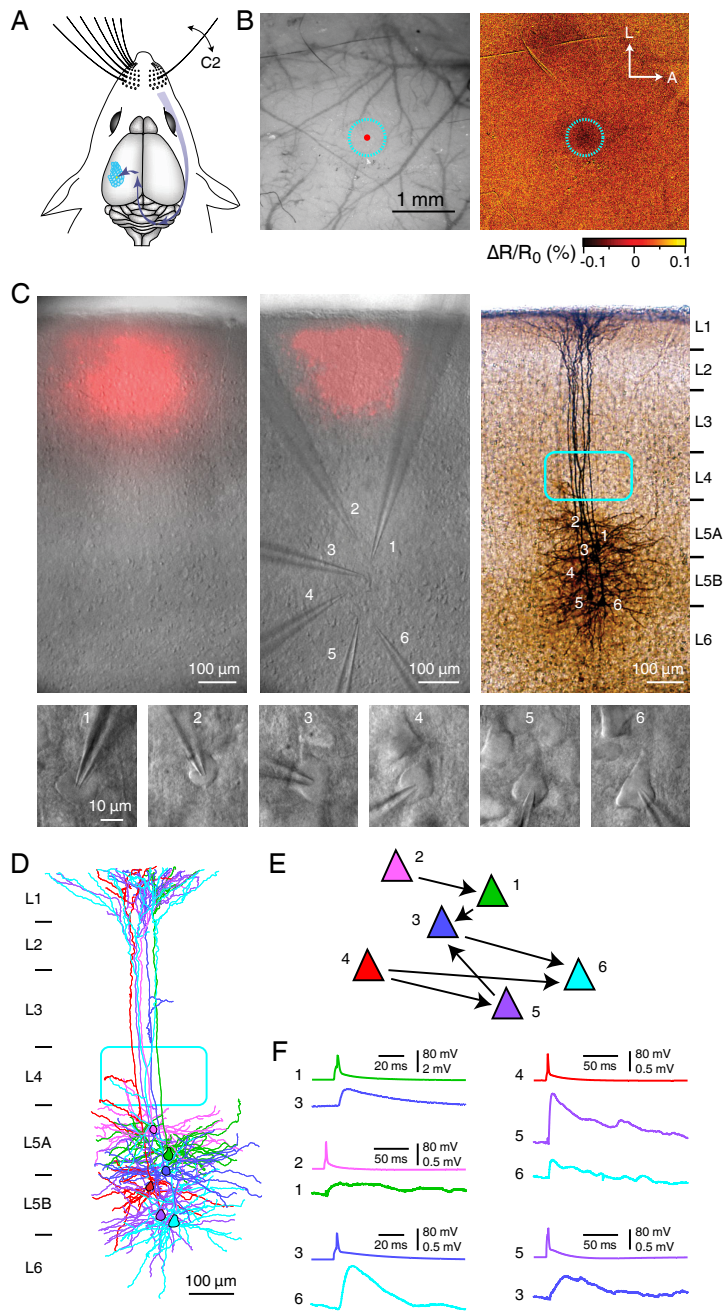


Figure 1.3: **Whole-cell *in vitro* recordings of the mouse C2 barrel column**

A Single deflection of the C2 whisker. **B** Intrinsic imaging shows a decreased reflectance at the position of the C2 barrel. **C** The C2 column is identified by an injection of fluorescent dye into the area found in **B**. This injection can be found in brain slices (*left*). Recording electrodes are lowered into the slice (*middle*). These electrodes were filled with biocytin, which allowed for the visualisation of neuronal structure (*right*). **D** Dendritic reconstruction of single cells. **E** Example connectivity diagram of the recorded cells. **F** Membrane potential traces of the recorded cells. Each cell was stimulated to emit a spike and the responding postsynaptic neuron responses are shown for each stimulation. (from Lefort et al., 2009)

cortex is sparse. The chances of finding a group of multiple connected neurons is rather slim (Lefort et al., 2009). Few studies are able to investigate some features of network connectivity other than pure pairwise statistics using electrophysiology (Song et al., 2005; Perin et al., 2011).

In these studies, multiple electrodes are used to find interconnected groups of neurons. These groups are then analysed to quantify the occurrence of specific patterns of interconnected groups (so called 'motifs', Milo et al., 2002). The main conclusion from both publications is that in general, groups of three or more interconnected neurons are more frequent than expected from a standard random network.

But even with an outstanding number of 12 electrodes for intracellular recordings (Perin et al., 2011) the largest group that could be analysed consisted of just 8 neurons which is very small in the scope of cortical networks. Even cortical networks on a small scale, such as one barrel consist of thousands of neurons. Thus, methods to acquire data on network connectivity need to investigate larger groups of neurons.

1.2.3 Network Connectivity Measurements

In recent years, more and more techniques have been developed to circumvent the problems of electrophysiology. I focus on two developments that have proved to be particularly useful to the analysis that employed throughout this work. These are the use of glutamate uncaging and channelrhodopsin (ChR2) for stimulating neurons.

Glutamate Uncaging

Glutamate uncaging is a technique used to stimulate neurons in cortical slices (Callaway and Katz, 1993; Boucsein et al., 2005; Nikolenko et al., 2007). Glutamate itself is a neurotransmitter, released from the presynaptic terminal of excitatory neurons and taken up at the postsynaptic membrane. In the glutamate uncaging technique the whole slice is bathed in a 'caged' glutamate compound. This means that everywhere in the slice glutamate is present but due to an alteration in its molecular structure it is unable to excite neurons.

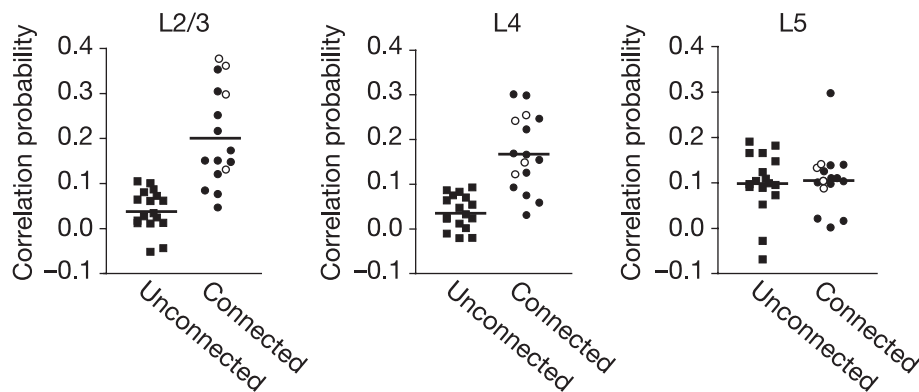


Figure 1.4: Connected pairs of excitatory neurons share input

Correlation probabilities for all stimulation sites in each layer for connected (circles) and unconnected (squares) pairs of recorded neurons. Open circles indicate reciprocal connections, filled circles unidirectional connections. Mean values for each group are indicated by horizontal lines. (Modified from Yoshimura and Callaway, 2005)

The configuration of this caged compound changes when exposed to strong light and the glutamate will be able to excite synapses. Using a two photon laser, the localisation of the uncaging is sufficiently high to stimulate single neurons (Fino and Yuste, 2011; Packer and Yuste, 2011). The main advantage here is that it is relatively easy to record from just one cell intracellularly and test many possible inputs to this cell with the light stimulus. This technique was used in multiple studies to probe network connectivity (Yoshimura and Callaway, 2005; Yoshimura et al., 2005; Fino and Yuste, 2011; Packer and Yuste, 2011).

One of the main problems with this technique is that it is nearly impossible to record the connection strength since the caged glutamate can affect the postsynaptic response (Fino and Yuste, 2011).

Nevertheless the existence of connections can be extracted from these experiments. The large number of possible inputs that can be accessed leads to additional information on the convergence and clustering of connections in comparison with the paired recordings.

In the course of this work (Chapters 3 and 5), results from one set of experiments are used (Yoshimura and Callaway, 2005; Yoshimura et al., 2005). Here, glutamate uncaging is used to scan the inputs to pairs of neurons.

The main finding of the experiments is that connected pairs of excitatory neurons are more likely to share input from other excitatory cells than unconnected pairs. These findings are shown in Figure 1.4. Here, the probability of sharing input (correlation probability) is plotted for pairs of excitatory neurons. The inputs are tested from layer 2/3 (Figure 1.4 left), layer 4 (Figure 1.4 middle) and layer 5 (Figure 1.4 right) with the recorded pair in layer 2/3. The inputs from layer 2/3 and layer 4 are different for connected and unconnected pairs, while layer 5 input shows no difference.

When taking inhibitory neurons into account, the results indicate that pairs of fast-spiking and excitatory neuron in layer 2/3 share more input only when they are connected bidirectionally, while one-way connected and unconnected pairs show the same, lower level of shared input. Pairs of excitatory and other (adapting) interneurons share the same amount of input regardless of the connectivity. This indicates that different cell types show different levels of fine-scale connectivity.

Channelrhodopsin Stimulation

The second advance that makes network connectivity more accessible is Channelrhodopsin. This is a light activated sodium channel that was originally found in green algae (Nagel et al., 2002). Using either genetic manipulations or viral vectors, this channel can be expressed in neurons (Nagel et al., 2003; Boyden et al., 2005), effectively activating the neurons on a rapid timescale when illuminated by blue light.

This activation is different from glutamate uncaging in that channelrhodopsin activates the cells intrinsically since the channel is embedded directly into the membrane. The usage of channelrhodopsin can be quite similar to that of glutamate uncaging. Using a laser it is possible to stimulate single neurons and perform a similar scanning of inputs as with glutamate (Zhang et al., 2006; Wang et al., 2007).

A striking advantage of channelrhodopsin is that it can be genetically targeted to specific classes of cells and using viral vectors it can also be locally targeted (Aronoff and Petersen,

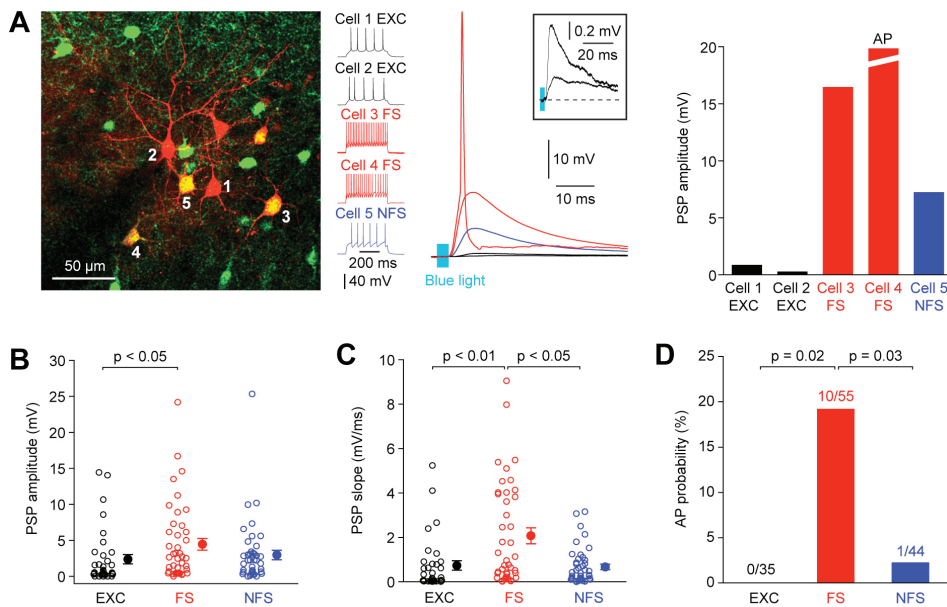


Figure 1.5: **Channelrhodopsin stimulation in layer 2/3 of mouse barrel cortex**

A Example channelrhodopsin stimulation experiment. *Left* Two-photon image stack. Inhibitory cells are green, recorded excitatory cells are red and recorded inhibitory cells are yellow. *Middle* Firing patterns of recorded cells and postsynaptic responses (Excitatory cells (EXC, black), inhibitory fast-spiking cells (FS, red) and inhibitory non-fast-spiking cells (NFS, blue)) *Right* Postsynaptic potentials (PSP) in response to the channelrhodopsin stimulation for all recorded cells. Cell 4 (fast-spiking) fired a spike reliably in response to the light stimulation. **B** Distribution of peak response amplitudes in response to the light stimulation across all experiments with spiking cells excluded. **C** Slopes of postsynaptic potential (PSP) responses. **D** Probability of cells spiking in response to the stimulation. (Modified from Avermann et al., 2011)

2008). This can be used to specifically stimulate multiple cells of one type and record the response of other cells to this complex yet confined stimulus.

Such an approach is used in Avermann et al., 2011 in an *in vitro* situation. Here, channelrhodopsin was used alongside standard pairwise connectivity measurements. This allows the unravelling of the connectivity parameters of different cell classes. Measurements are taken from excitatory cells, inhibitory fast-spiking cells and inhibitory non-fast-spiking cells of layer 2/3 of mouse barrel cortex. The results of the channelrhodopsin stimulation are depicted in Figure 1.5. One example experiment is shown in Figure 1.5 A. The image in Figure 1.5 A left illustrates the injection site, while the middle panel shows membrane potential recordings

of the cells labelled on the left responding to a light stimulus. The right hand side shows the peak amplitude of the recorded cells. One fast-spiking interneuron (cell 4) reliably spikes in response to the light stimulus. Figure 1.5 B depicts the distribution and mean value of the peak amplitudes across all experiments, while Figure 1.5 C shows the same for the slope of the postsynaptic response. Finally, Figure 1.5 D depicts the probability of firing an action potential in response to the light stimulus for all three cell classes. All classes show a highly skewed distribution of PSP amplitudes with the fast-spiking populations responding strongest, even emitting spikes with a probability of about 20%. I use these distributions of PSP amplitudes shown in Figure 1.5 B in Chapter 4 to compare different network architectures.

A similar approach is used in an *in vivo* setup by Mateo et al., 2011. Here the same channelrhodopsin stimulation is applied during ongoing activity. Intracellular *in vivo* recordings show periods of silence with almost no spiking activity where the membrane potential is roughly equal to the resting membrane potential, while other periods show spiking activity with an average membrane potential that is strongly depolarised in comparison to the resting potential. These two periods are called down- and upstate respectively, referring to their average membrane potential.

Applying the channelrhodopsin stimulation reveals two things: first, the membrane potential amplitude in postsynaptic neurons depends strongly on the state of the network. For upstates, neurons tend to respond little if at all, while in the downstate neurons respond quite strongly to the channelrhodopsin stimulation.

The second observation is that the probability of emitting a spike in response to the stimulus depends on network state and cell type. The spiking probability of excitatory neurons is higher in the up- than in the downstate, but only to a small degree, whilst the spiking probability of non-fast-spiking neurons strongly increases from the down- to the upstate. The probability of a fast-spiking neuron emitting a spike increases in the upstate compared to the downstate although not significantly. Figure 1.6 shows the spiking probabilities for all populations in the up and downstate. I reproduce parts of these results with a simplified model of the upstate in

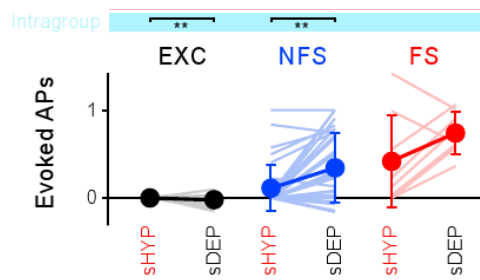


Figure 1.6: **Probability of spiking in response to a channelrhodopsin stimulus *in vivo***
Shown are the spiking probabilities for excitatory (black), non-fast-spiking (blue) and fast-spiking (red) cells. Significant inside a population between up and downstate are marked in teal. (Modified from Mateo et al., 2011)

Chapter 6.1.

Other Network Connectivity Measurements

There are other techniques available that can be used to investigate network connectivity. The most direct one would be electronmicroscopy (EM). With this technique it is possible to visualise the synapses and discern with 100% accuracy whether or not two neurons are connected. The main problem is that due to the extremely high resolution of the acquired images, the resulting amount of data is very hard to analyse on a sensible timescale. Recently, studies have shown that it is indeed possible to extract connectivity from EM and that it is also possible to link this information to *in vivo* data (Bock et al., 2011). However, the scale at which this is possible at the moment barely exceeds that of intracellular recordings with a sufficient number of electrodes.

Another very interesting approach is to use fluorescent markers for the recording of neuronal responses. The best examples are calcium imaging (Smetters et al., 1999; Peterlin et al., 2000) and voltage sensitive dyes (Grinvald et al., 1984; Shoham et al., 1999) or voltage sensitive proteins (Mutoh et al., 2011).

Voltage sensitive dyes have been used in the past to study the activity of neuronal populations on a relatively large scale (Grinvald et al., 1986; Shoham et al., 1999; Ferezou et al., 2006). Since

the dyes do not enter the cell bodies of neurons, it is rather difficult to record single cell activity (Ferezou et al., 2006; Peterka et al., 2011). The use of voltage sensitive dyes is thus a potentially interesting mechanism for recording multiple neuronal responses at the same time. However, it is currently not possible to do so at a single cell level. Recently, voltage sensitive proteins have been developed that are targeting single cells with a very high resolution (Mutoh et al., 2011). This technique is very recent and will likely provide insights into neuronal responses in the future.

Calcium imaging is another technique used to visualise neuronal responses (Smetters et al., 1999; Peterlin et al., 2000). During the action potential of a neuron, there is a transient change in calcium concentration (Borst and Helmchen, 1998). This change can be made visible by fluorescent markers. Calcium ions can bind to these markers and change their fluorescence, thus making transient changes in calcium levels visible. This technique can be used to extract spike times of populations of neurons with a high precision (Grewe et al., 2010; Lütcke et al., 2010). This approach is very similar to the classical multi-electrode recordings, where spikes of multiple neurons at the same time can be extracted. However, since only spikes are recorded, the extraction of network connectivity is limited. Weak connections may not be sufficient to elicit a spike and remain largely undetected, while disynaptic connections might be detected as a single connection, if their activation is sufficiently strong. However, there are studies which extract this effective connectivity information from spike train data (Pillow et al., 2008; Gerhard et al., 2011).

Another possibility is to infect certain cells with viruses that are able to propagate through synapses to other neurons. This would effectively allow the visualisation of all inputs or targets to a single infected cell, depending on the direction in which the virus travels (Wickersham et al., 2007). This technique is promising, although it is unknown which proportion of the post- and presynaptic neurons are labeled and thus the usefulness for complete circuit mapping is unclear. Another drawback is that in a single experiment only one cell can be targeted in order to get a clear estimate on the number of connected cells. Thus, acquiring statistics on network connectivity requires an extremely high number of experiments and is at this stage not feasible.

In general, this technique is more useful to investigate long-range projections where a larger volume is infected and predominant projection targets or sources can be distinguished (Mao et al., 2011).

1.3 Non-random Network Architectures

As pointed out before, theoretical neuronal network models have been using the uniform random network paradigm in the past. However, more and more recent studies try to investigate the role of more complex network structures.

Small-world networks (Watts and Strogatz, 1998) are an important example of complex network structures. They are characterised by groups of highly connected nodes that are linked to each other through sparse connections. These networks are predominantly found in social networks (Davidsen et al., 2002). They are also used in modeling economic markets (Janssen and Jager, 2001) or epidemics (Keeling and Eames, 2005).

Another widely used network structure is the scale-free network (Barabási and Albert, 1999). These are networks that show no characteristic scale on the number of connections per node. The distribution of these values over the whole network is called the degree distribution. The main characteristic of scale-free networks is thus that the degree distributions show no characteristic scale and are thus powerlaw distributed. This implies also that certain nodes will have an unexpectedly large number of connections and would serve as ‘hubs’ that gather and send a lot of information. Examples for scale-free networks are the network of airports and corresponding flight routes in the United States (Wang and Chen, 2003) or the topology of the internet (Vazquez et al., 2002).

These network types can be used in computational models (Feldt et al., 2011; Prettejohn et al., 2011) and show similarities to biological networks. For example, developing hippocampus is shown to have GABAergic ‘hub’ neurons and thus resembles a scale-free network (Bonifazi et al., 2009). Another example is that small-world structures have been observed in extracted connectivity from spike train data in cortex, but the significance of such effects is questionable

(Gerhard et al., 2011).

Instead of using distinct network structures directly, it is also possible to perform specific changes to network connections in order to introduce complex patterns. One example of this is to change the shape of the degree distributions, which can be split into the in-degree and the out-degree distribution, only counting the incoming and outgoing connections respectively. This approach has been used by Roxin, 2011 to investigate oscillations in spiking activity. Here the asynchronous irregular random network model from Brunel, 2000 is used. The only difference in network structure is that Roxin varies the in- and out-degree distributions systematically by their variance. The main result shows that broad in-degree distributions increase oscillatory activity, while broadening the out-degree distribution does not contribute to oscillations in the spiking activity.

Another approach is taken by Pernice et al., 2011 to characterise the influence of structure on network activity. Here a mathematical model of interacting point processes is used to simulate the neuronal network. With this approach it is possible to directly calculate spike train correlations and firing rates in the network. One of the main results is that the shape of the out-degree distribution and thus the occurrence of output hubs lead to a strong increase in spike train correlations in the network.

I use the method of changing degree distributions of the network in Chapters 3 and 5. To link the resulting networks to existing network types, I quantify the resemblance of a given network to the small-world structure. I employ the so called *small-world-ness* (Humphries and Gurney, 2008) as a quantitative measure of similarity. This is done by computing the average shortest path length L_{rand} and the average clustering coefficient C_{rand} for the uniform random network and computing the equivalent values L and C for the network to be tested. The small-world-ness S is then calculated as follows:

$$S = \frac{C}{C_{rand}} * \frac{L_{rand}}{L} \tag{1.2}$$

Chapter 1. Introduction

The shortest path length is the number of nodes that need to be visited when travelling from one node to another. The average shortest path length is the average of this number across all pairs of nodes. The clustering coefficient for a single node is the number of existing connections between neighbouring nodes divided by the maximal possible number of connections (Watts and Strogatz, 1998). While initially defined for undirected networks, I use an extension to directed networks where neighbouring nodes are nodes that receive a connection from the node in question. The clustering coefficient therefore indicates how dense connections are locally.

It is important to note that all changes to network structure can be done, while keeping the connection probability of the whole network the same as before. Thus, these more complex network structures are still in agreement with the basic experimental findings from pairwise recordings.

In addition to specific structural changes, it is also possible to investigate complex features in the distributions of synaptic weights. Most experimental approaches that are able to elucidate complex network structures are unable to report the synaptic strengths. This is true for calcium imaging, since only spikes are recorded and also for glutamate uncaging because of the specifics of the stimulation paradigm. However, it has been shown theoretically that different weight distributions can drastically affect the behaviour of neuronal networks (Morrison et al., 2007; van Rossum et al., 2008; Koulakov et al., 2009). Thus, the impact of specific weight distributions might be as important as the network structure itself.

In Chapter 2, I investigate the impact of different global weight distributions on network excitability. Similar to changing the network structure it is also possible to manipulate the weight distributions with a more fine-scaled approach, while keeping the global weight distribution intact. One approach to this fine-scaled change is investigated in Koulakov et al., 2009. It is shown that networks can have different distributions of spontaneous activity by only manipulating the local weight distributions. This is done by scaling the incoming or outgoing weights per neuron with a specific scaling value. These scaling values are drawn in

a way that keeps the global weight distribution constant. Since the weights are scaled on a single neuron basis, the local weight distribution is changed. I make use of this approach in Chapters 4 and 5.

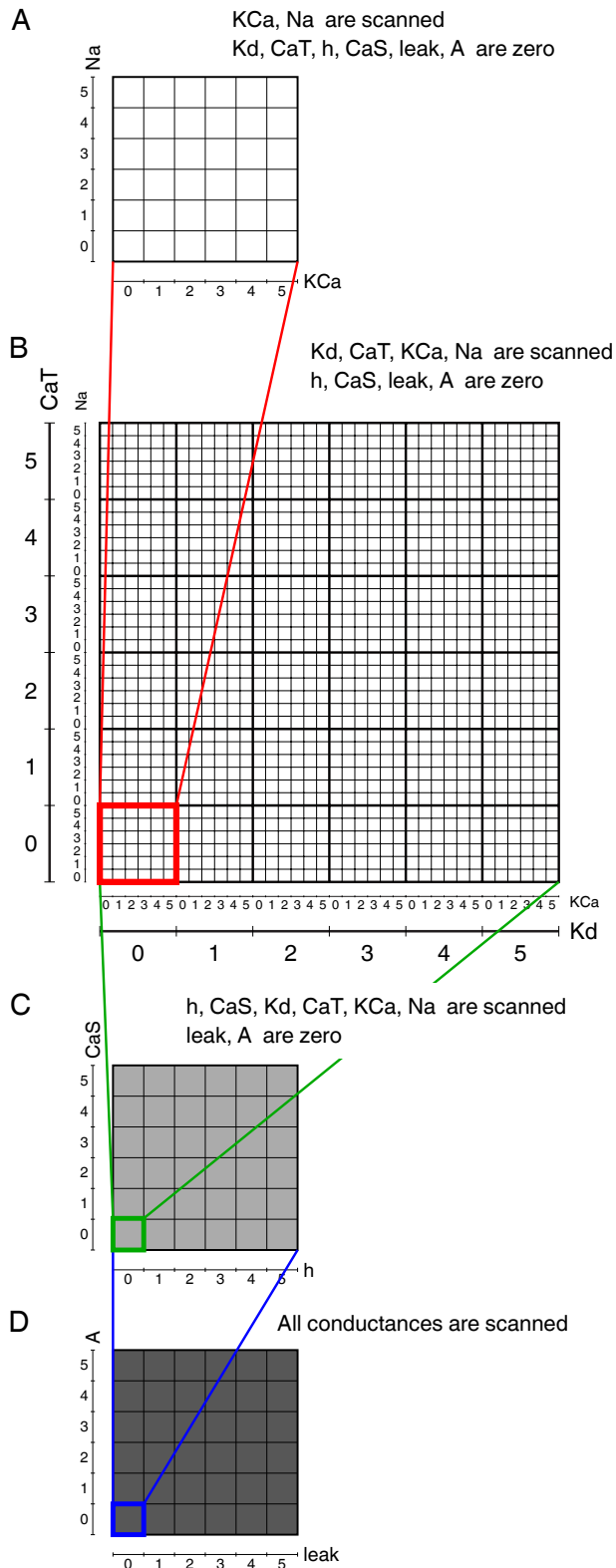
1.4 Visualising High Dimensional Parameter Spaces

The network changes used throughout this thesis result in high dimensional parameter spaces. To analyse these spaces, I adopt the idea of clutter based dimensional reordering (cbdr) (LeBlanc et al., 1990; Peng, 2005; Taylor et al., 2006). This technique is used to construct two dimensional images of high dimensional spaces, revealing their underlying structure. To construct these images, the algorithm starts with two parameters (p_1 and p_2) that yield a two dimensional parameter space. Next, two more parameters (p_3 and p_4) are taken and for each point of this new two dimensional parameter space, p_1 and p_2 are varied to create a nested four dimensional parameter space. This process is reiterated until all parameters are used. An example of this technique being used to scan a set of eight parameters is shown in Figure 1.7.

The constructed dimensional ‘stack’ is not necessarily helpful, as even structured data can appear as random if displayed in a non-optimal fashion. To optimise the order of parameters, a measure of goodness is introduced called ‘edginess’. This measures the difference of one pixel in the image to the four principal neighbours for all pixels and indicates the smoothness of the image. The desired image should have a low edginess (high smoothness) since similar areas should be grouped together. The optimisation is done as follows: For a constructed image, the edginess is computed. Next, two parameters are switched and if the edginess is lower, the process is repeated until no lower edginess can be found by further switching of two parameters. The resulting image is then optimal in a sense that it shows the smallest number of changes across the picture and should therefore sort parameters in their order of impact. Parameters with almost no impact should be scanned first (see Figure 1.7 A), while parameters with a strong impact should be scanned last (see Figure 1.7 D).

Figure 1.7: **Example of dimensional stacking**

A Visualization of two conductances (KCa and Na), with other conductances set to zero. Each conductance is varied independently, resulting in a 6x6 grid. Each square would then be coloured according to some property of the corresponding neuron (e.g., spontaneous activity type). *B* To visualize an additional two conductances, the grid from *A* is embedded in a larger grid. The larger grid scans an additional two conductances (Kd and CaT), and within each square of this larger grid is a 6x6 grid scanning the original two conductances (KCa and Na). The 6x6 grid in *A* is found in the bottom-left corner because it corresponds to Kd=0 and CaT=0. Overall, a 36x36 grid is formed, scanning four conductances total (Kd, CaT, KCa, and Na). *C* This process is then repeated, embedding the grid from *B* in another 6x6 grid that scans *h* and CaS, thus forming a 216x216 grid that scans 6 conductances. *D* This process is repeated once more, embedding the grid from *C* in another 6x6 grid that scans leak and A, thus forming a 1,296x1,296 grid that scans all 8 conductances. This grid contains a single pixel for each model in the database (1,296x1,296 = 1.7 million models). (Modified from Taylor et al., 2006)



1.5 Optimisation Techniques

In order to obtain an optimal solution to the investigated parameter spaces, genetic algorithms are used. Given a specific fitness measure, these algorithms usually use multiple sets of parameters simultaneously and try to improve their fitness by introducing small changes to these sets. Two different classes of genetic algorithms are used: swarm optimisation and evolutionary algorithms.

1.5.1 Particle Swarm Optimisation

In particle swarm optimisation (Kennedy and Eberhart, 1995) the goal is to find the optimal value of an error surface. To this end, a swarm of multiple sets of parameters called particles are spread all over the parameter space. Each particle has a specific position (set of parameters) and speed. The particles move in each timestep to a new set of parameters determined by the former position and their speed. For each location, the error is evaluated and the best local error and position is stored. The new speed is then computed by taking into account the former speed of the particle, the best solution found by the particle and the global best solution found by any particle in the swarm. This algorithm is iterated until a desired error is reached or until a sufficient number of steps is reached. This algorithm works best for complex error spaces and inexpensive error evaluations. I use this algorithm in Chapter 4. Due to the complexity of the further parameter spaces increasing drastically, I could not use the particle swarm optimisation in Chapter 5.

1.5.2 Strength Pareto Evolution Algorithm (SPEA-2)

To investigate the high dimensional parameter space in Chapter 5 an evolutionary algorithm is used. These algorithms use a population of sets of parameters. The main idea is that the individuals of this population can mate and mutate much like biological individuals. The term evolutionary algorithm refers to the fact that through the mating and mutations an evolution is simulated. Mating (or crossover) means that two individuals are combined. For this step,

Chapter 1. Introduction

the so called two points crossover is used in this work. This means that two parameters are chosen and all parameters between the two chosen values are taken from the other individual. The mutation step is applied to a single individual and changes the single parameters. I use a Gaussian mutation for this step, meaning that each parameter can be modulated by a value drawn from a Gaussian distribution of mean zero and unit variance.

The most important part of this algorithm is the selection of 'good' individuals to carry over into the next generation. For this the approach of the strength pareto evolution algorithm is used (SPEA-2, Zitzler and Thiele, 1999; Zitzler et al., 2001). The initial step is that all 'pareto dominant' solutions are chosen for the next step. A solution is pareto dominant, if there are no solutions that are better in all parameters (Voorneveld, 2003). If the set of all pareto dominant individuals is smaller than the desired population size, the next population is completed with the best non-dominant individuals. If the set of dominant individuals is too large for the next population, the dominant individual that is closest to another dominant individual is removed. This is iterated until the set has the desired population size.

There is no problem to use multi dimensional fitness values for the pareto dominance evaluation. Thus, I employ this algorithm in Chapter 5 to optimise the solution for the adjustments of networks in the structural and in the weight domain.

2 Random Layered Networks

Synaptic weight distributions have been shown to be made of many weak connections and rare very strong connections (see Chapter 1.2.2). Many theoretical studies do not take into account these characteristics, but only use a fixed weight per connection (see Chapter 1.1.6). This chapter investigates the impact of such a simplification on network behaviour.

I constructed model networks with six layers, using three distinct weight distributions. The effects of these different weight distributions were measured through the excitability of the network. As a measure of excitability, the threshold of further excitation was introduced. This threshold was the number of neurons that needed to fire synchronously in order to evoke at least one further spike in the network.

The beginning of the chapter consists of a description of the biological data used to constrain the model network. Following this, the construction of the network is discussed, followed by the description of the three different types of weight distributions. Then, I define the stimulation paradigm that was employed to probe network excitability, and the measure used to quantify the network excitability. In the results section, I analyse and explain the impact of weight distributions on the excitability of the six cortical layers individually. The results indicate that the sparse strong connections are a key component for the excitability of networks.

2.1 Experimental Basis

Data from intracellular recordings done in slices were used to constrain the network models (Lefort et al., 2009). As explained in Chapter 1.2.2, these types of recordings are commonly used to extract connection probabilities and weight distributions. These measurements as well as recordings of single cell properties were used to constrain the model networks.

2.1.1 Connectivity Data

In Lefort et al., 2009, groups of up to six excitatory neurons are recorded intracellularly. When stimulating one of these cells to emit a spike, the membrane potentials of the other cells is recorded (see Chapter 1.2.2 for details of this technique). If one of the other recorded cells is connected to the stimulated cell, then this cell shows a response to the stimulus in form of an increase in membrane potential. Single cell stimulations are repeated 20 times per cell and it is only the average response that is used in further analysis. The amplitude change in the average membrane potential trace of the postsynaptic cell is taken as the weight of this connection. Repeating this experiment multiple times with different sets of neurons in different locations allows to extract weight distributions and connection probabilities across layers.

The shape of the measured weight distributions is highly skewed. Figure 2.1 shows a histogram of the synaptic strengths found in the experiments in (Lefort et al., 2009). It can be seen that a lot of the connections show weak synaptic strengths with some connections having very large synaptic strengths up to 8 mV.

The results of the analysis of connectivity and evoked amplitudes are summarised in Table 2.1. In this table, each connection between two layers is described by the previously determined probability of connection, the mean and the median amplitude change that is evoked and the total range of recorded amplitudes.

Table 2.1: **Excitatory synaptic connectivity and uEPSP amplitudes in the mouse C2 barrel column**

P denotes the probability of a connection from the pre- to the postsynaptic layer (L). Mean, median and range are describing the characteristics of the unitary excitatory postsynaptic potential (uEPSP) evoked by the connection.
(Modified from Lefort et al., 2009)

| | | Presynaptic | | | | | | |
|--------------|------------------|------------------|--------------------|--------------------|--------------------|--------------------|--------------------|--------------|
| | | L2 | L3 | L4 | L5A | L5B | L6 | |
| Postsynaptic | L2 | P (found/tested) | 9.3% (88/950) | 12.1% (22/182) | 12.0% (25/208) | 4.3% (9/209) | 0.96% (1/104) | 0% (0/50) |
| | | mean \pm sem | 0.64 \pm 0.06 mV | 0.71 \pm 0.15 mV | 0.98 \pm 0.24 mV | 0.52 \pm 0.13 mV | 0.21 mV | |
| | | median | 0.46 mV | 0.59 mV | 0.58 mV | 0.52 mV | | |
| | | range | 0.08 - 3.88 mV | 0.04 - 2.67 mV | 0.07 - 5.54 mV | 0.08 - 1.09 mV | | |
| | L3 | P (found/tested) | 5.5% (10/183) | 18.7% (96/513) | 14.5% (25/172) | 2.2% (2/89) | 1.8% (3/167) | 0% (0/64) |
| | | mean \pm sem | 0.44 \pm 0.09 mV | 0.78 \pm 0.07 mV | 0.58 \pm 0.13 mV | 0.67 mV | 0.26 \pm 0.08 mV | |
| | | median | 0.35 mV | 0.48 mV | 0.35 mV | | 0.32 mV | |
| | | range | 0.09 - 1.02 mV | 0.08 - 2.76 mV | 0.07 - 3.33 mV | 0.15 - 1.19 mV | 0.10 - 0.35 mV | |
| | L4 | P (found/tested) | 0.96% (2/208) | 2.4% (4/170) | 24.3% (254/1046) | 0.7% (2/275) | 0.7% (1/137) | 0% (0/94) |
| | | mean \pm sem | 0.31 mV | 0.36 \pm 0.09 mV | 0.95 \pm 0.08 mV | 0.48 mV | 0.17 mV | |
| | | median | | 0.31 mV | 0.52 mV | | | |
| | | range | 0.18 - 0.45 mV | 0.22 - 0.61 mV | 0.06 - 7.79 mV | 0.22 - 0.74 mV | | |
| | L5A | P (found/tested) | 9.5% (20/211) | 5.7% (5/87) | 11.6% (32/276) | 19.1% (178/934) | 1.7% (3/174) | 0.6% (1/160) |
| | | mean \pm sem | 0.55 \pm 0.10 mV | 0.93 \pm 0.26 mV | 0.54 \pm 0.09 mV | 0.66 \pm 0.06 mV | 0.24 \pm 0.09 mV | 0.08 mV |
| | | median | 0.40 mV | 1.09 mV | 0.38 mV | 0.37 mV | 0.19 mV | |
| | | range | 0.08 - 2.03 mV | 0.08 - 1.54 mV | 0.06 - 1.98 mV | 0.05 - 5.24 mV | 0.11 - 0.41 mV | |
| | L5B | P (found/tested) | 8.3% (9/108) | 12.2% (20/164) | 8.1% (11/136) | 8.0% (14/175) | 7.2% (40/555) | 2% (2/100) |
| | | mean \pm sem | 0.22 \pm 0.04 mV | 1.01 \pm 0.24 mV | 0.88 \pm 0.25 mV | 0.88 \pm 0.36 mV | 0.71 \pm 0.19 mV | 0.30 mV |
| median | | 0.20 mV | 0.51 mV | 0.44 mV | 0.60 mV | 0.29 mV | | |
| range | | 0.09 - 0.47 mV | 0.06 - 4.05 mV | 0.07 - 2.61 mV | 0.13 - 5.45 mV | 0.08 - 7.16 mV | 0.12 - 0.48 mV | |
| L6 | P (found/tested) | 0% (0/50) | 0% (0/61) | 3.2% (3/93) | 3.2% (5/158) | 7.0% (7/100) | 2.8% (15/532) | |
| | mean \pm sem | | | 2.27 \pm 1.72 mV | 0.28 \pm 0.09 mV | 0.49 \pm 0.16 mV | 0.53 \pm 0.19 mV | |
| | median | | | 0.96 mV | 0.27 mV | 0.43 mV | 0.26 mV | |
| | range | | | 0.17 - 5.67 mV | 0.06 - 0.58 mV | 0.14 - 1.36 mV | 0.09 - 3.00 mV | |

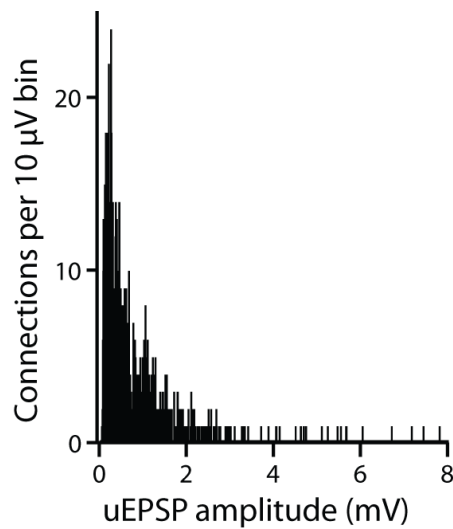


Figure 2.1: **Distribution of synaptic strengths**

The number of connections having a given synaptic strength is plotted against the measured unitary excitatory postsynaptic potential (uEPSP) amplitude for all experiments and layers combined. (Modified from Lefort et al., 2009)

2.1.2 Single Cell Data

To model single cells in the simulation, the leaky integrate-and-fire model was used (see Chapter 1.1.5 and Gerstner and Brette, 2009). The important parameters for this neuron model are the resting membrane potential (Resting V_m), the input resistance (R_{in}), the membrane time constant (τ) and the action potential threshold (AP threshold). Since the neurons are recorded intracellularly in the experiments, it is possible to extract these parameters from the single cells in the same experiments as the connectivity measurements.

The resting membrane potential is measured by averaging the membrane potential over 5 ms prior to any stimulation. The input resistance, membrane time constant and action potential threshold are extracted from step current injections (Lefort et al., 2009). All parameters are measured for each cortical layer independently (see Table 2.2).

Table 2.2: **Intrinsic electrophysiological properties of excitatory neurons in the mouse C2 barrel column**

Shown are the average resting membrane potential (Resting V_m), input resistance (R_{in}), membrane timeconstant (Tau), action potential threshold and amplitude (AP threshold, AP amplitude) and the rheobase for all layers. All values are mean \pm s.e.m. (from Lefort et al., 2009)

| | Layer 2 | Layer 3 | Layer 4 | Layer 5A | Layer 5B | Layer 6 |
|--|-----------------|-----------------|-----------------|-----------------|-----------------|-----------------|
| Resting V_m (mV) | -72.0 ± 0.3 | -71.4 ± 0.4 | -66.0 ± 0.3 | -62.8 ± 0.2 | -63.0 ± 0.3 | -66.8 ± 0.4 |
| R_{in} (M Ω) | 188 ± 3 | 193 ± 5 | 302 ± 4 | 210 ± 3 | 162 ± 5 | 277 ± 4 |
| Tau (ms) | 28.3 ± 0.3 | 30.0 ± 0.6 | 34.8 ± 0.5 | 37.6 ± 0.6 | 25.8 ± 0.7 | 28.2 ± 0.5 |
| AP threshold (mV) | -38.3 ± 0.2 | -38.7 ± 0.2 | -39.7 ± 0.2 | -38.9 ± 0.2 | -41.1 ± 0.2 | -40.2 ± 0.3 |
| AP amplitude - from threshold to peak (mV) | 72.4 ± 0.4 | 73.5 ± 0.5 | 70.9 ± 0.4 | 70.2 ± 0.5 | 73.1 ± 0.5 | 69.9 ± 0.5 |
| Rheobase (pA) | 126 ± 3 | 132 ± 4 | 56 ± 1 | 68 ± 2 | 98 ± 3 | 76 ± 3 |

2.2 Network Model

The networks I studied here were standard random sparse networks as described in Chapter 1.1. To make the networks more related to biology, the experimental results described above were used to constrain the model networks.

The networks studied in this chapter consist of six different layers as measured in Lefort et al., 2009. Each layer was represented as a single population of homogeneous neurons sharing the same parameters (Table 2.2). The connections between layers were modeled according to the experimental results (Table 2.1). Thus, almost all layers were connected to each other with different connection probabilities and weight distributions. Beyond the connection probability, the type of weight distribution was only weakly constrained by the experimental data.

2.2.1 Weight Distributions

As described in Chapter 1.1.6, theoretical models use a variety of weight distributions. Here, I investigated three different weight distributions. First, only a single weight per connection was used, second a lognormal fit of the experimental data and third the same lognormal distribution as before, but in which the connections with small weights were pruned.

In this section, I describe each distribution individually and explain how it was fitted to the available data and how close the similarity of each distribution was to the experimental observations.

Fixed Single Weight

The simplest weight distribution is to only assign to all connections between two given layers the same weight. This type of weight distribution is used widely in previous theoretical models (see Chapter 1.1).

Here, for each pair of layers, the mean evoked amplitude measured in the experiments was used as the synaptic weight for all connections between these two layers (Table 2.1). Thus, single neurons in one layer evoked the same postsynaptic response in all connected cells in another layer.

This distribution by definition showed an accurate mean connection strength when compared to the experimental observations. However, since only a single value was used per pair of layers, the variance and the shape of the experimentally observed distributions were not captured.

Lognormal Weight Distribution

Another approach was to consider a lognormal distribution as an approximation of the experimental findings. A distribution of a variable x is lognormal if the logarithm of x is distributed normally. The parameters of a lognormal distribution are μ and σ , the mean and the standard

deviation of the normal distribution underlying the lognormal distribution. A particular feature of lognormal distributions is that these show an increased skewness in comparison to normal distributions. This skewness is determined by the parameter σ . For σ close to zero, the distribution is not skewed, while for increased σ the skewness increases.

The lognormal distribution of synaptic weights w can be written as:

$$f(w) = \frac{1}{w\sigma\sqrt{2\pi}} e^{-\frac{(\ln w - \mu)^2}{2\sigma^2}} \quad (2.1)$$

To fit the lognormal distribution to the experimental data, I used the maximum likelihood estimators for the parameters μ and σ . These were then calculated for each connection between two layers as follows:

$$\mu = \frac{1}{N} \sum_{i=1}^N \ln(x_i) \quad (2.2)$$

$$\sigma^2 = \frac{1}{N} \sum_{i=1}^N [\ln(x_i) - \mu]^2 \quad (2.3)$$

with x_i being the measured amplitudes for connections between two layers and N the number of experimental measurements.

The lognormal weight distribution captured the experimental data well. One particular feature of the lognormal fit was that it matched the high skewness of the biological distribution of synaptic strengths. The mean amplitude also was the same as measured in the experiments.

Lognormal Weight Distribution with Cutoff - 'Big connections'

The third weight distribution used was the so-called 'big connections' network. This network used the same weight distribution as the lognormal network, but after network construction, all connections that were smaller than 0.5 mV were cut.

This procedure destroyed approximately 50% of the network connections. Thus, this network does not fit the connectivity observations. Neither the mean nor the variance of the weight distributions found in experiments were reproduced.

Although not biologically plausible, using such a network allowed to investigate the role of the rare strong connections. If the network stimulation explained in the next part evoked similar responses than those found in the lognormal network, it would indicate that the strong connections are the relevant ones despite the fact that they are sparse.

2.2.2 Network Stimulation

In order to compare the network excitability, a synchronous spike in a single layer was used as a stimulus. The spike was evoked synchronously in a random subgroup of the specific layer. Figure 2.2 shows the network behaviour in response to this stimulus when using a lognormal weight distribution.

The peak EPSP amplitudes for each cell in the simulation after stimulating either one neuron (top row) or ten neurons (bottom row) evoke qualitatively similar network responses (Figure 2.2). In either cases, the network response reflects the underlying connectivity matrix of Table 2.1. For each stimulated layer (columns), the peak membrane potential following the stimulation is plotted. The figure illustrates the connections between different layers. For layers 2 and 3 the activity pattern was similar in that both activate layers 2, 3, 5a and 5b and to a lesser degree also layer 4, but the specific amount of activation was different. Layer 5b was strongly activated by layer 3 but only weakly activated by layer 2, although the overall number of activated cells was similar. Layer 6 was rather special because it had very few connections to other layers, only layers 5b and 6 were activated by it. The input to layer 6 came mostly from layers 4 and 5b. The connection from layer 4 to layer 6 was very sparse (3%) but each single weight was very strong (mean amplitude 2.27 mV) which is visible in Figure 2.2 bottom row, L4 column.

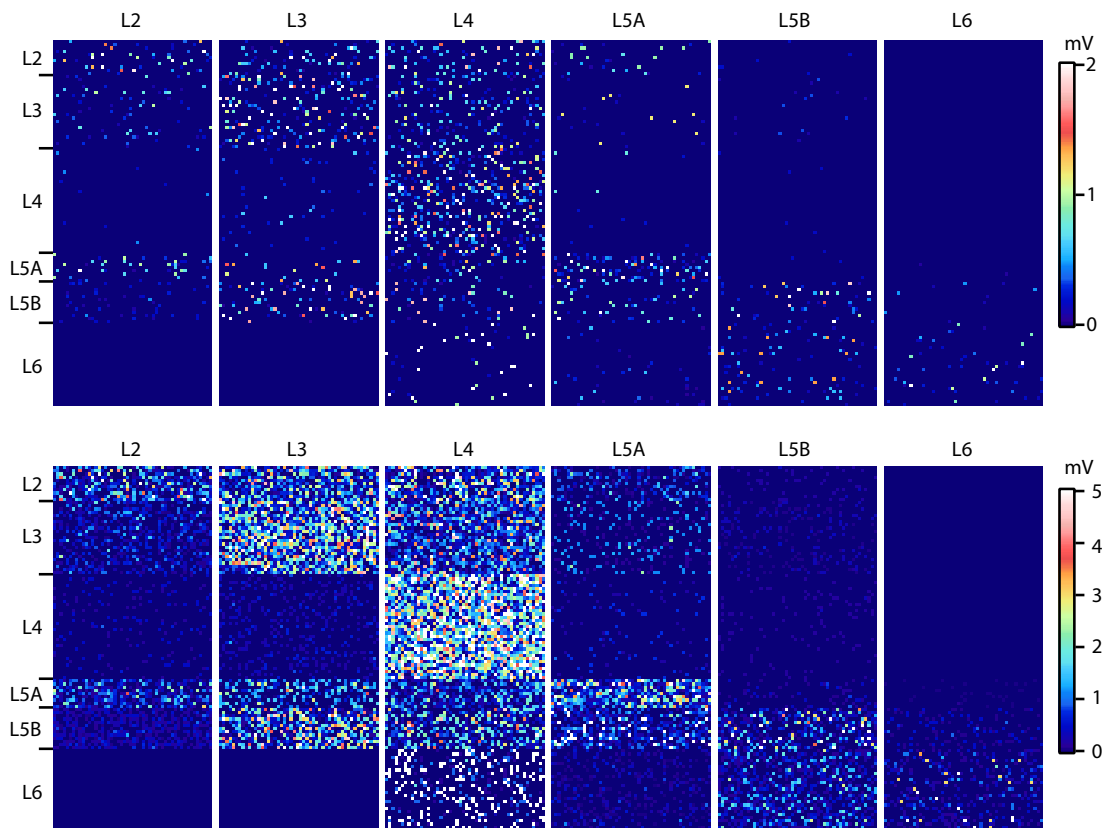


Figure 2.2: Network responses for a layered network

Shown are response amplitudes following a stimulus of one (*top*) or ten (*bottom*) neurons in a specific layer (noted above each column). Colour coded is the amplitude of the evoked response in the postsynaptic cells in mV. The network used had a lognormal weight distributions (Modified from Lefort et al., 2009)

2.2.3 Threshold for Further Excitation

To quantify the excitability of the networks in a reliable way, the threshold of further spiking was introduced. This threshold was the number of neurons that needed to be stimulated in one layer in order to evoke at least one spike in at least one non stimulated neuron. As can be seen from Figure 2.2, the activity pattern following stimulation in a single layer is different for each layer. Thus, the threshold is computed for each layer separately.

The threshold for further excitation constituted the minimal requirements to propagate infor-

mation in the network. If less neurons were activated than found by the threshold, no further spikes were evoked and no information could be propagated.

To investigate the differences in threshold between the lognormal weight distribution and the other weight distributions, the threshold ratio was employed. This was the threshold computed in the tested network divided by the threshold for the lognormal network.

2.3 Results

In this section, I investigate how different weight distributions affect the network excitability. The network excitability is quantified for every layer by the threshold of further excitation for different weight distributions. I then focus on the question how and why the resulting threshold differences measured are layer specific. Finally, the role of the connectivity parameters in explaining the threshold differences is described.

2.3.1 Impact of Different Weight Distributions Network Excitability

This part describes the excitability of the lognormal network first. Then the excitability of fixed single weight and 'big connection' networks are compared to the excitability of the lognormal distribution. This is done by computing the threshold ratios for each layer.

Lognormal Weight Distribution

Figure 2.3 shows the thresholds of further excitation for the lognormal network. Here, layer 4 showed further spikes with only 30 ± 6 neurons stimulated. This was the smallest number of stimulated cells needed in the whole network. Layers 3 and 5a showed also relatively low numbers for the threshold (L3 61 ± 9 , L5a 60 ± 15). The other layers needed considerable more stimulation to evoke further spiking (L2 238 ± 60 , L5b 276 ± 118) with layer 6 being very hard to excite. Almost 50% of the whole layer needed to be stimulated in order to evoke further spikes (L6 568 ± 310 with a size of 1154 for the layer 6 population).

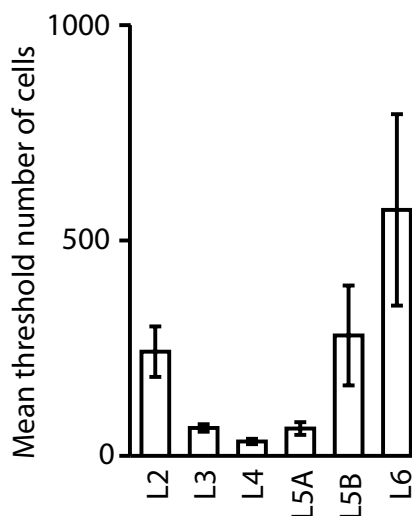


Figure 2.3: **Threshold for further excitation**

Plotted is the minimal number of neurons needed to stimulate in a specific layer in order to evoke one further spike in the whole network. Values are mean \pm std (Modified from Lefort et al., 2009)

To compare the impacts of different weight distributions, I determined the thresholds of further excitation for the other distributions and computed the ratios of the results of these networks and the results of the lognormal network. This ratio was one if the threshold was the same in both networks, while larger values indicated a higher threshold in the tested network than in the lognormal network. Figure 2.4 shows the resulting threshold ratios for all networks and layers. The specific results for each weight distributions are described individually in the next parts.

Fixed Single Weight

In Figure 2.4, the green bars indicate the threshold ratio for the fixed weight network to the lognormal network. It can be seen that this change in weight distribution induced a strong change in network excitability.

In this architecture, layer 4 had to be stimulated in 60 ± 4 neurons to evoke further spikes. This was double the amount of stimulation needed than in the lognormal network. Simi-

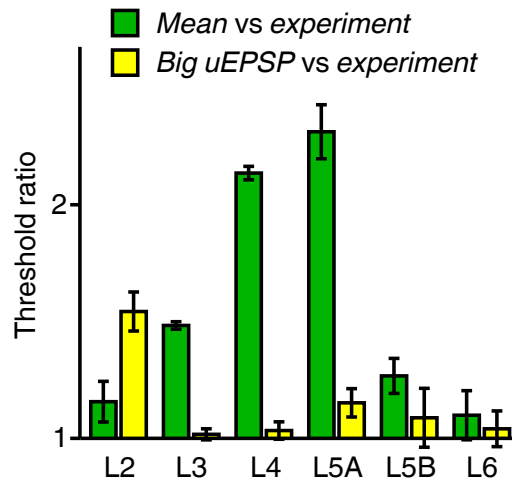


Figure 2.4: **Comparison of different global weight distributions**

Plotted is the ratio of stimulated neurons needed to evoke one further spike in the network using only the mean per connection as synaptic weights (labelled 'mean', ratio shown in green) or the network with full weight distributions but with all connections smaller than 0.5 mV cut after network setup (labelled 'Big uEPSP', ratio shown in yellow) and the network with full weight distributions (labelled 'experiment'). (Modified from Lefort et al., 2009)

larly, layer 5b also needed double the stimulation size to evoke further spikes (L5a 139 ± 36). The other layers also were all less excitable in the mean network than in the lognormal network although with lower ratios ranging from 1.1 to 1.5 (Thresholds: L2 276 ± 108 , L3 91 ± 5 , L5b 350 ± 108 , L6 623 ± 310).

The results indicated that although the mean input per neuron was equivalent in the lognormal and mean architecture the lognormal network was easier to excite. This might have been due to the lack of sparse strong connections in the fixed weight network.

Lognormal Weight Distribution with Cutoff - 'Big connections'

The big connection network showed only small differences from the lognormal fits. This can be seen from the results depicted as yellow bars in Figure 2.4.

Layer 4 had to be stimulated in 31 ± 6 neurons to evoke further spiking which was the same amount of excitation than in the lognormal network. This indicated that indeed the con-

vergence of the sparse very strong connections drove the threshold for further excitation in random networks. Even in a network that had only half of the original connections, the threshold was not significantly different. The other layers also showed very little increase in excitability with ratios close to one (thresholds: L3 62 ± 9 , L5a 69 ± 19 , L5b 300 ± 181 , L6 590 ± 225). The only difference visible was in layer 2, where indeed the small connections may have had a higher impact than in other layers. Here the ratio was 1.54 with the threshold being 368 ± 104 .

2.3.2 Layer Specific Differences

It is important to note that the connections that directly drove the threshold for further excitation were predominantly the recurrent connections inside each layer. The reason for this was, that the recurrent connection provided the strongest output for a stimulation in any given layer (compare Table 2.1). Thus, the non-stimulated neurons in the stimulated layer were most likely to spike in response to the stimulation and thus defined the threshold of further excitation.

To understand why some layers were more affected by changes in the weight distribution than others, it was crucial to see what the threshold of further spikes was measuring. It measured only the fact that enough activation was present in the network to evoke further spikes. There were multiple scenarios which could explain the sufficient amount of activation that evoked the spike.

One possibility was that a few very strong connections were converging. Layer 4 was an example of this. Here the experimentally measured weight distribution for the recurrent connections showed a heavy tail. This was indicated by the high difference in mean and median for the recurrent layer 4 to layer 4 connection and the wide range of synaptic weights shown in Table 2.1. Since the 'big connection' network showed no difference to the lognormal network, these strong connections were sufficient to drive the activation. The mean network, in which the few strong connections were missing, needed to be stimulated a lot stronger which also indicated that the sparse strong connections were most important in evoking

spikes in layer 4.

One other possibility was, that enough small connections converged. This was most likely the case in layer 2. Here the ratio for the 'big connection' network was higher than for the mean network. This indicated that the small connections (< 0.5 mV) that were cut in the 'big connection' network played a substantial role in the excitability of layer 2.

For the other layers, the determining factors for the differences in threshold were more complex. Layer 5a recurrent connections showed a more skewed distribution and higher connection probability than layer 2 recurrent connections, although the mean strength was comparable. In comparison to the behaviour of layer 2, here there were still enough large connections to dominate the threshold of further spikes.

For layer 5b the principle was the same as for layer 5a but the connection probability was lower and thus large connections were not as dominant. Since the connection probability was low, the overall number of strong connections was low. Consequently, convergent input of strong connections had a low probability and their impact was reduced.

Layer 3 was very similar to layer 2, but had a higher mean connection strength and connection probability. Due to the high connection strength, less connections were cut in the 'Big connection' network. Thus, layer 3 was less affected by the cutoff. In comparison to layer 2, the recurrent connection here showed a slightly stronger tail and thus the effect of using only the mean synaptic strength was higher.

Layer 6 connections were very sparse so that in any case about 50% of layer 6 neurons needed to be stimulated to evoke further spikes. This number was sufficient almost regardless of network setup.

2.4 Summary

In conclusion it was shown here that the global distribution of synaptic weights does play a significant role in the network dynamics. The big connection network and the full network

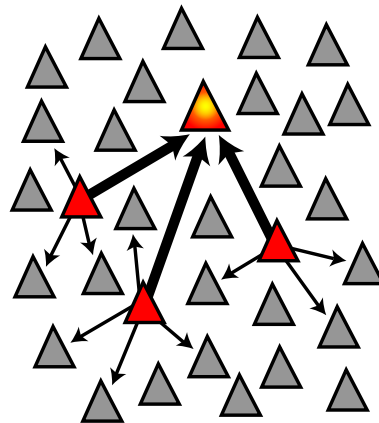


Figure 2.5: **Schematic of possible network interactions**

The convergence of few large-amplitude synaptic connections might dominate network activity. (Modified from Lefort et al., 2009)

differed only very little in their stimulation threshold which indicated that the propagation of excitation in the network was mediated by very sparse strong connections. This can be seen prominently in the excitability of layer 4. The assumption of a single connection strength for a network model was shown to have a strong impact on network excitability. Networks with only the mean connection strength were less excitable and thus might not represent the biological networks accurately.

A hypothesis arising from these findings would be that the convergence of very few of these large connections could dominate network activity. Figure 2.5 illustrates the most probable network architecture responsible for propagation of activity in the network simulations. Few stimulated neurons (red) activate a post-synaptic neuron (orange) via sparse converging strong connections.

These findings indicated that there might be features, in this case convergences of large multiple connections, that influenced network behaviour but were not specifically modeled in the uniform random framework. In the further chapters I show how networks can be adjusted to incorporate non-random structures in network architectures.

3 Modifying Local Connectivity

Experimental data indicate that biological neuronal networks exhibit complex connectivity features. Uniform random networks as widely used in theoretical studies cannot reproduce these complex features. This chapter focusses on the introduction of structure into random network models.

To this end I introduced a measure that quantified the network similarity to experimental findings. This measure was then used to determine important network parameters and to optimise network structure. Structural changes in the network were induced by changing the degree distributions.

In the first part of the chapter the experimental results to which the constructed networks are compared are described. The specific network model is introduced and a method for structural changes is explained. To quantify network similarity, a measure is introduced and parameter significance is discussed. These are used to investigate the space of possible networks and to optimise network structure. The results show that the needed structure is highly connection specific and especially the recurrent excitatory connections must be highly structured to reproduce the biological findings.

3.1 Experimental Basis

The data used to construct random networks relies mostly on recordings of relatively small groups of neurons (2-6 neurons at the same time). Thus, only pairwise statistics can be robustly extracted (Markram et al., 1997; Holmgren et al., 2003; Feldmeyer et al., 2006; Helmstaedter et al., 2008; Lefort et al., 2009).

Some publications however, make an effort to characterise connectivity on a more complex level (Yoshimura et al., 2005; Yoshimura and Callaway, 2005; Song et al., 2005; Fino and Yuste, 2011; Bock et al., 2011; Perin et al., 2011; Packer and Yuste, 2011). The overall conclusion is that connectivity was not purely random, but that there are cell-type specific differences in connectivity and that connectivity is not uniform throughout a single population.

3.1.1 Probabilities of Shared Input

I made use of one particular type of experiment to evaluate different model networks (Yoshimura and Callaway, 2005; Yoshimura et al., 2005, see also Chapter 1.2.3). These experiments use glutamate uncaging to scan for synaptic inputs of simultaneously recorded cells.

To this end a brain slice is bathed in a caged (inactivated) glutamate compound. Using a laser beam the compound can very locally be uncaged (activated) and thus it is possible to stimulate single neurons. The whole slice is stimulated systematically at various positions aligned on a grid and for each position the evoked responses of the two patched cells are recorded.

This information is then used to infer the probabilities of receiving input from the same stimulus location conditioned on the connectivity between the two patched cells. These experiments are done for pairs of excitatory neurons (Yoshimura and Callaway, 2005) and for excitatory and fast-spiking neurons as well as for excitatory neurons and adapting interneurons (Yoshimura et al., 2005).

The results show that connected pairs of excitatory neurons share more input than uncon-

nected pairs ($20.1 \pm 2.7\%$ for connected versus $3.8 \pm 1.1\%$ for unconnected pairs). Pairs of fast-spiking and excitatory neurons only show an increase in shared input for bidirectionally connected pairs ($17 \pm 2\%$ for bidirectionally connected pairs, $5 \pm 1\%$ for unconnected pairs and $1 \pm 3\%$ for pairs with one-way connections), while pairs of adapting interneurons and excitatory neurons show no dependency on connectivity.

These measurements can not be reproduced by a uniform random network since the connections are independent of each other. To be able to reproduce the experiments it is necessary to introduce local changes into the connectivity of the model network.

3.2 Network Model

Due to the need for detailed experimental data on the connectivity of excitatory and inhibitory populations, I chose to focus the modeling on only a small part of the whole 6 layered network explained in the previous chapter. Because the layer 2/3 was best constrained by the experimental data, the network was constructed to mirror only the layer 2/3 network of mouse barrel cortex.

3.2.1 Network Populations

Instead of using only excitatory populations like in the previous chapter, three distinct populations of excitatory and inhibitory neurons were used. One population consisted of only excitatory neurons and the two other populations consisted of inhibitory fast-spiking and inhibitory non-fast-spiking neurons. The excitatory population comprised 1691 neurons, the fast-spiking 97 neurons and the non-fast-spiking population 133 neurons. All population sizes were taken from experimental data (Lefort et al., 2009; Gentet et al., 2010).

The two inhibitory types were chosen because the distinction between them is relatively clear (Avermann et al., 2011; Helmstaedter et al., 2009; Thomson and Lamy, 2007). Fast-spiking interneurons in this definition were parvalbumin positive and were electrophysiologically identifiable by a shorter action potential half-width (Avermann et al., 2011). The adapting

Chapter 3. Modifying Local Connectivity

interneurons measured in Yoshimura et al., 2005 are a subclass of the non-fast-spiking interneurons.

Both types, the fast-spiking and the non-fast-spiking interneurons, can in principle be further subdivided into multiple subclasses (Thomson and Lamy, 2007; Helmstaedter et al., 2008). However, since connectivity data on all subclasses is very sparse, I concentrated on only two interneuron classes.

3.2.2 Connectivity

The connection probability between all populations was directly taken from experimental data (Table 3.1, Lefort et al., 2009; Avermann et al., 2011). Since the analysis took into account only the presence or absence of connections, no statement could be made about weight distributions.

The general setup of the connections differed from the standard random sparse paradigm described in Chapter 1.1.1. Instead of constructing the connections in a uniform random way, I introduced structure in the connectivity. The method used to introduce structure is explained in the next section.

3.3 Changing Network Structure

To modify the structure of the network, the in- and out-degree distributions were varied independently. The in-degree was the number of connections a neuron receives and the out-degree was the number of connections a neuron sends.

In a uniform random network, all neurons are equally probable to be a pre- or postsynaptic neuron thus the distribution of in- and out-degrees had a low variance. In the following part, a method used for changing degree distributions is described.

Table 3.1: **Synaptic connectivity and uEPSP amplitudes in layer 2/3 of the mouse C2 barrel cortex**

P denotes the probability of a connection from the pre- to the postsynaptic layer (L) for all three populations (excitatory (EXC), inhibitory fast-spiking (FS) and inhibitory non-fast-spiking (NFS)). Mean, median and range are describing the characteristics of the evoked postsynaptic response for this connection. Inhibitory amplitudes were always measured with the postsynaptic neuron depolarised to -55 mV. (from Avermann et al., 2011)

| Presynaptic | | EXC | FS | NFS |
|--------------|------------------|--------------------|---------------------|---------------------|
| Postsynaptic | | | | |
| EXC | P (found/tested) | 16.8% (16/95) | 60.0% (21/35) | 46.5% (20/43) |
| | mean \pm SEM | 0.37 \pm 0.10 mV | -0.52 \pm 0.11 mV | -0.49 \pm 0.11 mV |
| | median | 0.20 mV | -0.29 mV | -0.30 mV |
| | range | 0.06 to 1.42 mV | -0.10 to -2.00 mV | -0.10 to -2.00 mV |
| FS | P (found/tested) | 57.5% (23/40) | 55.0% (11/20) | 37.9% (11/29) |
| | mean \pm SEM | 0.82 \pm 0.10 mV | -0.56 \pm 0.14 mV | -0.37 \pm 0.10 mV |
| | median | 0.68 mV | -0.44 mV | -0.23 mV |
| | range | 0.16 to 1.94 mV | -0.07 to 1.46 mV | -0.12 to -0.99 mV |
| NFS | P (found/tested) | 24.4% (11/45) | 24.1% (7/29) | 38.1% (8/21) |
| | mean \pm SEM | 0.39 \pm 0.11 mV | -0.83 \pm 0.25 mV | -0.49 \pm 0.20 mV |
| | median | 0.19 mV | -0.60 mV | -0.15 mV |
| | range | 0.12 to 1.21 mV | -0.09 to 1.85 mV | -0.07 to -1.47 mV |

3.3.1 Modifying Degree Distributions

A change in the degree distribution was achieved by manipulating the connection drawing paradigm. For each connection, a pre- and a postsynaptic neuron was drawn. In the standard case, the probability for each neuron to be a pre- or postsynaptic neuron was equal, the distribution of neurons was uniform.

Here, instead of drawing neurons from a uniform distribution, I used an exponential distribution to determine the pre- and postsynaptic partners. The resulting degree distributions were then different because some neurons were more probable to be a pre- or postsynaptic neuron and thus form more connections.

Chapter 3. Modifying Local Connectivity

Exponential distributions offered a high variance and a single parameter, the rate λ , to tune. This made it easier to investigate the effects of this change on the network structure since the number of free parameters was limited.

The index of a pre- or postsynaptic neuron i was drawn according to this distribution:

$$f_{pre/post}(i) = \lambda_{pre/post} e^{-\lambda_{pre/post} i} \quad (3.1)$$

$$\lambda_{pre} = \frac{d_{out}}{n_{pre}} \quad (3.2)$$

$$\lambda_{post} = \frac{d_{in}}{n_{post}} \quad (3.3)$$

with n_{pre} and n_{post} being the sizes of the pre- and postsynaptic neuronal populations and d_{out} and d_{in} being the parameter used to characterise the skewness of the distribution for the out-degree or in-degree.

The characterising parameters d_{in} and d_{out} were either 0 or 5. For a value of 0, a uniform distribution was used since the exponential distribution would have an undefined λ . For a value of 5 the distribution was highly skewed with some neurons connecting to all possible partners.

Due to the general construction of the network explained in Chapter 1.1.1 higher values for d_{out} (or d_{in}) were impractical because highly probable neurons would occur more often and thus increase probability of finding the same connection twice. This would increase the amount of redrawing and thus make the algorithm very slow to converge.

The effect on the degree distribution is shown in Figure 3.1. The basis was the uniform random network (top) with a low variance (histogram left, black bars) in the degree distribution. From there I varied the in- or out-degree distributions (in-degree bottom left, out-degree bottom right) to be highly skewed (histogram left, grey bars).

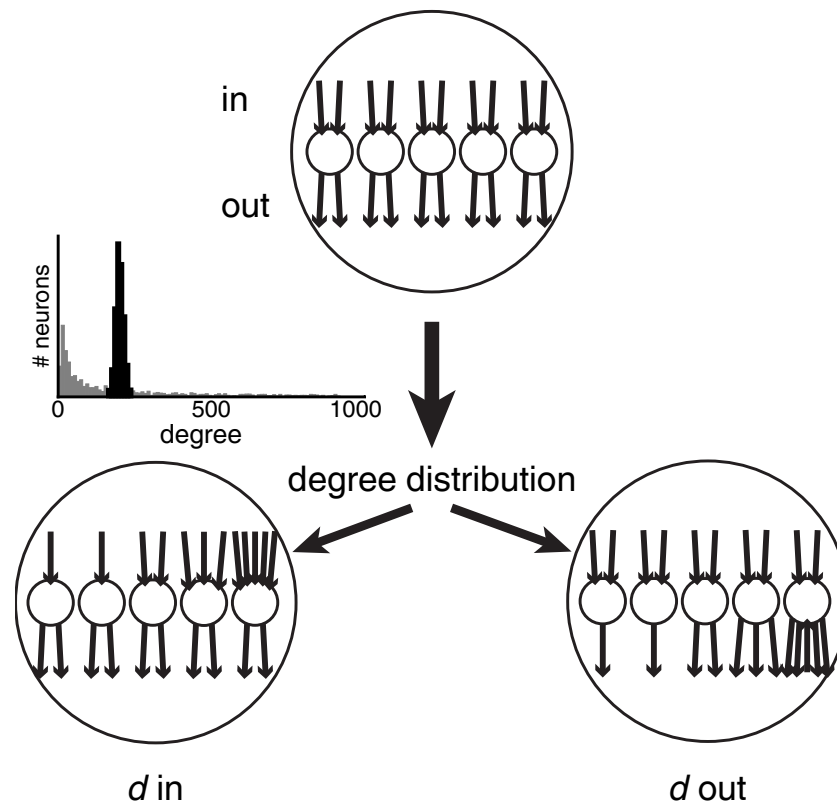


Figure 3.1: **Diagram of the idea of changing degree distributions**

Using a uniform random network as the starting point (*top*) effects of changing the degree distribution in the output and input are shown (*bottom*). *Left*: Histogram showing the degree distribution for the uniform network in black and for imposed weight correlations in grey ($d = 5$).

3.3.2 Quantification of Network Similarity

The similarity of the constructed networks to biological networks was quantified by calculating the same probabilities as reported in Yoshimura and Callaway, 2005 and Yoshimura et al., 2005 and computing the summed square error between model and experiment. This gave a single value which described the similarity between the model and the biological measurements. A low summed square error indicated a similar network, while networks that are far from the biological observations would have a high summed square error.

The error was calculated for all pairings of neuron types (excitatory/excitatory, excitatory/fast-spiking interneuron, excitatory/adapting interneuron) and for all reported probabilities of

Chapter 3. Modifying Local Connectivity

sharing inputs given the connectivity of the neuron pair recorded from (unidirectional P_1 and P_2 , bidirectional P_3 and not connected P_4). These probabilities are extracted from the whole network and thus show only small variations for multiple realisations of the same network.

$$\text{summed square error} = \sum_{A,B \in \text{pairings}} \sum_i (P_{i,\text{experiment}} - P_{i,\text{model}})^2 \quad (3.4)$$

with P_i :

$$P_1 = P(\text{shared input} | A \rightarrow B)$$

$$P_2 = P(\text{shared input} | A \leftarrow B)$$

$$P_3 = P(\text{shared input} | A \leftrightarrow B)$$

$$P_4 = P(\text{shared input} | A \not\leftrightarrow B)$$

3.3.3 Parameter Significance

I calculated the significance of changing a single parameter in the parameter space with the Student's t-test. Using an iterative approach, I computed the significance level on the whole parameter space first, then fixing the significant parameters and repeating the procedure until no further parameters were significant.

This was necessary because the significance of changing a single parameter may have been different depending on the area which was taken into account. Significance levels were denoted as $p < 0.05(*)$, $p < 0.01(**)$ and $p < 0.001(***)$

3.4 Results

Since no pairs of inhibitory neurons are tested in Yoshimura and Callaway, 2005 and Yoshimura et al., 2005, the connectivity between inhibitory populations could not be taken into account in the fitting. Only connections involving the excitatory population were used, leading to

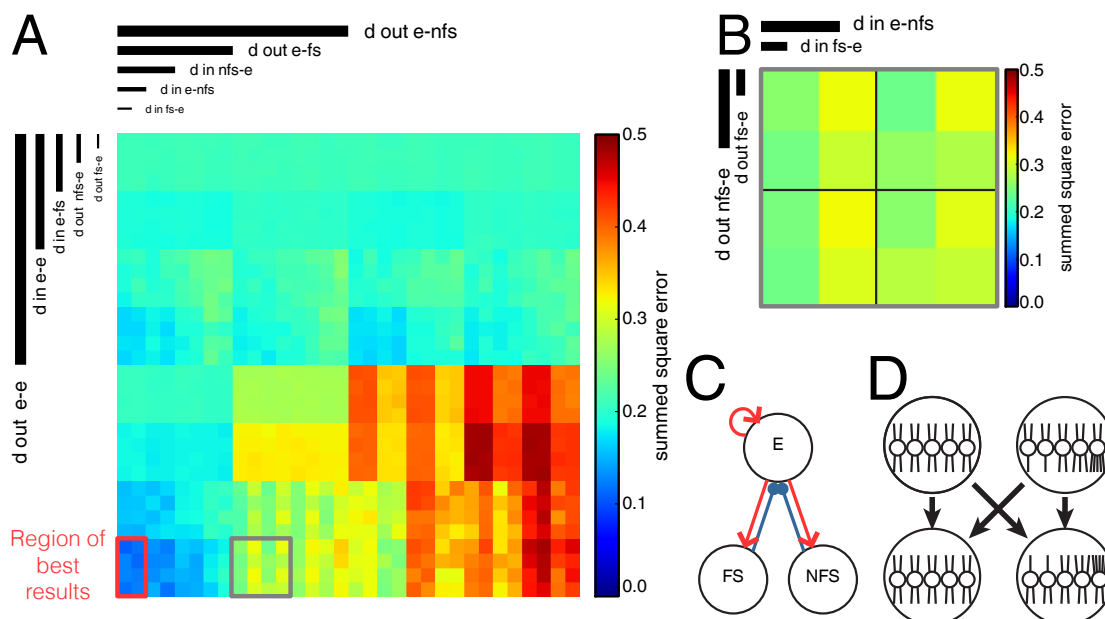


Figure 3.2: **Dimensional stacking for the parameter space spanned by varying the structural parameters**

A Dimensional reordering of the parameter space created by varying the structural parameters affecting the similarity to observed connectivity patterns. Colour indicates the summed square error of the observed probabilities in biology and in the model. The red outline shows the region of best results. *B* Closer zoom into the four dimensional region indicated in *A*. Each pixel represents one parameterset. The quadrants delineated by the thin black lines are the parameter space spanned by d_{in} e-nfs and d_{out} nfs-e, while the four pixels inside each quadrant are the parameter space spanned by d_{in} fs-e and d_{out} fs-e. *C* Diagram of the network connections affected by the fitting for all populations (excitatory (E), fast-spiking (FS) and non-fast-spiking (NFS)). *D* Diagram of the changes of network connections that were used in the fitting. Significant parameters: d_{out} e-e(***) , d_{out} e-fs(***) , d_{out} e-nfs(***) , d_{in} e-e(***) , d_{in} e-fs(***) , d_{in} e-nfs(**) , d_{in} nfs-e(***) . Significance levels using Student's t-test: $p < 0.05$ (*) , $p < 0.01$ (**) and $p < 0.001$ (***).

ten parameters tested. Two parameters (d_{in} and d_{out}) for each connection: excitatory to excitatory (e-e), excitatory to fast-spiking (e-fs), fast-spiking to excitatory (fs-e), excitatory to non-fast-spiking (e-nfs), non-fast-spiking to excitatory (nfs-e).

3.4.1 Significant Parameters

Figure 3.2 shows the setup and results for the structural fitting. In Figure 3.2 C, the connections that were used in the fitting are depicted. Since five connections were tested and the in- and

Chapter 3. Modifying Local Connectivity

the out-degree were varied, ten parameters were used as described above.

Figure 3.2 D shows what alterations were made to these connections. Each connection was tested in four configurations. The out-degree of the presynaptic population could be unchanged or altered with the method described above, and the same was true for the in-degree of the postsynaptic population. This led to 4^5 or 1024 networks tested.

To visualise the similarity of all networks in an intuitive way, the Clutter Based Dimensional Reordering described in Chapter 1.4 was used. This technique nested all dimensions of the parameter space into a single two dimensional image. The ten parameters used here are depicted in the dimensional stacking in Figure 3.2 A. Here all parameters were scanned and for each network the colour indicates the summed square error as a measure of dissimilarity. Blue indicates a low error and thus a high similarity and red indicates a high error and low similarity.

The standard uniform random network was in the top left corner and showed a summed square error of 0.21.

It can be seen that the outgoing connections of the excitatory population had a strong influence on the similarity to experimental results. The specific configuration of parameters, however, was different for each target population.

For the connections from excitatory to excitatory neurons (e-e), both a high variance in the in- and in the out-degree was needed for a high similarity. This was affecting the parameters d_{in} e-e and d_{out} e-e. A strong difference can be seen from the top half of the image to the bottom half (change in d_{out} e-e). Inside one half, the difference between the top part and the bottom part was due to the difference in d_{in} e-e. Thus, the two parameters had a strong influence on the network similarity measure.

This was different for the excitatory to fast-spiking connection (e-fs). Here only the in-degree (d_{in} e-fs) was required to have a high variance. The out-degree (d_{out} e-fs) had to be unchanged.

In the connection to the non-fast-spiking neurons (e-nfs) the purely random network was

Table 3.2: **Constraining parameters on the structural fitting technique**

Parameters that had a significant effect on the measures are marked by the value that provided the better result. Tested but not significant parameters are marked with '-'. Untested parameters are left empty.

| | d | |
|---------|-----|-----|
| | in | out |
| e-e | 5 | 5 |
| e-fs | 5 | 0 |
| e-nfs | 0 | 0 |
| fs-e | - | - |
| fs-fs | | |
| fs-nfs | | |
| nfs-e | 0 | - |
| nfs-fs | | |
| nfs-nfs | | |

Table 3.3: **Shared input probabilities**

Probabilities of sharing input for the structurally adjusted network with all significant parameters (model) and the corresponding experimental findings. Shown are the probabilities for all tested pairings. Neurons were either unconnected (\emptyset), unidirectionally connected (\rightarrow , \leftarrow) or bidirectionally connected (\leftrightarrow). Experimental data from Yoshimura and Callaway, 2005 and Yoshimura et al., 2005.

| | | | \rightarrow | \leftarrow | \leftrightarrow |
|-------|------------|-------|---------------|--------------|-------------------|
| e-e | model | 0.078 | 0.173 | | |
| | experiment | 0.038 | 0.201 | | |
| e-fs | model | 0.027 | - | 0.076 | 0.151 |
| | experiment | 0.051 | - | 0.013 | 0.172 |
| e-nfs | model | 0.066 | 0.070 | 0.069 | 0.067 |
| | experiment | 0.04 | 0.03 | 0.05 | 0.05 |

fitting the data best. All changes to the structure in these connections would lead to an increased error.

The region constrained by the significant parameters found with this approach is marked in red in Figure 3.2 A. The significant parameters are summarised in Table 3.2. The network with all significant parameters fixed showed very similar probabilities of sharing input to those found in experiments (Table 3.3).

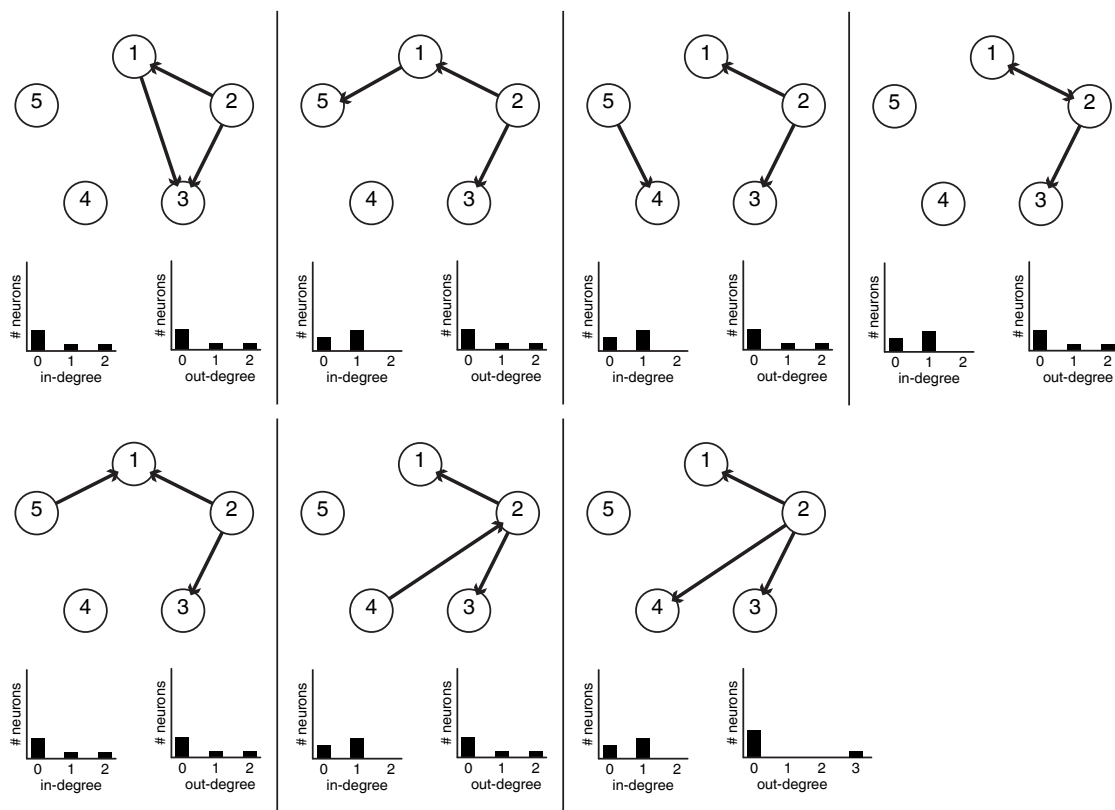


Figure 3.3: Shared input networks consisting of five neurons

All network configurations (except isomorphisms) are shown for a network of 5 neurons with 15% connection probability. For each configurations, the in- and out-degree distributions are depicted underneath the network diagrams.

3.4.2 Effects of Degree Distributions on Shared Input

The changes in the degree distributions were a complex manipulation of the network structure and it was not apparent why this change affected the probabilities of shared input. To elucidate this impact a simplified example network of five neurons with 15% connection probability was investigated.

Figure 3.3 shows all possible networks of five neurons with three connections (15% connection probability) in which shared input was present. Since labels of neurons could be reassigned without changing the network architecture, permutations were considered as equivalent. It was therefore arbitrarily decided that shared input was originating from cell 2, while cells 1 and 3 shared this input. The corresponding degree distributions for the networks are shown

underneath each network. From these distributions it is clear that for this simplified example, all networks that showed shared input also showed sparse high out-degree nodes. This is especially apparent in Figure 3.3, bottom right. Here three pairs of neurons show shared input and the degree distribution shows a higher variance as in the other networks and a sparse high out-degree node.

A second observation was that the only network that showed shared input to connected cells (top left in Figure 3.3) showed sparse high in- and outdegree nodes. This was only visible in one other network (bottom left in Figure 3.3). Thus, the occurrence of shared input given a connection between two neurons was only possible if high degree nodes are present both the in- and the outdegree case.

Thus, in this simple example the occurrence of shared input only occurred with skewed out-degree distributions. Skewed in- and out-degree distributions were necessary for shared input to connected cells to occur. This is the case for the recurrent excitatory connections.

When taking into account the connection from excitatory to fast-spiking neurons, this picture changes slightly. In the experimental findings, the probability of sharing input for pairs of excitatory and fast-spiking neurons was only increased for bidirectionally connected pairs. When staying with the previous example network, the probability for two (connected) excitatory cells to connect to a given fast-spiking cell is 0.3 (for a connection probability from excitatory to fast-spiking of 0.6 as observed in experiments). Since the probability for the fast-spiking neuron to connect to a specific excitatory neuron is also 0.6, the overall probability in this example of observing a shared input between bidirectionally connected cells is $0.3 * 0.6 = 0.18$. A highly skewed out-degree distribution for the excitatory to fast-spiking connection would lead to the same results, since the average probability of receiving a connection for a fast-spiking neuron would remain the same. When assuming an increased variance in the in-degree distribution of the excitatory to fast-spiking connection, there will be fast-spiking input hubs which have a high probability of getting input from two given excitatory neurons. In the extreme case of a fully connected fast-spiking neuron, the probability of a reciprocal shared input pattern is

then $1 * 0.6 = 0.6$, this results in an increase in the average probability of sharing input given a bidirectionally connected pair.

Thus, a high variance in the in-degree of the fast-spiking population would increase the occurrence of bidirectional shared input patterns, while a changed out-degree distribution would not increase the occurrence of such patterns.

3.4.3 Covariation Effects of Multiple Parameters

While the identification of the significant parameters was the most important result, it was no less interesting to investigate the impact of single parameters on the effect of all other parameters. d_{out} e-e for example was a parameter that affected the behaviour of almost all other parameters in the network.

When d_{out} e-e was zero, there was only little influence on the summed square error from all other parameters. Only when this parameter was changed, the other parameters gained more influence.

For example, the influence of d_{out} e-nfs was negligible in the case where d_{out} e-e was zero. But when d_{out} e-e was increased, a change in d_{out} e-nfs would drastically reduce the network similarity. This came from the fact that pairs of excitatory and non-fast-spiking neurons showed the same amount of shared input for all possible connections.

In the framework of an increased d_{out} e-e, some neurons had a very high probability of being the source of shared input, while in a random network there was no such preference. If there was a change in the connection from excitatory to non-fast-spiking neurons in the case of a random excitatory network, it did not affect the similarity to biological results because the excitatory network could not show a preference in the input. Only for a structured excitatory network the change in the excitatory to non-fast-spiking connection could have an effect since the chance of sharing input was substantially increased.

A similar effect could be observed for almost all other parameters. Thus, structure in the

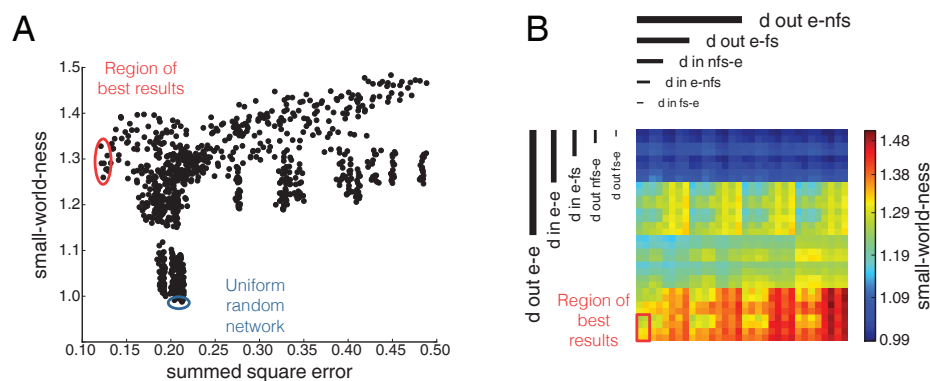


Figure 3.4: **Network structure and Small-World-ness**

A Scatterplot showing the small-world-ness of the constructed networks and the corresponding summed square error depicted in Figure 3.2. The red ellipse indicates the region of best results, while the blue ellipse shows the uniform random network. *B* Dimensional reordering of the parameter space created by varying the structural parameters (d_{in} and d_{out}) affecting the similarity to observed connectivity patterns. Colour indicates the small-world-ness of the network. The ordering is the same as in Figure 3.2, the red outline shows the region of best results of Figure 3.2.

excitatory network was key to a network model that reflected the experimental findings.

3.4.4 Small-World Networks

I also investigated whether the changes in single parameters would make the studied networks more similar to small-world networks (see Chapter 1.3). To this end, the small-world-ness for each constructed network was computed.

It was found that changes in the significant parameters increased the small-world-ness of the network (1.29 ± 0.02 for the region of best results). However, the reverse was not true, a high small-world-ness did not imply a good network fit. Figure 3.4 shows the distribution of small-world-ness in the tested networks, while in Figure 3.4 A the overall histogram for all networks is shown.

From this it can be seen that the small-world-ness in the region of best results was ranging between 1.25 and 1.32. The dimensional stack in Figure 3.4 B shows the small-world-ness in the same way as Figure 3.2 A was shown. Here it can be seen that the network with high

Chapter 3. Modifying Local Connectivity

small-world-ness were in the lower right corner where the summed square error was very high (compare to Figure 3.2).

Thus, high small-world-ness did not imply a plausible network. This was mostly due to the fact that I was using a specific type of network with three distinct populations and changes in the significant parameter were highly cell type specific. The small-world-ness as a general measure did not take into account the identity of the populations but only the overall network structure.

3.4.5 Scale-Free Networks

Since the construction of the network was imposing an approximately exponential degree distribution, there would be so called 'hub' neurons in the network and thus part of the definition of scale-free networks would be met. However, since the degree distributions were approximately exponential, the networks I constructed were by definition not scale-free networks. This would imply a powerlaw degree distribution (see Chapter 1.3).

3.4.6 Network Motifs

Some experimental studies showed that specific connectivity patterns of three or more neurons were more frequent in biological recordings than to expect from a uniform random network (Song et al., 2005; Perin et al., 2011, Chapter 1.2.2). The occurrence of these connectivity patterns, also called motifs (Milo et al., 2002), indicated that network connectivity was not uniform random.

The networks studied here were constructed to show an approximately exponential degree distribution. It has been shown previously, that such degree distributions do lead to an overrepresentation of triplet and higher order motifs (Roxin et al., 2008). Thus, the changes proposed here are in agreement with the experimental results of Song et al., 2005 and Perin et al., 2011.

3.5 Summary

In conclusion I was able to show that adjustments in the network structure through degree distributions was sufficient to model networks that capture biological measurements on complex connectivity patterns. This was true for studies of shared input (Yoshimura and Callaway, 2005; Yoshimura et al., 2005) and for electrophysiological studies of network motifs (Song et al., 2005; Perin et al., 2011).

Having a structured excitatory network turned out to be of paramount importance to construct network models that capture the complex connectivity patterns found in biological networks. The structure in the excitatory network was enabling the other parameters to be effective and also increased the occurrence of network motifs.

A strong impact of inhibitory connections was not evident from this approach. This was mostly due to the fact that the experimental paradigms used to fit the parameters were focussing on excitatory networks or excitatory inputs. Thus, a more thorough fitting of the networks was not possible at this stage.

One possible extension to alleviate this problem is to introduce experimental data of network activity and not solely rely on structural information. This is what is discussed in the next chapters.

4 Modifying Local Weight Distributions

Experimental results from pairwise recordings are used widely to construct network models. A remaining question is how well the dynamic properties of these networks generalise to different stimulations. In this chapter, experiments using channelrhodopsin to stimulate multiple neurons at the same time were used to investigate the network response properties.

To this end, I used a network stimulation that corresponded to the channelrhodopsin stimulus in the experiments and a measure was found that quantifies the similarity of the two distributions of responses. It was shown that the classical network models failed to reproduce the results observed in the experiments. To improve network performance, a method to change synaptic weight distributions at a single neuron of the network was introduced. This method was then used to adapt the local weight distributions so that the biological findings were reproduced more correctly. The results show that the necessary changes were highly specific to the type of the pre- and postsynaptic neuron.

In this chapter, the biological experiments used are explained first. Then the network model and the stimulus used to reproduce the biological findings are detailed. Following this it is explained how the weight distributions are altered to show local changes and how the calculation of the similarity of the model network and the experimental results is performed. These techniques are then used to investigate the role of local weight distributions in the network response distributions.

4.1 Experimental Basis

In order to investigate the effects of local changes in random networks it is necessary to use experimental data that goes beyond pairwise measurements. One conceptually simple experiment that allows for this is described in Avermann et al., 2011.

4.1.1 Channelrhodopsin Evoked Responses

Here a local volume of layer 2/3 mouse barrel cortex is infected by a lentiviral vector which expresses channelrhodopsin (ChR2) in excitatory cells. Channelrhodopsin is a light activated sodium channel and thus neurons that are expressing channelrhodopsin can be stimulated to spike with a flash of blue light.

In this experiment the postsynaptic responses of non-expressing excitatory neurons, fast-spiking interneurons and non-fast-spiking interneurons following such a channelrhodopsin stimulation are recorded. These responses are compound responses from multiple excitatory sources and thus are not only probing pairwise connections.

With this kind of data it is possible to test networks based on data of pairwise recordings whether or not they are adequately close to biological neuronal networks.

4.1.2 Connectivity

Avermann et al., 2011 also measure the pairwise connectivity between cells in all populations. This data is the same that was used for modeling networks in the previous chapter. In addition to the connection probabilities the measured weight distributions are also taken into account.

4.2 Network Model

The network model that I used in this part showed the same basic setup as that presented in the previous chapter. Thus the network consisted of three populations: excitatory, inhibitory

fast-spiking and inhibitory non-fast-spiking neurons. Population sizes were chosen according to biological measurements for layer 2/3 of a single mouse barrel cortex column (Lefort et al., 2009; Gentet et al., 2010). 1691 excitatory neurons were used, 97 fast-spiking and 133 non-fast-spiking neurons.

The main difference was that this network was analysed with respect to its response properties. It was thus necessary to complete the network model with a specific neuron model and realistic weight distributions.

4.2.1 Neuron Model

The single neurons in each population were simulated using the AdEx neuron model (Brette and Gerstner, 2005; Gerstner and Brette, 2009, Chapter 1.1.5). The parameters of these neurons were taken from Mensi et al., 2011, where recordings of layer 2/3 of mouse barrel cortex were used to extract all neuronal parameters.

4.2.2 Connectivity

The connection probabilities used were the same as in the previous Chapter (see Table 3.1). These connections were formed according to the standard uniform random paradigm (Chapter 1.1.1).

The global weight distribution used were lognormal fits to the distributions measured by Avermann et al., 2011. The lognormal fitting was the same as shown in Chapter 2.2.1. With keeping the global weight distributions fixed, I modified the local weight distributions as described below to investigate the effects on the network response behaviour.

4.2.3 Stimulation in the Model Networks

To reproduce the Channelrhodopsin experiments, 25 randomly chosen excitatory neurons were stimulated to emit a single, synchronous spike. This stimulus was close to the biological

Chapter 4. Modifying Local Weight Distributions

stimulus as neurons there emitted a single spike upon light stimulation. These spikes were temporally reliable across neurons (Avermann et al., 2011).

The stimulation size of 25 neurons was chosen because at this stimulation size, the mean response of the excitatory population fits in the mean response measured in the experiments. Thus, it provided a useful starting point at which the excitatory response was modeled as accurate as possible (see Figure 4.2).

The model was in a silent state and showed no spontaneous activity similar to the *in vitro* situation in Avermann et al., 2011. To acquire the network responses, the model was stimulated ten times with interstimulus intervals of 300 ms. After each stimulation, the peak membrane potential of all cells was recorded in a 50 ms window.

4.2.4 Quantification of Model Networks

To evaluate the performance of the constructed networks in comparison to biological results, I compared the network response distributions. These were obtained by the stimulation protocol described above.

The distribution of these responses was then compared to the ones measured in the experiments. To quantify the similarity of the distributions I used the log-likelihood ℓ as a measure. This was computed for a single neuronal population as follows:

$$\ell = \sum_i \log P(x_i|Y) \tag{4.1}$$

with x_i being values from the experimental network response distribution and Y being the model generated dataset. For the whole network consisting of three populations, the average log-likelihood across all populations was used.

4.2.5 Parameter Significance

The significance of single parameters was determined in the same way as in the previous chapter. This means that significant parameters were identified in the whole parameter space by using Student's t-test. After all significant parameters were fixed, the significant parameters for the resulting subspace were computed. This process was repeated until no more significant parameters were found.

4.3 Changing Local Weight Distributions

Single neurons in a uniform random network receive on average the same input. This is due to the fact that although global weight distributions can show a high variance, the number of incoming connections is high and thus, due to the central limit theorem, the averaging effect of a random network is strong. To allow for more variance, I altered the local weight structure in a way that preserved the global weight distribution, but changed the average input per neuron.

To alter the weight structure, the approach of weight correlations (Koulakov et al., 2009) was used. Here the idea was that some neurons received mostly very strong connections, while others received mostly weak connections. In Figure 4.1 the general outline of weight correlations is shown.

With the uniform random network as the basis (Figure 4.1 top) I aimed to change the weight correlations in the output of single neurons (Figure 4.1 bottom left) and in the input to single neurons (Figure 4.1 bottom right).

The distribution of average synaptic weights per neuron was strongly affected by this approach. While the random network showed a very sharply peaked distribution with low variance (Figure 4.1 histogram left, black bars), introducing weight correlations changed this distributions to a skewed distribution with high variance (Figure 4.1 histogram left, gray bars). This approach thus correlated the synaptic weights on a single neuron level.

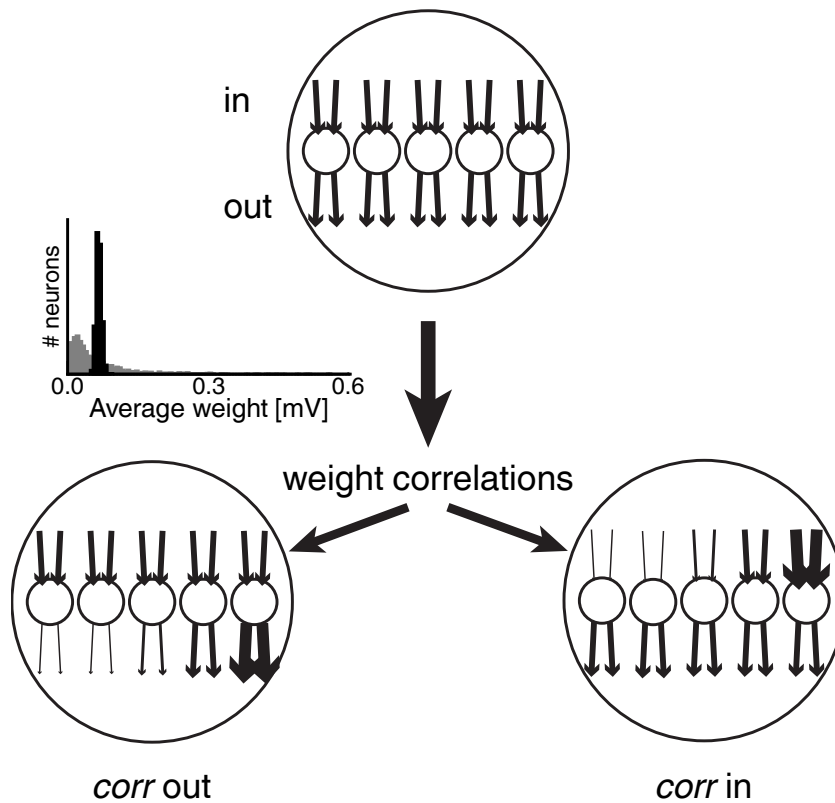


Figure 4.1: **Diagram of the idea of weight correlations**

Using a uniform random network as the starting point (*top*), effects of changing the weight correlations in the output and input are shown (*bottom*). *Left*: Histogram showing the distribution of average weights for the uniform network in black and for the network with imposed weight correlations in grey ($corr=1$).

To introduce these correlations of weights correctly two scaling values, ω_{pre}^i and ω_{post}^j were drawn from two lognormal distributions for each neuron. The distributions needed to be lognormal in order to preserve the global weight distribution since the lognormal distribution was preserved under multiplication. Furthermore the lognormal distributions from which ω_{pre}^i and ω_{post}^j were drawn had to have unit mean not to alter the mean of global weight distribution. The parameters μ and σ of these distributions were thus calculated as follows:

$$f_{in/out}(\omega) = \frac{1}{\omega\sigma_{in/out}\sqrt{2\pi}} e^{-\frac{(\ln\omega - \mu_{in/out})^2}{2\sigma_{in/out}^2}} \quad (4.2)$$

$$\mu_{in/out} = -(\sigma_{in/out}^2)/2 \quad (4.3)$$

$$\sigma_{in/out} = corr_{in/out} \quad (4.4)$$

I then multiplied the original weight matrix with ω_{pre}^i of the presynaptic partner and ω_{post}^j of the postsynaptic partner (Figure 4.1 left and Koulakov et al., 2009). The variance of the lognormal distribution, $corr_{in}$ for the input weights ($corr_{out}$ for the output weights) was used to parameterise the strength of the induced correlations.

Each parameter was taken to be either 0 or 1. For a value of 0, the distribution collapses to a single value thus no correlations are induced, for a value of 1 a high skewness and variance are induced. Choosing a value of 1 as the value for scanning parameter spaces is arbitrary since higher values are also possible. However, this value induced highly skewed distributions and thus would sufficiently show the effect of local weight correlations if there was any.

4.4 Results

I compared the evoked response distributions in the model and in the experiments, first in the uniform random case and then for all parameter combinations. The weight correlations in input and output were varied independently for each excitatory connection, leading to a total of six parameters. Finally, I looked at the results for a network in which the significant parameters were fixed.

4.4.1 Results for a Uniform Random Network

Applying the channelrhodopsin-like stimulus in the uniform random network did evoke a distribution of responses in the excitatory population that was close the experimental results (Figure 4.2 B, model: solid bars, experiment: outlined bars), but failed to reproduce the responses of the inhibitory populations (Figure 4.2 C,D).

The main difference between model and experimental results could be seen in the response distribution of the fast-spiking population. Here the model showed a Gaussian shape of the response distribution, while the experimental results showed a highly skewed distribution.

Figure 4.2 E depicts the amplitude distribution of the whole network. Here each pixel cor-

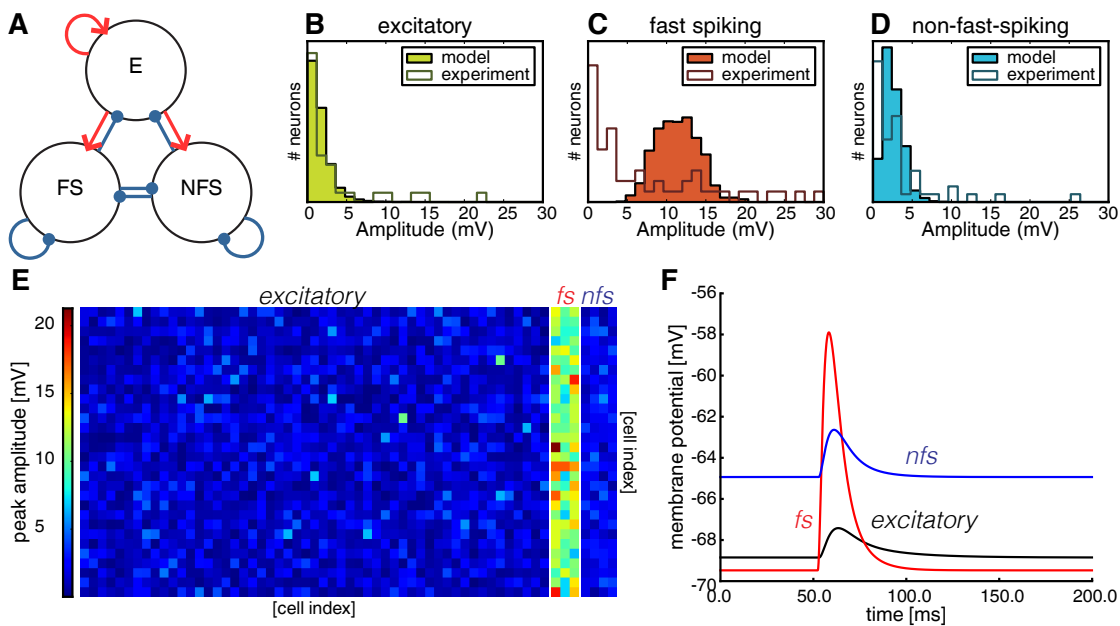


Figure 4.2: **A ChR2 like stimulus in a uniform random three population network model**

A General network setup and interactions. Each circle denotes a single population with the type of the contained neurons. Blue lines indicate an inhibitory connection, red lines are excitatory connections. B,C,D Distributions of response amplitudes in excitatory (B), fast-spiking (C) and non-fast-spiking neurons (D). Outlines are experimental results from Avermann et al., 2011, while solid bars show the model predictions for a channelrhodopsin like stimulus in 25 neurons for a uniform random network architecture. E,F Example experiment for a channelrhodopsin like stimulus in 25 excitatory neurons. E Plot of peak amplitudes for each neuron 50 ms after stimulus. Stimulated neurons are not shown. F Average traces for excitatory (black), fast-spiking (red) and non-fast-spiking populations (blue).

responded to one neuron and the colour codes the peak membrane potential change with respect to the resting potential. Again the shape of the response distributions is easily visible. While the excitatory and non-fast-spiking (nfs) response showed many weakly activated neurons and only few strongly active neurons, the fast-spiking population showed only strong activation throughout the whole population.

Figure 4.2 F shows the average membrane potential for each population following the stimulus at 50 ms. While the strong fast-spiking response was expected (Avermann et al., 2011), the overall magnitude was overestimated in the model. The experimental results showed an average response in the fast-spiking population of 5.3 mV, while the model response was 11.4 mV.

Since the stimulus size in the biological observations may have varied from experiment to experiment, this could explain some of the differences in the variance and shape of the distributions. However, since the stimulus size was a common parameter that affects all distributions equally, a change in the distribution of stimulus sizes so that the fast-spiking population showed more similarity to the experimental observations would in turn weaken the similarity of the excitatory and non-fast-spiking responses.

Furthermore, the Gaussian shape of the model response distribution in the fast-spiking neurons could almost completely be explained by the strong averaging effect of a uniform random network. Since the connection of excitatory to fast-spiking cells had a high probability ($P_{E \rightarrow FS} = 0.6129$) and there are vastly more excitatory than fast-spiking neurons in layer 2/3 of mouse barrel cortex (E: 1691, FS: 97 (Lefort et al., 2009; Gentet et al., 2010)), the majority of the excitatory input onto fast-spiking interneurons was shared.

It was possible to calculate the expected response distribution of the fast-spiking population by using a binomial distribution of the number of connections. The expected number of connections c from 25 stimulated excitatory cells to a given fast-spiking cell was

$$c = 0.575 \times 25 = 14.3750 \tag{4.5}$$

Chapter 4. Modifying Local Weight Distributions

with 0.575 the connection probability and 25 being the number of stimulated presynaptic neurons. The expected mean depolarisation r of the fast-spiking population was

$$r = c \times 0.82 = 11.7875 \quad (4.6)$$

with the calculated expected number of connections c and 0.82 being the average synaptic strength from the excitatory to the fast-spiking population. The expected variance ν of the responses was

$$\nu = 0.6129 \times 0.3871 \times 25 \times 0.82 = 5.0097 \quad (4.7)$$

The measured values in the simulations shown in Figure 4.2 were 11.3944 for the mean and 7.4403 for the variance. Thus, the response distribution could roughly be approximated without taking into account the specific shape of the weight distribution from excitatory to fast-spiking neurons indicating a strong averaging effect of the random network. This strong averaging was only visible in cases where the connection probability was high. The excitatory and the non-fast-spiking populations were sparse and thus the averaging effect was not as prominent as in the fast-spiking population.

The fact that the shape of the response distribution from excitatory to fast-spiking neurons was already defined by the average weight indicated that the averaging effect of random networks was too strong. The weight distribution for the excitatory to fast-spiking connection was rendered meaningless. Thus, changes to the random network architecture seemed necessary to increase the similarity of network response distributions.

4.4.2 Significant Parameters

To investigate whether the similarity of response distributions could be increased, all parameter combinations of weight correlations in the in- and output for the excitatory connections (excitatory to excitatory (e-e), excitatory to fast-spiking (e-fs) and excitatory to non-fast-spiking (e-nfs)) were tested.

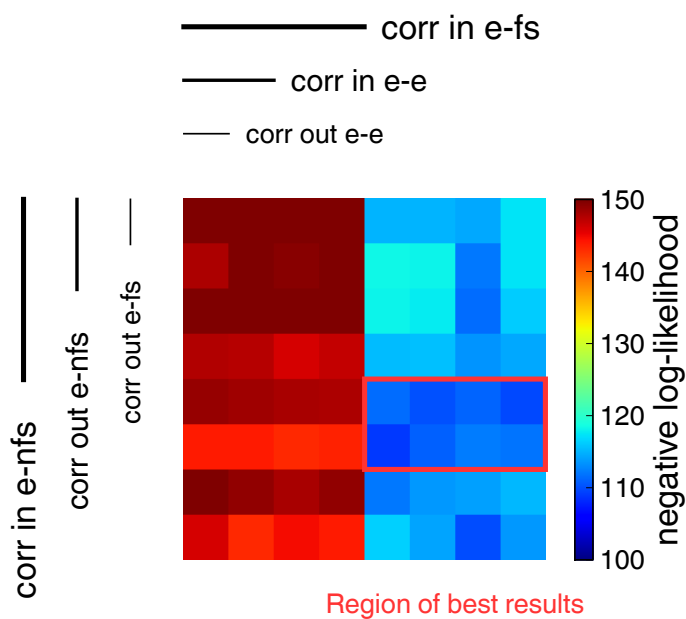


Figure 4.3: **Dimensional stacking for the parameter space spanned by varying the excitatory weight correlations**

Significant parameters: *corr in e-fs*(***), *corr in e-nfs*(***), *corr out e-nfs*(***). Significance levels using Student's t-test: $p < 0.05$ (*), $p < 0.01$ (**) and $p < 0.001$ (***).

Figure 4.3 shows the resulting parameter space. Here a dimensional stacking illustrates the similarity of the responses in the model and in the experimental data for all tested parameter combinations.

From this image, it is clear that introducing correlations in the input to the fast-spiking population (*corr in e-fs*) had the strongest influence on the similarity of the network response distributions. This was to be expected since this response was the one that fitted the data the least in the uniform random network.

Similarly, introducing the correlations in the input to the non-fast-spiking neurons (*corr in e-nfs*) also showed an influence albeit weaker than the one of the fast-spiking population. Finally, the correlations in the output of the excitatory to non-fast-spiking connection also had a small influence on the response distributions.

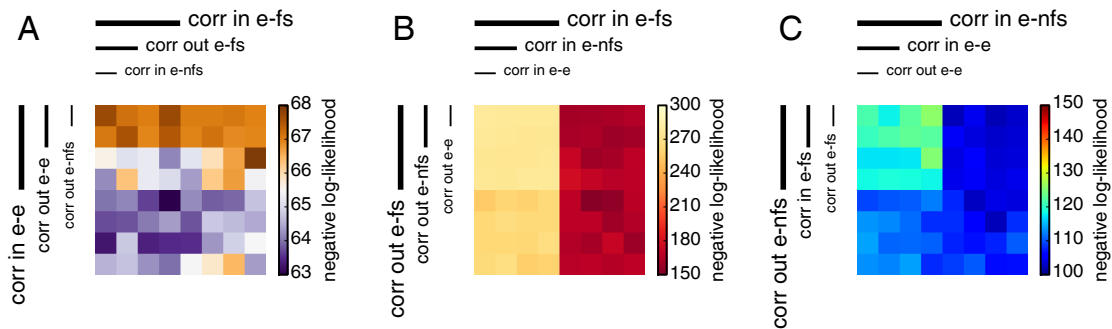


Figure 4.4: **Dimensional stackings for each population for the parameter space spanned by varying the excitatory weight correlations**

The stackings are based on the responses of the excitatory (e, A), the fast-spiking (fs, B) and the non-fast-spiking population (nfs, C).

4.4.3 Particle Swarm Optimisation

Particle swarm optimisation (see Chapter 1.5.1) confirmed the results from this approach. The best-fitting parameters were *corr out e-e*: 0.70, *corr in e-e*: 0.02, *corr out e-fs*: 0.93, *corr in e-fs*: 2.27, *corr out e-nfs*: 0.00, *corr in e-nfs*: 0.47.

Here the importance of the change in input correlations to the fast-spiking population was even more prominent. Interestingly the weight correlations in the output of the recurrent excitatory connection (*corr out e-e*) should also be increased. This modification was not visible from the results shown in Figure 4.3. Thus, I investigated the response similarities for each population separately.

4.4.4 Effects of Parameters on Individual Populations

When looking at the individual results for each response distribution, the same parameter turned out to be affecting the response distributions in different ways. Figure 4.4 shows the dimensional stacks for the responses of the excitatory, the fast-spiking and the non-fast-spiking populations separately.

The correlations in the recurrent excitatory connections only affected the excitatory response

(Figure 4.4 A), while the responses in the fast-spiking and non-fast-spiking populations remained unaffected (Figure 4.4 B-C).

Similarly, while in the average picture *corr* in e-fs was the most important parameter, in the response of the excitatory population (Figure 4.4 A) the optimal region would request *corr* in e-fs to be 0. However, the scale of this improvement was small in comparison to the large benefit of a high *corr* in e-fs on the fast-spiking response (Figure 4.4 B). Since the non-fast-spiking response showed no dependence on *corr* in e-fs (Figure 4.4 C), the parameter should be increased for an optimal network. The final values for all tested parameters are shown Table 4.1.

4.4.5 Results for an Adjusted Random Network

Figure 4.5 summarises the resulting network responses using the adjusted network derived in Chapter 4.4.2. The affected connections in the network model are outlined in Figure 4.5 A, while B-D depict the network response distributions for the different populations.

Looking at the response of the adjusted network shows that the response distributions of the model fitted those of the biological measurements more faithfully (Figure 4.5 B-D). This is true especially in comparison to the response distributions of the uniform random network (Figure 4.2 B-D).

Table 4.1: **Constraining parameters on the weight domain fitting technique**

Parameters that had a significant effect on the measures are marked by the value that provided the better result. Tested but not significant parameters are marked with '-'. Values found using particle swarm optimisation are listed in brackets.

| | <i>corr</i> | |
|-------|-------------|----------|
| | in | out |
| e-e | - (0.02) | - (0.70) |
| e-fs | 1 (2.27) | - (0.93) |
| e-nfs | 1 (0.47) | 0 (0.00) |

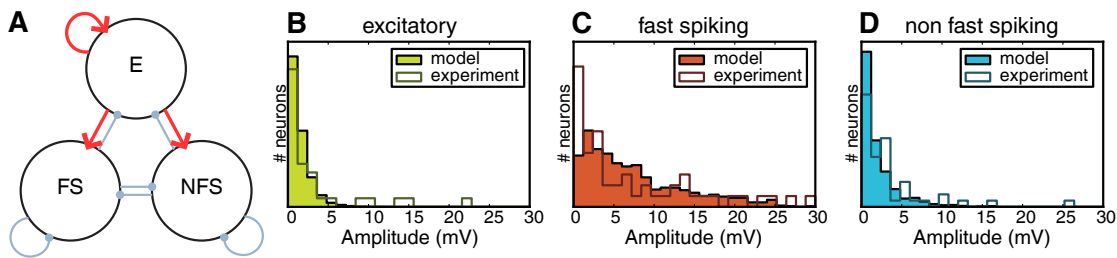


Figure 4.5: **A ChR2 like stimulus in a three population network model with adapted excitatory local weight distributions**

A General network setup and interactions. Each circle denotes a single population with the type of the contained neurons. Blue lines indicate an inhibitory connection, red lines are excitatory connections. The network was setup with all connections with the thick connections having at least one significant parameter that was determined by the fitting procedure. B, C, D Distributions of response amplitudes in excitatory (B), fast-spiking (C) and non-fast-spiking neurons (D). Outlines are experimental results, while solid bars show the model predictions for a channelrhodopsin like stimulus in 25 neurons.

4.5 Summary

The technique of weight correlations could thus be used to adjust the local weight distributions of a uniform random network to better match the response distributions observed in biological experiments.

The results showed that the shape of the network response distributions could be changed by introducing local weight correlations. Especially the changes in the input weight correlations to inhibitory neurons improved the similarity of response distributions in the model and in the experiment. For the fast-spiking and excitatory populations, an increase in the output weight correlations slightly improved the similarity of the response distributions further, although this effect was not significant.

The existence of such local weight correlations was until now not studied in experiments. This is due to the fact that large scale studies of synaptic weights that investigate large number of in- and outgoing synapses are technically limited (see also Chapter 1.2.3). However, it has been shown in Koulakov et al., 2009, that local weight correlations could be generated by a hebbian learning rule (see also Chapter 7.2). Thus, the concept of weight correlations is plausible but not proven and the results presented here and also in the next chapter are predictions of the

weight distributions that should be observed in experimental data.

The approach used here did only try to fit the excitatory connections and thus the most direct connections when applying a channelrhodopsin-like stimulus. Since in the adjusted network, the fast-spiking population showed spiking in response to the stimulus, it may be necessary to further increase the quality of the network models by taking into account all connections instead of only the excitatory ones. This approach thus uses more parameters and is more difficult to address.

In the next chapter, I show how to combine the fitting in the structural and weight domain, while taking into account all possible parameters.

5 Combining Architectural Changes

In the previous chapters, it was shown how the structure of neuronal networks can be adapted to yield a higher similarity to biological observations and how the local weight structure of networks can be changed in order to display response properties that resemble the experimental findings better than those of classical random networks. In this chapter, these techniques are combined to form adjusted networks that show both, a high structural similarity and a biologically plausible response behaviour.

The chapter begins with the effects of the two fitting steps presented in the previous chapters on each other. I show how the structurally adapted network described in Chapter 3 can reproduce the response behaviour analysed in Chapter 4 and whether the networks extracted in Chapter 4 match the experimental observations described in Chapter 3. Since analysing all network parameters at the same time is computationally expensive, I go on to explain how to split the fitting procedure into multiple steps and show the results of this fitting. An evolutionary algorithm is employed to verify the results obtained in this chapter. Finally, the role of inhibition in the network architecture is investigated.

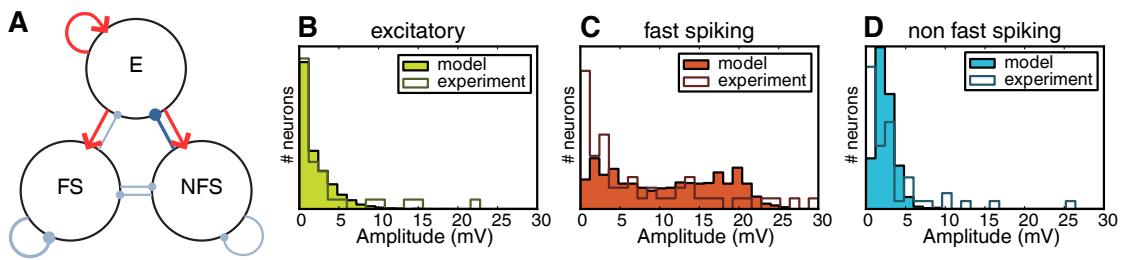


Figure 5.1: **Response distributions for optimal structure**

A Diagram of non-random connections. The network was setup with all connections with the thick connections having at least one parameter that was determined by our fitting procedure. B,C,D Distribution of response amplitudes in excitatory (B), fast-spiking (C) and non-fast-spiking neurons (D). Outlines were experimental results, while solid bars show the model predictions.

5.1 Response Properties and Structured Networks

As shown in Chapter 3, changes in the degree distributions helped to shape the network structure to express the complex connectivity patterns found in experiments. The question remained how these structural changes affect the response distributions that were introduced in Chapter 4.

Figure 5.1 shows these response distributions for the structurally adapted network. The connections with significant parameters found in Chapter 3 are depicted in the network diagram in Figure 5.1 A. The response distributions are shown in Figure 5.1 B-D.

Looking at the fast-spiking population (Figure 5.1 B) makes it immediately clear that the structure was not sufficient to shape the response distributions correctly. While the variance of the distribution was increased and matched the variance in the biological distribution better, the overall shape was not reproduced. The non-fast-spiking response (Figure 5.1 D) did not change from the uniform random picture (compare to Figure 4.2 D) due to the fact that the connections from excitatory to non-fast-spiking neurons remained unchanged from the uniform random paradigm (Table 3.2). The excitatory response distribution was fitted very well (Figure 5.1 C). Thus, a change only in the degree distributions was not sufficient to evoke biologically plausible network response distributions.

The changes in the network architecture introduced in Chapter 4 to fit the biologically observed response distributions were affecting the local weight distributions of the networks. The structure of the connections remained uniform random and thus there were no changes in the complex connectivity patterns analysed in Chapter 3.

Each of the two paradigms analysed in Chapters 3 and 4 alone was not sufficient to provide a network that is both, showing a high similarity to biological results in network structure and response distributions matching those found in experiments. It remained to show that a combination of weight correlations and changed degree distributions could provide a network with plausible structure and response distributions.

5.2 Combined Approach

A major problem when trying to fit all possible network parameters was that this spans a very high dimensional parameter space. Weight correlations in the in- and output and change in in- and out-degree distributions for all connections in the three population network amounted to 36 parameters that would have to be investigated.

This high dimensional space was very difficult to analyse. To simplify the analysis and to reduce the computational load, I decided to split the fitting procedure into multiple steps.

First, the structure of the biological experiments discussed in Chapter 3 was reproduced. With the respective parameters fixed, the network was then altered to reproduce the network response distributions discussed in Chapter 4.

As a starting point for the combined fitting, the structurally adapted network derived in Chapter 3 was chosen. Thus, the structure of the model was already fitted to reproduce the experimental data and it only remained to fit the other parameters in order to improve the similarity of the network responses.

I chose the order of the single fitting steps in this way because of the dependencies of each step. The similarity in structure did not depend on the weight correlations, consequently, the

Chapter 5. Combining Architectural Changes

first step should be the structural fitting.

With such a restricted network, there were still many parameters free to be fitted. In order to further reduce the possible parameters, the spiking behaviour of the inhibitory populations was investigated. The idea was that only populations that did spike in response to the stimulus could have an impact on other populations and have parameters that could improve the network response distributions. Populations that did not spike could not have influence on any network response distributions and thus could be neglected.

Since the excitatory population was stimulated, it would always provide spikes. Therefore, the two inhibitory populations remained to be tested. To analyse the spiking behaviour of these populations, I varied the weight correlations of the excitatory connections. This was done in the same way as described in Chapter 4. The only difference was that here the structurally adapted network was used as a starting point instead of the uniform random network.

Figure 5.2 shows the average number of spikes in each population following a channel-rhodopsin like stimulus in the excitatory population. While the fast-spiking population showed a substantial amount of spiking for a large range of parameters (Figure 5.2 A), the non-fast-spiking population remained mostly silent, rarely emitting a single spike or more for all parameters (Figure 5.2 B). This is consistent with experimental results (Avermann et al., 2011). In these experiments, the fast-spiking neurons fired with a probability of 18% in response to channelrhodopsin stimulation, while the non-fast-spiking neurons responded with a spike with a probability of only 0.2%.

These results showed that the non-fast-spiking population did not contribute to the network response distributions of the other populations and thus can be excluded from the fitting protocol for the next step. The response distribution of the non-fast-spiking population itself will be fitted in a final step.

5.3. Fitting Response Distributions in a Structurally Adjusted Network

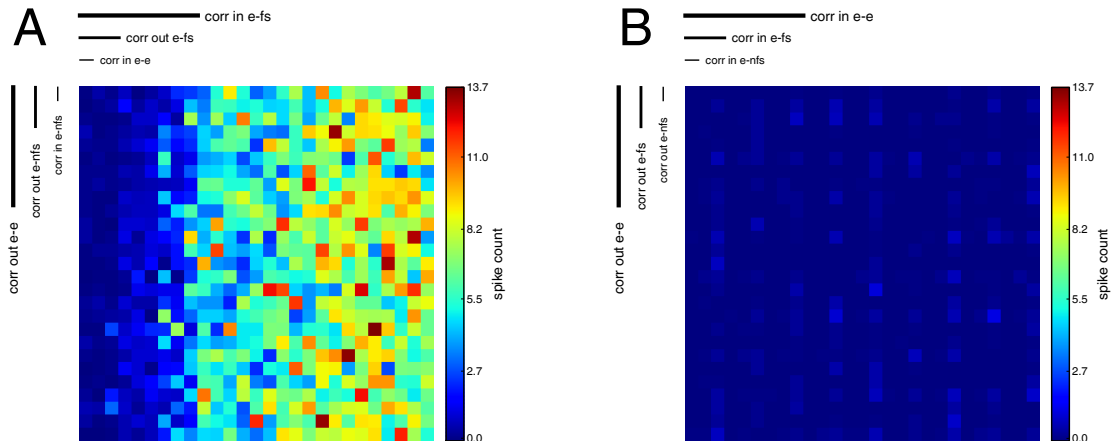


Figure 5.2: **Spiking in inhibitory network populations**

Dimensional stacking showing the number of spikes following a channelrhodopsin-like stimulation in the excitatory population (*A*: fast-spiking population (fs), *B*: non-fast-spiking population (nfs)).

5.3 Fitting Response Distributions in a Structurally Adjusted Network

After the exclusion of the non-fast-spiking population, all parameters that have not been used before were taken into account. This resulted in a mixture of weight correlation parameters and degree distribution parameters.

The results in this parameter space are shown in Figure 5.3. Since only the excitatory and fast-spiking populations were taken into account, the network diagram in Figure 5.3 A shows no connections to the non-fast-spiking population.

In Figure 5.3 B the dimensional stacking of the results for the average negative log-likelihood is shown. It is immediately clear that *corr in e-fs* had the strongest impact on the network responses which was very similar to the results in Chapter 4. The second observation was that *corr out e-fs* was also strongly affecting the response distributions. The analysis of significance showed that *corr out e-e*, *corr in e-e*, *corr out fs-fs* and *d out fs-fs* were also impacting the responses.

These results were not directly visible from the average picture. When focusing on the single

Chapter 5. Combining Architectural Changes

response distributions of the excitatory population in Figure 5.3 C, a different layout became apparent. Here *corr* in e-e had a strong effect on the negative log-likelihood. And similar to the results in Chapter 4, the optimal result for the excitatory population was in a region where *corr* in e-fs was zero. Since again the scale was rather small for the excitatory responses, the effect of *corr* in e-fs was governed by the strong impact on the fast-spiking population (Figure 5.3 D). Here the only affecting parameters were *corr* in e-fs and *corr* out e-fs. These parameters changed the response distributions on such a large scale that the adverse effect on the excitatory population was overwhelmed by the improvement in the fast-spiking response distribution.

Once all significant parameters were fixed, the remaining parameters for the connections to the non-fast-spiking population could be taken into account. Figure 5.4 summarises these results.

The network diagram in Figure 5.4 B shows the incoming connections to the non-fast-spiking population that were investigated. The dimensional stack in Figure 5.4 A is organized mainly in stripes which indicated a strong effect of the parameters on the x-axis, but no effect of the parameters on the y-axis. The two significant parameters were *corr* in e-nfs and *corr* out e-nfs. This was not entirely surprising given that the same parameter were shown to be important in Chapter 4.

More interesting was the fact that none of the connections from the fast-spiking population affected the behaviour of the non-fast-spiking population. Neither the degree distribution parameters nor the weight correlation parameters showed any effect. This might be due to the fact that although the fast-spiking population did emit spikes, the overall number of spikes and their timing were not sufficient to impact the response distribution of the non-fast-spiking population. Also, the inhibitory reversal potential of the excitatory cells was relatively close to their resting membrane potential (see Chapter 6.1).

In the end, some connections remained untested because the firing of the non-fast-spiking population was too sparse to influence other response distributions. Thus, the parameters

5.3. Fitting Response Distributions in a Structurally Adjusted Network

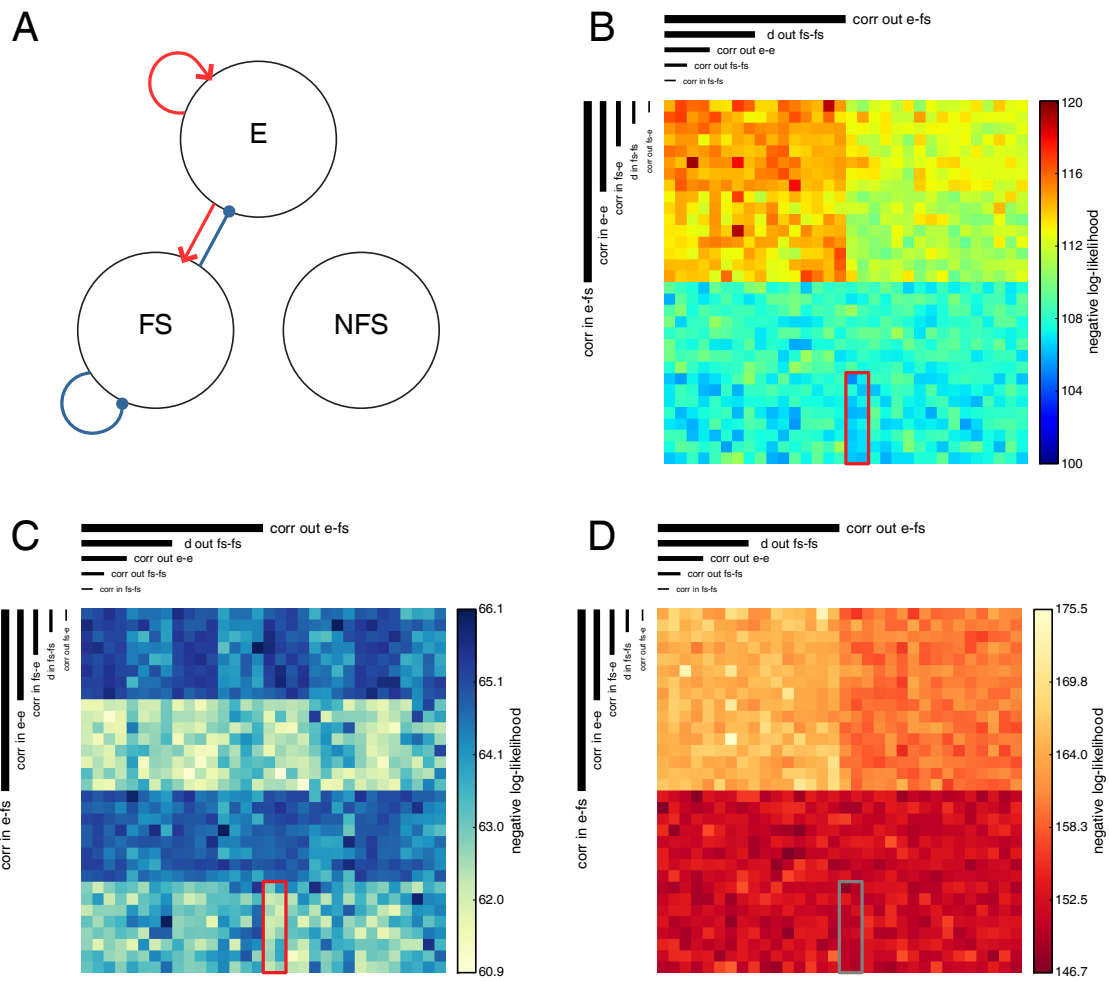


Figure 5.3: **Parameter space for the connections of excitatory (e) and fast-spiking (fs) neurons**

A Diagram of the network connections affected by the fitting. *B* Dimensional reordering of the average negative log-likelihood of the experimental data given the model data for the excitatory and fast-spiking populations. The red outline shows the region of best results. *C, D* Dimensional reorderings of the negative log-likelihood only for the excitatory (*C*) or for the fast-spiking population (*D*). Significant parameters: d out fs-fs (***) , $corr$ out e-e(***) , $corr$ out fs-fs(**) , $corr$ in e-e(***) , $corr$ in e-fs(***) . Significance levels using Student's t-test: $p < 0.05$ (*) , $p < 0.01$ (**) and $p < 0.001$ (***).

affecting connections from the non-fast-spiking population could not be tested. The only exception here was the connection from non-fast-spiking to excitatory in which the degree distribution parameters could be tested in the first step of the fitting. All parameters that were tested are summarised in Table 5.1.

Using these summarised values I could investigate the network response distributions in the

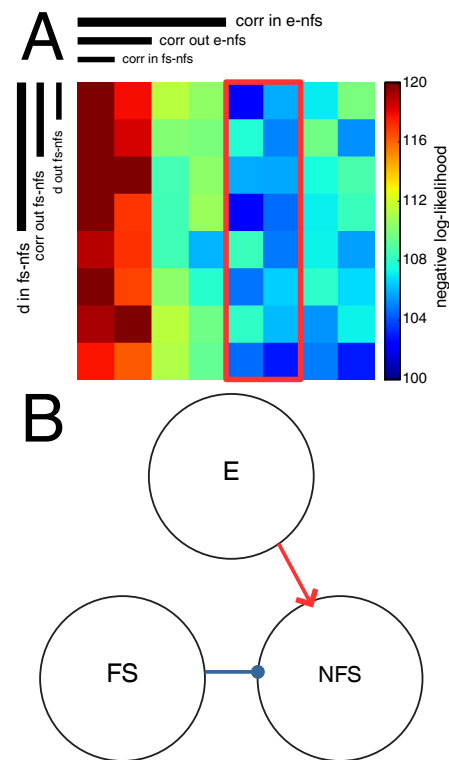


Figure 5.4: **Parameter space for the non-fast-spiking population**

A Dimensional reordering of the average negative log-likelihood of the experimental data given the model data for the non-fast-spiking (nfs) population. The red outline shows the region of best results. *B* Diagram of the network connections affected by the fitting. Significant parameters: *corr* out e-nfs(*), *corr* in e-nfs(***) . Significance levels using Student's t-test: $p < 0.05$ (*), $p < 0.01$ (**) and $p < 0.001$ (***).

same way as for the uniform random network that was the starting point of the fitting. This is illustrated in Figure 5.5.

In the network diagram in Figure 5.5 connections with significant parameters are highlighted in comparison to those without significant parameters. All excitatory connections had significant parameters, while only few inhibitory connections (recurrent fast-spiking and non-fast-spiking to excitatory) had significant parameters. Interestingly these parameters had to be fixed to zero for the optimal result. This indicated a non-specific inhibitory connectivity which has also been reported in new experimental findings (Packer and Yuste, 2011).

The response distributions in Figure 5.5 B-D show a high degree of similarity to those measured in biological experiments. When looking at Figure 5.5 E it becomes apparent that the overall behaviour of the network was more similar in all populations. Most neurons were weakly activated with sparse strong responses. Figure 5.5 F shows the average membrane potential traces of the three populations. Here it can be seen that in comparison with Figure 4.2 the response in the fast-spiking population was less high in amplitude.

5.3. Fitting Response Distributions in a Structurally Adjusted Network

Table 5.1: **Constraining parameters on the combined fitting technique**

Parameters that had a significant effect on the measures were marked by the value that provided the better result. Tested but not significant parameters were marked with '-'. Untested parameters were left empty.

| | <i>corr</i> | | <i>d</i> | |
|---------|-------------|-----|----------|-----|
| | in | out | in | out |
| e-e | 1 | 0 | 5 | 5 |
| e-fs | 1 | 1 | 5 | 0 |
| e-nfs | 1 | 0 | 0 | 0 |
| fs-e | - | - | - | - |
| fs-fs | - | 0 | - | 0 |
| fs-nfs | - | - | - | - |
| nfs-e | | | 0 | - |
| nfs-fs | | | | |
| nfs-nfs | | | | |

This came from the fact that the average membrane potential was computed without taking into account spiking neurons. Since spiking neurons must have received strong inputs, these strong inputs were taken out of the averaging by excluding spiking neurons. The same approach was also used in the experimental results (Avermann et al., 2011) where the amplitude of the fast-spiking response was less than expected from the uniform random network model.

Overall the results shown here were in agreement with experimental results on structure (Yoshimura and Callaway, 2005; Yoshimura et al., 2005; Packer and Yuste, 2011) and with network response behaviour (Avermann et al., 2011).

Another approach would have been to use other optimisation techniques to circumvent the problem of having to use a hierarchical approach. One problem was that this would require a multi objective approach, since both structure and response properties have to be matched.

Genetic algorithms were an appropriate way of approaching such problems. I used Strength Pareto Evolutionary Algorithm (SPEA2, Zitzler and Thiele, 1999; Zitzler et al., 2001) to confirm the observations made from the analysis. Table 5.2 shows the parameters as found by the SPEA-2 algorithm.

The results showed small differences in few parameters. Notable parameters showing different

Chapter 5. Combining Architectural Changes

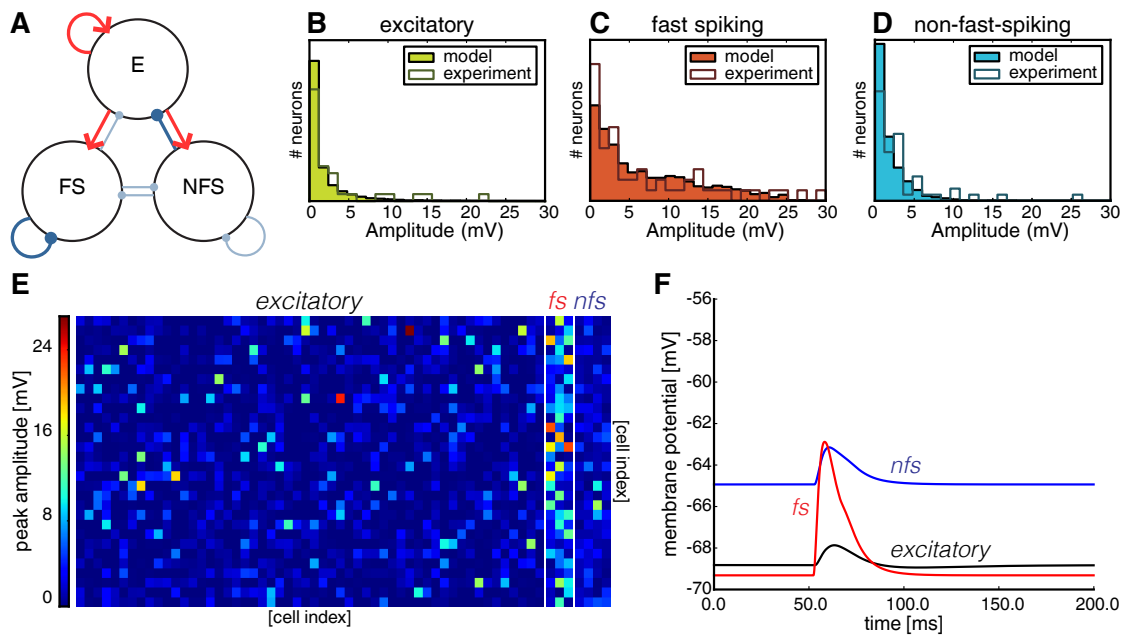


Figure 5.5: **Response distributions for an all adjusted network**

A Diagram of non-random connections. The network was setup with all connections with the thick connections having at least one parameter that was determined by our fitting procedure. B,C,D Distribution of response amplitudes in excitatory (B), fast-spiking (C) and non-fast-spiking neurons (D). Outlines were experimental results, while solid bars show the model predictions. E Plot of peak amplitudes for each neuron in 50 ms after stimulus for one example run of the network. Stimulated neurons were not shown. F Average traces for excitatory (black), fast-spiking (red) and non-fast-spiking populations (blue) after stimulation of 25 excitatory at 50 ms.

results were *corr* in e-e and *corr* out e-e. While the previous analysis showed that *corr* in e-e should be increased, the evolutionary algorithm showed no increase. The reverse was true for *corr* out e-e, while the previous analysis required no change in this parameter, here it was 0.88 and thus close to one. However, both changes only affect the results in a minor way (see Figure 5.3). Also it was notable that the evolutionary algorithm did not find a solution that was significantly better than the solution found through the splitted approach. This indicates that there may be multiple optima for different parameters and furthermore that the parameterspace is not approachable as a whole due to the expensive evaluation of single data points.

However, both algorithms agreed in the connections with the strongest impact as pointed out above and thus show that the extracted parameters were indeed important for network

5.4. Effects of Inhibitory Activity in Network Simulations

Table 5.2: **Optimal parameter found by SPEA-2 optimisation**

All parameters were taken into account for the optimisation. The fitness was computed by using the negative log-likelihood and the summed square error normalised to the network constrained by the found parameters in Table 5.1.

| | <i>corr</i> | | <i>d</i> | |
|---------|-------------|------|----------|------|
| | in | out | in | out |
| e-e | 0.04 | 0.88 | 2.53 | 3.33 |
| e-fs | 1.60 | 0.54 | 1.90 | 1.04 |
| e-nfs | 0.87 | 0.00 | 2.04 | 0.13 |
| fs-e | 0.00 | 0.90 | 0.46 | 1.53 |
| fs-fs | 0.48 | 0.00 | 0.00 | 0.09 |
| fs-nfs | 1.00 | 0.00 | 2.17 | 0.67 |
| nfs-e | 0.41 | 0.50 | 0.20 | 0.27 |
| nfs-fs | 0.00 | 0.15 | 0.00 | 1.01 |
| nfs-nfs | 0.15 | 0.03 | 0.00 | 0.41 |

construction.

5.4 Effects of Inhibitory Activity in Network Simulations

One interesting property from the network architecture extracted in the last section is the lack of impact from the connection from fast-spiking to excitatory neurons. None of the parameters that altered the connection from the fast-spiking to the excitatory population showed a significant effect on the fitness measures. Intuitively, this connection should have a strong impact on the network response, since the connections from fast-spiking to excitatory neurons are strong and frequent.

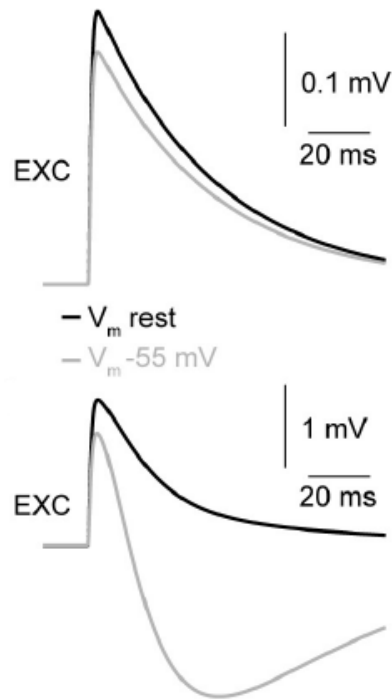
Here two explanations for this lack of impact are given. First, the role of the inhibitory reversal potential is described and then the effects of stimulus size are elucidated.

5.4.1 Inhibitory Reversal Potential

One important reason for the lack of impact from the fast-spiking neurons was that the inhibitory reversal potential of the excitatory cells was rather close to the resting potential ($V_{\text{rest}} = 68.1$ mV, $V_{\text{revI}} = -75$ mV). The distance of reversal potential and resting potential

Figure 5.6: **Single neuron responses on different membrane potentials show disynaptic inhibition**

Shown are typical single neuron responses to a synchronous spike in one neuron (*Top*) or in 50 neurons (*Bottom*). Each trace is shown for the neuron at its resting membrane potential (*black*) or depolarised to -55 mV (*grey*). (Modified from Avermann et al., 2011)



scales the amplitude of a synaptic input to the postsynaptic cell. When the resting membrane potential and the inhibitory reversal potential are similar, inhibitory activity shows almost no impact in the excitatory cells.

This is illustrated in simulations of the basic uniform random model described in Chapter 4.2. Figure 5.6 shows example membrane potential traces for excitatory neurons. The black traces show a typical single neuron response to single presynaptic spike in an excitatory neuron at the top and the response to a synchronous spike in 50 excitatory neurons at the bottom.

Even in the case of 50 stimulated neurons, the impact of inhibition is barely visible, since the black trace shows the stereotypical shape of an EPSP (Figure 5.6, bottom, black trace). Only when depolarising the neuron to -55 mV the inhibition becomes apparent (grey traces). For a single presynaptic spike, there was no recruitment of inhibitory cells thus the difference between the grey and the black trace is solely due to the membrane potential being closer to the excitatory reversal potential (Figure 5.6, top). In the bottom panel, the inhibitory effect becomes apparent and decreases the excitatory response substantially with even a hyperpolarising effect after the excitatory peak (Figure 5.6, bottom).

5.4. Effects of Inhibitory Activity in Network Simulations

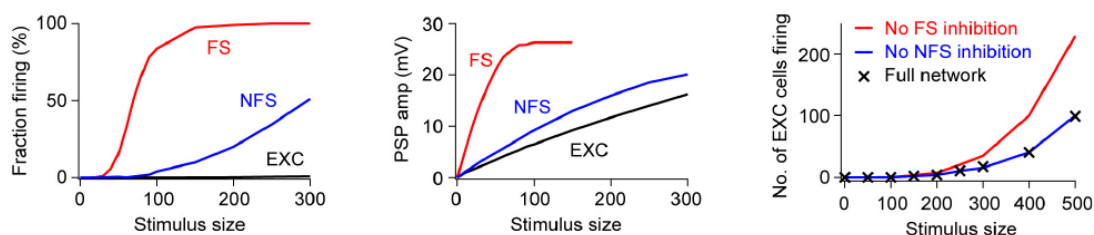


Figure 5.7: **Random network responses for different stimulation sizes**

Left: Fraction of firing cells as a function of stimulus size. Plotted are excitatory neurons (EXC, black), fast-spiking neurons (FS, red) and non-fast-spiking neurons (NFS, blue). *Middle:* Peak membrane potential of cells that did not spike as a function of stimulus size. Colours are the same as on the left panel. *Right:* Number of non-stimulated excitatory cells that did spike in response to the stimulus as a function of stimulus size. Networks used are the full setup with all three populations (black crosses), a network with only excitatory and fast-spiking cells (blue) or a network with only excitatory and non-fast-spiking cells (red). (Modified from Avermann et al., 2011)

These results indicated that for small stimulus sizes, there was no strong inhibition visible in the excitatory neurons, which is also seen in experimental recordings (Avermann et al., 2011).

5.4.2 Stimulus Size

Another reason for the lack of impact from the fast-spiking neurons was the stimulus size. Although the stimulation of 25 neurons evoked spikes in the fast-spiking population (see also Figure 5.2), these might have been insufficient to alter the responses of the excitatory population.

In order to see at which stimulus sizes the inhibitory input becomes apparent, a range of stimulus sizes from 10 to 300 neurons was tested. The results of the simulations are shown in Figure 5.7.

In the leftmost part of Figure 5.7, the fraction of spiking neurons is plotted for each population as a function of the stimulus size. The fast-spiking population shows an early and steep rise of the fraction of spiking neurons indicating strong recruitment of inhibition. The non-fast-spiking cells show a moderate increase to about 50% of the population firing in response to a stimulus of 300 excitatory neurons. The excitatory neurons show a very weak increase in

Chapter 5. Combining Architectural Changes

the fraction of spiking neurons. This is also due to the large number of excitatory cells in comparison to the inhibitory cells (1691 excitatory cells, 97 fast-spiking and 133 non-fast-spiking cells).

The middle panel of Figure 5.7 shows for each population and stimulus size the average peak membrane potential change of all cells that did not spike. Here the fast-spiking neurons show also a steep increase which saturates quickly close to the threshold of spiking. Non-fast-spiking and excitatory cells show a similar increase in amplitude. The non-fast-spiking population is slightly higher in amplitude than the excitatory population which is also reflected in the fraction of spiking cells.

The right side of Figure 5.7 shows the number of non-stimulated excitatory cells firing as a function of the number of stimulated neurons for different network configurations. To investigate the effect of inhibition with larger stimulus sizes, the network was constructed either normally, with all populations (black crosses), with only the excitatory and the fast-spiking population (blue) or with only the excitatory and the non-fast-spiking population (red). For stimulus sizes up to 150 neurons, the number of non-stimulated spiking excitatory cells is very similar in all network types. Only for stimulus sizes larger than 200 neurons, the network without fast-spiking neurons shows a higher number of firing excitatory cells. This indicates that the fast-spiking activity is only affecting the excitatory firing for large stimulus sizes. The non-fast-spiking neurons did not affect the number of spiking excitatory cells because their inhibition was overruled by the fast-spiking inhibition.

These results indicated that *in vitro* networks only showed effects of inhibition for large stimulus sizes. In these cases, the full fast-spiking population is recruited and it affects the number of excitatory cells that spike in response to the stimulation.

5.5 Summary

In this chapter, the approaches to improve network structure in Chapter 3 and to improve network response behaviour in Chapter 4 were combined. This led to networks that were able

to reproduce both the structure and the response behaviour found in biological experiments.

Since this approach involved a high dimensional parameter space, the fitting procedure was divided into multiple steps. First the structure was fitted, then the response properties were fitted. The results show that the choice of parameters is highly specific for the combination of pre- and the postsynaptic neurontype.

The final results were compared to parameters extracted with a genetic algorithm. The parameters of both approaches agreed in the main parameters, indicating that the approach used here captured the parameters having the highest impact.

Strikingly, the significant parameters extracted in this chapter did not involve parameters affecting the inhibitory connections from fast-spiking to excitatory neurons. This lack of effect was due to two reasons: the stimulus size and the relative closeness of the inhibitory reversal potential and the resting membrane potential in the excitatory cells.

This suggests that the inhibitory neurons will play a more prominent role in *in vivo* upstates, where the membrane potential of all cells is depolarised. Here the difference from the membrane potential to the inhibitory reversal potential in excitatory cells is larger than in the *in vitro* situation. In addition, the depolarisation is likely to increase the number of inhibitory cells firing and will thus make the inhibitory neurons more important. The implications of a simplified upstate model and the responses to sensory input for different network architectures are focussed in the next chapter.

6 Effects of Architecture on the Functional Behaviour of Networks

The focus in this chapter is to investigate the properties of the adjusted layer 2/3 network derived in Chapter 5 in more complex scenarios that resemble the *in vivo* situation instead of the silent *in vitro* state which was the basis of the previous chapters.

Two scenarios are taken into account: first, the behaviour of the network in simplified up- and downstates is described. Specifically, the network responses to a synchronous stimulation as in Chapter 4 are investigated for the uniform random network and the adjusted network both in the up- and in the downstate. The results indicate that adjusted networks show a closer fit to experimental data than uniform random networks.

In the second part of this chapter, the properties of the adjusted network with respect to sensory input are approached. To this end, sensory input from a single whisker is simulated and the temporal summation of these sensory inputs is studied in different network architectures. The results show again that adjusted networks show an increased performance in comparison with uniform random networks.

6.1 Simplified *in-vivo* Simulations

In this section, the behaviour of networks with different architectures is studied in a simplified *in vivo* setting. By depolarising the whole network to membrane potentials observed in

Chapter 6. Effects of Architecture on the Functional Behaviour of Networks

experiments, a simplified upstate is simulated. Using the same stimulation as in Chapter 4, I compare the evoked activity for different network architectures.

First, the effects of the simplified upstate in the model are studied by testing the response properties of single neurons with a synchronous stimulation as used in Chapter 4. Then the differences in response behaviour of the uniform random network and the adjusted network introduced in Chapter 5 are investigated.

6.1.1 Results

A simplified model of the *in vivo* up- and downstates (see Chapter 1.2.3 and Figure 1.6) was used to investigate the difference of the effects of inhibition on the network responses. The downstate was the silent network used in the previous chapters with membrane potentials and thresholds adapted to recordings *in vivo* (Mateo et al., 2011). The upstate was modeled by injecting a current step into each neuron that depolarised the single neurons to their average membrane potential in the upstate that was recorded *in vivo*. To investigate the response properties of the tested networks, a random subset of excitatory neurons was stimulated to emit a spike in each simulation. All non-stimulated cells were taken into account for the analysis of responses.

Effects on Simulations of Uniform Random Networks

First, the responses of a uniform random network without any changes in network architecture were simulated. For each condition (up- and downstate), a range of stimulus sizes between ten and 300 neurons was tested and the fraction of spiking, non-stimulated cells and their average response amplitude recorded. The results are shown in Figure 6.1.

The left panel shows the general stimulation paradigm and difference between up- and downstates. For each population an example trace is given that shows first a downstate with a stimulation followed by the transition to the upstate again with a stimulation eliciting a spike in the fast-spiking trace.

6.1. Simplified *in-vivo* Simulations

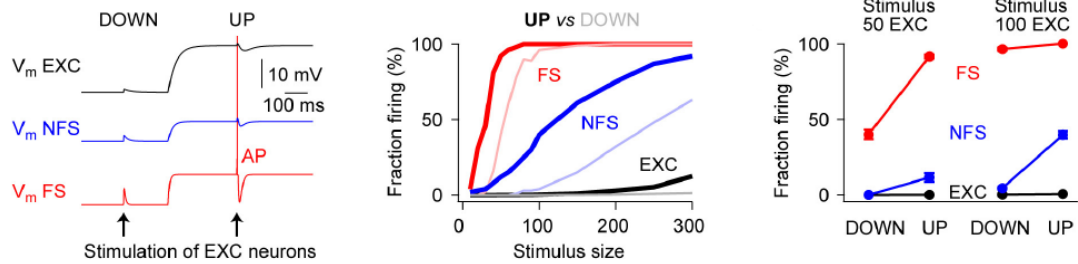


Figure 6.1: **Evoked spikes in simulations of up- and downstates in a uniform random network**

Left Traces of example neurons of all populations showing the transition from DOWN to UP state with a stimulus in each episode. Plotted are excitatory neurons (EXC, black), fast-spiking neurons (FS, red) and non-fast-spiking neurons (NFS, blue). *Middle* Fraction of firing cells as a function of stimulus size. Thick lines indicate values for the upstate (UP), thin lines indicate values for the downstate (DOWN). *Right* Difference in fraction of firing neurons for up- and downstate for 50 (left) and 100 (right) excitatory neurons stimulated. (Modified from Avermann et al., 2011)

The middle panel of Figure 6.1 shows the fraction of firing cells for excitatory, fast-spiking and non-fast-spiking cells for the upstate and the downstate condition. It can be seen that all populations show an increase in spiking mostly due to the higher prestimulus membrane potential in the upstate. The difference for fast-spiking cells is only visible in small stimulus sizes, since larger stimulus sizes evoke spikes in all fast-spiking neurons even in the downstate. Non-fast-spiking neurons show an increase in spiking for all stimulus sizes. Even a very small stimulus size of ten excitatory neurons in the upstate evokes spikes in the non-fast-spiking population. The change in the fraction of spiking excitatory neurons is very small but consistent across all stimulus sizes.

The right hand side of Figure 6.1 compares the fraction of spiking cells for the up- and downstates for 50 and 100 stimulated neurons. Here the difference between the increase in the fast-spiking and non-fast-spiking cells is apparent. The fast-spiking population shows a strong increase from the down- to the upstate when 50 neurons are stimulated, while for a stimulus size of 100 neurons, the population is already completely recruited and shows no large difference. For the non-fast-spiking population this effect is almost reversed. While the stimulus size of 50 neurons does not lead to a large difference in fraction of spiking neurons, the stimulation of 100 neurons shows a strong increase from the down- to the upstate. The

Chapter 6. Effects of Architecture on the Functional Behaviour of Networks

excitatory population shows a consistent but small increase in the fraction of spiking cells. The experimental recordings *in vivo* display a similar result (Mateo et al., 2011). In the experiments, fast-spiking cells increase slightly in probability of spiking, non-fast-spiking neurons increase strongly and excitatory neurons show a very small but significant decrease in firing probability (see Figure 1.6).

The model predicted a stimulus size of around 100 neurons for a scenario that would be equivalent to the experimental findings. This is the approximate number of stimulated cells estimated in the experiments (Mateo et al., 2011). Although the model fitted the data qualitatively, the actual fraction of spiking cells was not comparable to the experimental values. The experiment found spiking probabilities for the fast-spiking neurons of 0.42 ± 0.53 for the down- and 0.74 ± 0.24 for the upstate and for the non-fast-spiking neurons probabilities of 0.11 ± 0.26 for the down- and 0.34 ± 0.4 for the upstate (see Figure 1.6). For a stimulus size of 100 neurons, the fraction of fast-spiking neurons in the model increased from 0.96 ± 0.01 in the down- to 1.00 ± 0.00 in the upstate. The non-fast-spiking neurons increased from 0.04 ± 0.02 (down) to 0.40 ± 0.02 (up). Thus the uniform random networks did not provide a detailed agreement with the experimental results.

Effects on Simulations of Adjusted Random Networks

The same stimulation paradigm as used on the uniform random network was then used on the adjusted network described in Chapter 5. Figure 6.2 shows the results for an adjusted network.

In the left panel it can be seen that the general trends found in the random network still hold true. The upstate increases the fraction of spiking neurons in all populations. In the adjusted network, fast-spiking neurons fire less than in the random network and do not reach full recruitment. This is the reason why the increase in the fraction of firing cells can be seen in the fast-spiking population even for large stimulus sizes. The response in the non-fast-spiking cells is stronger than in the random network as is the excitatory response.

When comparing the fraction of spiking cells in the down- and in the upstate for a stimulus

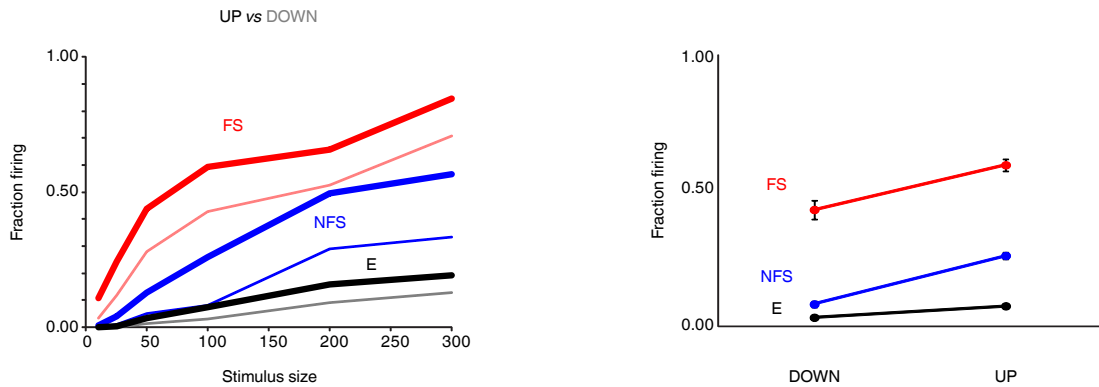


Figure 6.2: **Evoked spikes in simulations of up- and downstates in an adjusted network**

Left Fraction of firing cells as a function of stimulus size. Thick lines indicate values for the upstate (UP), thin lines indicate values for the downstate (DOWN). Fast-spiking neurons (FS) are shown in red, non-fast-spiking (NFS) in blue and excitatory (E) in black. *Right* Fraction of spiking cells for a stimulus size of 100 excitatory neurons in the DOWN (left) and UP (right) case.

size of 100 neurons, it can be seen that the qualitative result is the same as in the random network (Figure 6.2, right). The fast-spiking neurons increased from 0.43 ± 0.04 in the down- to 0.59 ± 0.2 in the upstate and the non-fast-spiking increased from 0.08 ± 0.01 to 0.26 ± 0.01 . This is much more in agreement with the numbers found in the *in vivo* experiments (see Figures 6.3 and 1.6).

6.1.2 Summary

To conclude, a random network model using simplified *in vivo* like up- and downstates could qualitatively account for the changes in postsynaptic firing probability in response to channelrhodopsin stimulation. This indicated that the underlying pairwise connectivity measurements used to construct these network were sufficient to evoke responses that were in general agreement with experimental data. However, the results showed only a qualitative agreement and differed greatly in the exact quantification.

An adjusted network showed responses that agreed qualitatively like the responses from uniform random networks, but the responses also fitted the experimental data quantitatively. Thus, the adjusted network was not only fitting the network responses *in vitro*, but it could also

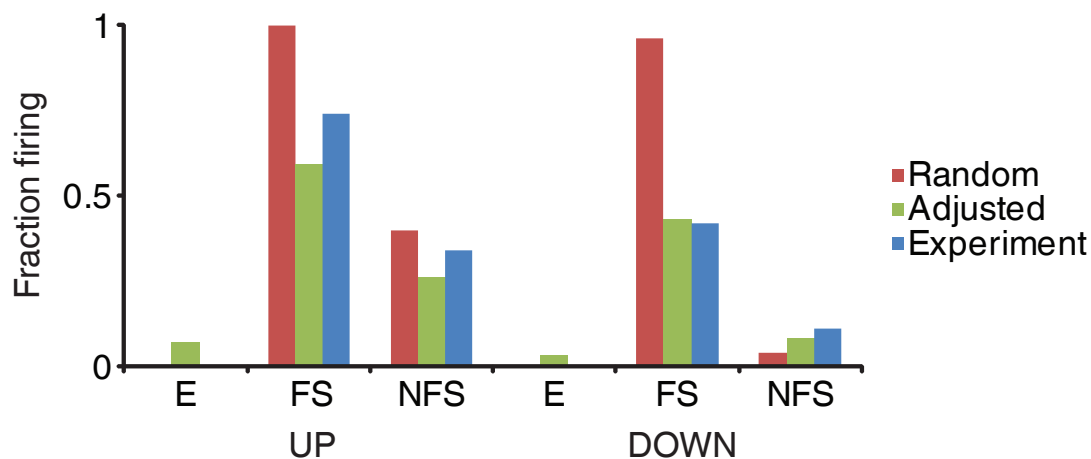


Figure 6.3: **Summary of *in vivo* fraction of firing neurons after stimulation**
 Shown is the fraction of neurons that fired in response to the channelrhodopsin stimulation in a uniform random network (red), in the adjusted network (green) and those found in the experiments (blue) for all three cell types (excitatory (E), fast-spiking (FS) and non-fast-spiking (NFS)).

reproduce *in vivo* experiments to a certain degree. This indicated that the adjusted network structure did capture the underlying network better and thus was able to generalise from *in vitro* to *in vivo* data.

6.2 Temporal Inputs to Multiple Barrels

In this part I use a sensory input paradigm to investigate how different network architectures are able to shape neuronal responses to an external stimulation. To this end, the experimental findings which should be reproduced are introduced. Then, using insights from a previous model by Wilson et al., 2011, the network models used earlier are extended to a show spatial profile. Finally, it is shown how different network architectures reproduce the results found in the experiments.

6.2.1 Experimental Basis

In order to further investigate possible functional consequences especially in the domain of sensory input, I focused on one particular experiment. Here, two adjacent whiskers are stimulated in a temporal sequence with varying interstimulus intervals (Shimegi et al., 2000, Chapter 1.2.1). The main results are shown in Figure 1.2.

The neuron response depends strongly on the position of the neuron and is stronger than expected from independent stimulation alone. Thus, they are able to show that the response magnitude of a neuron depends on the underlying geometry of the barrel field.

6.2.2 Modeling Basis

In Wilson et al., 2011 a model of this dependence is presented. This model makes use of the coincidence detection mechanism of Jeffress, 1948. Coincident temporal auditory inputs can be detected when using a bank of different neurons with different delays for each stimulus location. The active neuron therefore codes for a specific temporal distance of stimuli.

In Wilson et al., 2011, this idea is transferred to the barrel cortex. The single whisker deflections are modeled as an increase in activity in excitatory and inhibitory neurons in layer 4 of the corresponding barrel. This activity then propagates to the higher layer 2/3.

The excitatory and inhibitory connections from layer 4 to layer 2/3 show distance dependent delays, modeled to reflect biological observations (Feldmeyer et al., 2002; Helmstaedter et al., 2008). The excitatory delay is 10 ms/mm and the inhibitory delay is 3.3 ms/mm with an offset of 3.7 ms so that the inhibitory activity is propagated later to the layer 2/3 neurons than the excitatory activity. These values were chosen to match the parameters used in Wilson et al., 2011.

The model network consisted of a population of unconnected layer 2/3 neurons spatially distributed in one dimension with positions ranging from -0.6 mm to 0.6 mm and layer 4 inputs located at -0.2 mm and 0.2 mm. Neurons were grouped for the analysis into 'Above A'

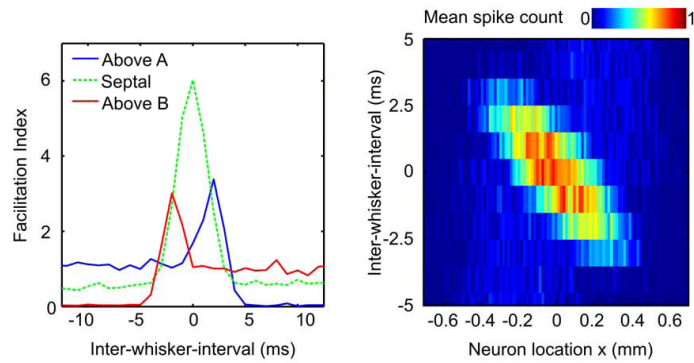


Figure 6.4: **Results for temporal stimulation of two whiskers in a simplified model**

Left: The facilitation index of three groups of neurons is plotted for different temporal spacings of the stimulus. Neurons in ‘Above A’ are located from -0.6 mm to -0.2 mm, Septal neurons are located between -0.2 mm and 0.2 mm and ‘Above B’ comprises neurons from 0.2 mm to 0.6 mm. *Right:* Activation map of the layer 2/3 population. Shown is the mean spike count per neuron for different neuron positions and temporal spacings of the stimulus. (Modified from Wilson et al., 2011)

for neurons in the positions from -0.6 mm to -0.2 mm, into ‘Septal’ from -0.2 mm to 0.2 mm and ‘Above B’ from 0.2 mm to 0.6 mm.

The results of this simple model are shown in Figure 6.4. The left panel of the figure shows the facilitation index for different temporal spacings of the stimulus. The facilitation index was the ratio of the recorded response to the estimated response from the linear sum of responses to independent stimuli.

This figure can be compared directly to Figure 1.2. Both figures show a strong facilitation for the septal area for small inter-whisker intervals and suppression of the neurons inside a barrel if the principal whisker was stimulated second with large interstimulus intervals. For small intervals the model showed a small peak in facilitation for neurons in both barrels which was shown in the experiment for the caudal population.

The right panel in Figure 6.4 shows the direct activation of each neuron as a function of neuron position and inter-whisker-interval. The highly activated, diagonal region was representing the cases in which both whisker stimulations evoke an excitatory response in the corresponding neurons. The faint bars downward from the left part of the diagonal activation (-0.4 mm to

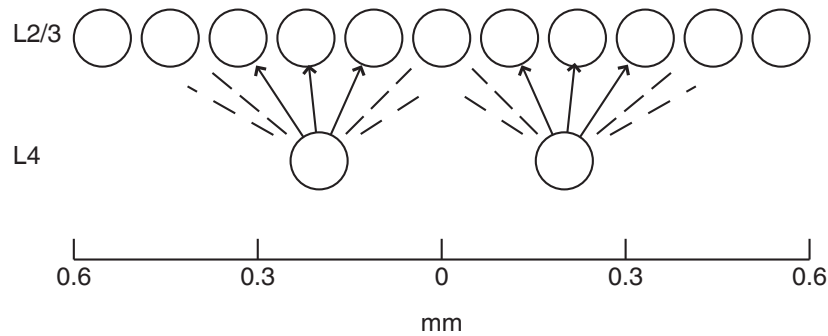


Figure 6.5: **Spatially extended layer 2/3 network with layer 4 inputs**

All layer 2/3 neurons are assigned positions between -0.6 mm and 0.6 mm uniformly. Layer 4 inputs, located at -0.2 mm and 0.2 mm, are providing excitatory and inhibitory input to layer 2/3 neurons (black lines).

-0.2 mm) and upward from the right part of the diagonal region (0.2 mm to 0.4 mm) showed approximately the normal level of activation expected from single whisker stimulations. These effects were all visible in the results presented in the left panel.

The small peaks of the left panel were an effect from the edges of the diagonal region in the right panel. Since the two Figures 6.4 and 1.2 were mostly in agreement, the model of Wilson et al., 2011 could model the temporal integration of multiple whisker stimuli.

6.2.3 Extension of the Previous Layer 2/3 Model to a Spatial Scale

Similar to the approach in Wilson et al., 2011, I constructed network model in which the neurons in the layer 2/3 model described in the previous chapters were spatially distributed. Figure 6.5 shows the general layout of the model. Each layer 2/3 neuron was assigned a position between -0.6 mm and 0.6 mm drawn from a uniform distribution (Figure 6.5, top).

I then assumed a population of layer 4 neurons that provided excitatory and inhibitory input with distant dependent delays corresponding to the existing model from Wilson et al., 2011 and experimental measurements (Helmstaedter et al., 2008). The layer 4 neurons were modeled as four pools of 450 unconnected spike sources, one excitatory and one inhibitory pool for

the barrel A located at -0.2 mm and one excitatory and one inhibitory for barrel B at 0.2 mm (Figure 6.5, bottom). The connection probabilities and strengths from layer 4 to layer 2/3 were taken from existing literature (Helmstaedter et al., 2008; Lefort et al., 2009).

The connection structure from layer 4 to layer 2/3 was always uniform random to all three populations of layer 2/3 neurons, while for the structure inside layer 2/3 three different networks were tested: unconnected, uniform random and adjusted.

6.2.4 Results

Although the networks were setup with all three populations (excitatory, fast-spiking and non-fast-spiking), I only report on the behaviour of the excitatory cells to be able to compare the results to the findings of Shimegi et al., 2000 and Wilson et al., 2011. To measure the effect of the stimulation, spikes from layer 2/3 neurons were recorded for the interval from -37 ms to 37 ms as used in Wilson et al., 2011. The results for 7 trials with different, randomly connected layer 4 pools were averaged and yield the mean spike count.

Impact of Network Architecture on the Facilitation Index

To measure the facilitation index, I performed the experiment with only one stimulation and recorded the mean spike count. The facilitation index was then the ratio of the tested response to the linear sum of the single stimulation experiments.

Figure 6.6 shows the facilitation index measurements for all three tested networks. As in Figures 6.4 and 1.2 before, the panels of Figure 6.6 show the average facilitation index for different spatial grouping of neurons for different stimulus intervals. While the overall facilitation index was higher than the results shown in Figure 6.4, the widths of the facilitated regions for the three groups were larger and thus more similar to those found in experimental results (Figure 1.2). There were only slight differences between the three network setups (unconnected, uniform random and adjusted). The adjusted network showed stronger facilitation than the other networks in the 'Above A' and 'Above B' group for small inter-whisker-intervals. The

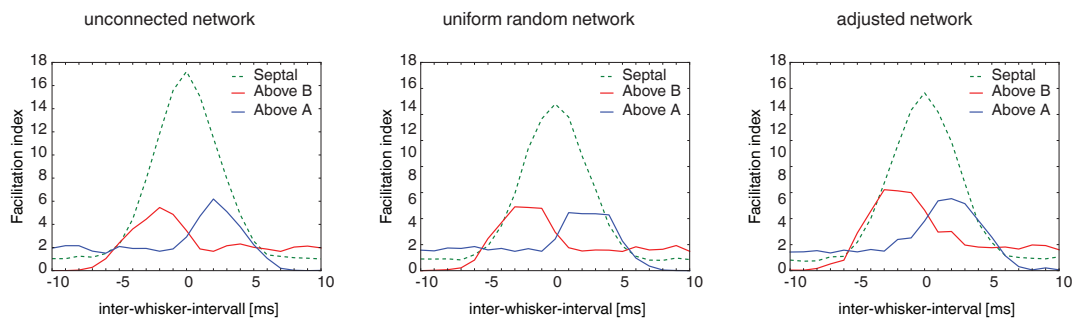


Figure 6.6: Facilitation of responses to temporal stimulations of two adjacent whiskers
 Plotted is the facilitation index averaged over different neuron positions. Neurons are grouped ‘Above A’ for positions -0.6 mm to -0.2 mm, ‘Septal’ for -0.2 mm to 0.2 mm and ‘Above B’ for 0.2 mm to 0.6 mm. The facilitation indices are shown for different interstimulus intervals from -10 ms (Whisker B first) to 10 ms (Whisker A first).

unconnected network showed the strongest facilitation of all networks in the septal group for small intervals. The effects of long inter-whisker-intervals remained the same for all networks.

Impact of Network Architecture on the Activity of Single Cells

Since this analysis was using a strong spatial averaging into only three groups, I investigated the network responses in a more detailed way by looking at the activation maps of the different network architectures depicted in Figure 6.7.

The activation maps show the same general structure as Figure 6.4, right panel. A diagonal region of highly active cells with two vertically extended regions of weak activity at the end of the diagonal. The scale with respect to the inter-whisker-interval is larger as in Wilson et al., 2011 similar to Figure 6.6.

Between the unconnected and the uniform random network there was only a slight difference in the amplitude of the highly active region. The adjusted network on the other hand showed an increased activation for neurons located at the far lateral end of the network (approximately at -0.6 mm to 0.4 mm and 0.4 mm to 0.6 mm). These neurons were silent in the unconnected and in the uniform random network as well as in the model of Wilson et al., 2011 (see Figure 6.4).

The differences of the activation map of the unconnected network and the adjusted network

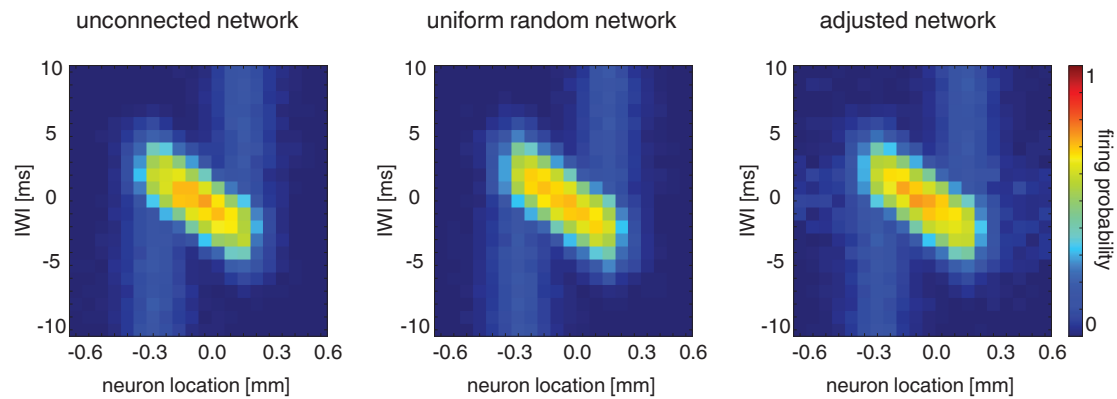


Figure 6.7: Activity distributions for multiple network setups

Shown is the firing probability for neurons at different locations for different inter-whisker-intervals (IWI). The activity maps are plotted for the unconnected network (*Left*), the uniform random network (*Middle*) and the adjusted network (*Right*).

are shown in Figure 6.8. Here, an increased activity in the adjusted network is depicted in red, while a decrease with respect to the activation in a unconnected network is shown in blue.

The most prominent changes in spiking probability were the increase in activity of the lateral cells as mentioned before. There was also a slight decrease in the vertically extended regions of weak activity around ± 0.2 mm. The slight decrease came from the fact that inhibitory neurons were affecting the behaviour of the excitatory cells in the adjusted network but not in the unconnected network. Since the stimulus was very strong, the inhibitory activity was fast enough to depress the activity in the excitatory neurons to a certain degree (compare Figure 5.6).

The increase in the lateral regions came from the fact that excitatory neurons that had a large out-degree were activated by the layer 4 stimulation. These out-degree hubs provided in turn activation to many other excitatory neurons, thus stimulating them more than in an unconnected network and also more than in the uniform random network (see also Figure 6.7).

6.3. The Adjusted Network Architecture in *in vivo* Scenarios

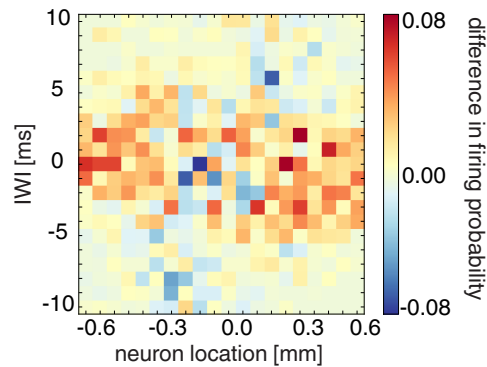


Figure 6.8: **Differences in activity distributions for adjusted and unconnected networks**
Plotted are the differences between the activation maps of the unconnected network and the adjusted network from Figure 6.7. Red indicates a higher activation in the adjusted network, while blue indicates a higher activation in the unconnected network.

6.2.5 Summary

I showed how the modeling results from Wilson et al., 2011 can be applied to complete network models. I further showed how these network models were able to reproduce the experimental data from Shimegi et al., 2000.

Using different network architectures, I was able to show that neurons in the adjusted network show a temporal specificity at positions at which neurons in the unconnected or uniform random network would be silent. This indicates that adjusted networks can use more neurons to determine the temporal sequence of stimuli than the other network architectures.

This enhanced specificity could not be seen in the experimental data (Figure 1.2), since the averaging into spatial groups would mask this rather weak effect. Only a more detailed analysis of the experimental data could shed light on how far the specificity reached.

6.3 The Adjusted Network Architecture in *in vivo* Scenarios

The adjusted network extracted in Chapter 5 is based solely on *in vitro* measures and thus it is necessary to test the constructed networks in more complex *in vivo* scenarios. The results presented in this chapter show that the adjusted network not only performed equally to a

Chapter 6. Effects of Architecture on the Functional Behaviour of Networks

uniform random network in the tested *in vivo* scenarios, but also showed a more accurate and plausible behaviour. This indicates that the adjusted network architecture captures elements of the biological network architecture.

7 Limitations and Perspectives

Here, I discuss the specific choice of architectural changes and the alternatives that were not explored in this thesis. It is described how synaptic plasticity may be a factor to generate and alter the network architectures shown throughout my work. I move on to explain how the network models studied could be changed to display ongoing activity and thus open the possibility to employ more *in vivo* data into the fitting procedure and analysis.

7.1 Other Architectural Changes

The improvements discussed in this work are only one possibility to manipulate network architecture. There are multiple other possibilities including the use of scale-free and small-world networks as discussed in Chapter 1.3 and distance dependent probabilities.

7.1.1 Scale-Free Networks

The scale-free approach is quite similar to the manipulations of the degree distributions as presented in Chapter 3. The presented approach constructs networks with an approximately exponential degree distribution. By using a different algorithm for the network formation like preferential attachment (Barabási and Albert, 1999), it would be possible to model scale-free networks directly.

Chapter 7. Limitations and Perspectives

However, the construction of the exponential networks is much faster and less memory intensive. This was the reason to stay with the exponential networks. The expected difference between scale-free and exponential networks is for the networks presented here rather small. This is due to the limited network size that truncates the degree distributions in both cases.

7.1.2 Small-World Networks

Small-world networks on the other hand are another option to model the network topologies. One of the main difficulties here is the sensible extension of small-world structure to multiple populations. I also showed that small-world-ness does not imply a high similarity to the experimental observations (see Chapter 3).

An extended approach to small-world networks that takes into account multiple neuronal populations might circumvent the problem of unspecificity of the standard small-world networks. Thus, small-world networks might be another possibility to investigate biologically plausible network structures.

7.1.3 Distance Dependent Probability

One other very interesting possibility is the use of distance dependent connection probabilities. For this, it would be necessary to extend the network models to a spatial representation, similar as in Chapter 6.2.

This approach is discussed as one possibility to model the occurrence of network motifs (Perin et al., 2011). Also, in Vogels and Abbott, 2009, a hybrid network model is used. Here a random network of excitatory and inhibitory neuron uses a second, embedded population of inhibitory neurons that only connect to neurons in their local neighbourhood. They then embed an excitatory 'sender' population that projects to excitatory and locally targeting inhibitory neurons into this network. Due to the local interneurons that are targeted an input into the sender population does not increase activity in the receiver population, since the inhibitory neurons effectively cancels the excitatory activation. However, by disrupting this

balance of excitation and inhibition, it is possible to 'gate' this signal. This means that by selectively modifying the responsiveness of the inhibitory receiver neurons, an input in the sender population can be propagated to the receiver population.

Thus, distance dependent networks can be used to model biological observations and important network properties.

One problem with the use of distance dependent probabilities is that their existence on the subcolumnar scale is still debated. While some studies report strong distance dependency even for distances smaller than $100\mu\text{m}$ (Holmgren et al., 2003; Perin et al., 2011), others report a noticeable distance dependency only for larger distances (Packer and Yuste, 2011) or do not find a distance dependency at all on the studied spatial scale (Lefort et al., 2009; Avermann et al., 2011).

This might also be dependent on species, since most reports of strong distance dependency studied rats, while most studies that did not find a distance dependency used mice for their recordings. In general, it seems undisputed that distance dependent connectivity properties exist on a larger scale. For example in long-range connections, neurons tend to connect to target clusters or patches that are rather localised at large distances to the presynaptic neurons. Models for this long-range patchy connections have already been proposed (Voges et al., 2010). The question remains whether distance dependency exist at the subcolumnar scale.

Thus, distance dependent probabilities are an interesting option and their implications on network properties will be extremely important in the future. However, it is unclear whether they are the underlying structure of the fine-scale connectivity or not.

7.2 Plasticity

One highly important and interesting field that is not covered in my work is the role of plasticity. Neural networks are plastic, their connections change over time, while the networks I studied were in a frozen state. No connections were changed after the network was setup. In this part,

I describe what roles plasticity may have in constructing complex network architectures.

7.2.1 Global Weight Distributions

In Chapter 2 it is shown how global weight distributions affect network excitability. The observed distribution of synaptic weights in biological experiments is highly skewed and the few strong connections are key to network excitability. These sparse strong connections could arise through spike time dependent plasticity (STDP, Gerstner and Sjöström, 2010). Using a STDP learning rule in a network showing asynchronous irregular activity (Brunel, 2000; Vogels et al., 2005) can lead to weight distributions with many small connections and few strong connections (Morrison et al., 2007).

7.2.2 Degree Distributions

The changes in the degree distributions that I used in Chapter 3 could arise from structural plasticity (Butz et al., 2009). It is shown in experiments that spine formation and pruning during development is highly activity and cell type dependent (Knott et al., 2002). This would offer a mechanism that could lead to connection specific changes in degree distributions.

7.2.3 Local Weight Distributions

Synaptic plasticity is also a way of introducing local weight changes like they were used in Chapter 4. Although the idea of weight correlations can be explained by a hebbian learning rule (Koulakov et al., 2009), this approach is difficult to tune and does not allow for a systematic analysis of the parameter space. It is still unclear whether STDP rules that depend assymmetrically on the pre- and the postsynaptic spike can account for such local changes.

7.2.4 Plasticity as a Mechanism for Shaping Network Architectures

Overall, plasticity can work on all different levels of network architecture and may be a unifying mechanism that can construct complex networks as presented in my work. The investigation

of rules that may construct such networks is an important step to understand the fine-scale architecture of neural networks.

7.3 Active Networks

The networks I studied in this work showed no spontaneous activity. This is to be expected, since the experimental results *in vitro* also showed no spontaneous activity. However, the living brain of course does show spontaneous activity.

One important step would thus be, to study the networks presented here in an active state. The active state refers to the fact that neurons in the network show spontaneous ongoing activity (Brunel, 2000; Vogels et al., 2005). This would be very similar to experimental observations *in vivo* and would thus enable the use of more experimental data measured as spiking activity over time to investigate network architectures.

A small step in this direction is the simplified up state model presented in Chapter 6.1 although here the spontaneous activity is still missing. How the network should be changed to display spontaneous activity, while preserving the biological parameters is unclear.

Using synaptic inputs from a background network would be an obvious solution, but this opens up a completely new set of architectural parameters to connect the background network to the studied network. Another possibility would be to add noise to each single neuron but again that would require the knowledge of the specific type and structure of the noise per neuron in order to not bias the analysis of network structure by the input.

With an extension of the findings presented here to a more faithful *in vivo* representation, it would also be possible to use different tools of network analysis like presented for example in Pernice et al., 2011 and Roxin, 2011. Thus, this direction will be very important to link the results discovered in this work to classical studies of neuronal network analysis.

8 Conclusions

In the course of this work, I have shown that the assumptions of classical uniform random networks have a strong impact on the behaviour and plausibility of neuronal networks.

First of all, it was shown that the choice of global weight distribution greatly changes the excitability of the network. Many network studies assume a fixed single weight for all connections in the network. This greatly reduces the network excitability in comparison to networks constructed with a more accurate, lognormal weight distributions.

Furthermore, uniform random networks do not show the complex connectivity patterns of higher orders as are found in experimental studies. Manipulations of degree distributions can be used to introduce changes in the fine-scale connectivity so that the similarity of network structure to experimental results is improved.

The response behaviour of uniform random networks showed a problematic behaviour for stimulations of groups of neurons that were connected with a high probability. Here the averaging effect of the network was too strong and would not reproduce the responses found in experimental results. I introduced a way of changing the local weight distribution of the network in order to circumvent the averaging effect. A network with adapted local weight correlations showed the expected response behaviour.

These adjustments can be combined to construct networks that are capturing a wide range of

Chapter 8. Conclusions

experimental findings on complex connectivity patterns, as well as an appropriate response behaviour. Furthermore, these adjusted networks even perform better in more complex, *in vivo* like, scenarios to which the network was not adapted.

The changes in network architecture that were extracted in this work are highly connection specific. This means that connections between excitatory neurons show a different architecture than connections between excitatory and fast-spiking or non-fast-spiking interneurons. This indicates a specific functional role for the different inhibitory populations.

To conclude, the adjustments to network architecture presented here are one possible improvement to the uniform random network architecture and provide a solid basis for further investigation of network properties.

A Source Code for the Generation of Structured Weight Lists

```
1 def cm(n,m,p,dOut,postInc,weights,delays,corrOut,corrIn):
2
3     mIn=-1.*(corrIn**2)/2.
4     if corrIn==0:
5         corrIn=0.00000001
6     wPost=utils.ScaledRandomDistribution(distribution='lognormal',parameters=[mIn
7         ,corrIn])
8     vPost=wPost.next(m)
9
10    mOut=-1.*(corrOut**2)/2.
11    if corrOut==0:
12        corrOut=0.00000001
13    wPre=utils.ScaledRandomDistribution(distribution='lognormal',parameters=[mOut
14        ,corrOut])
15    vPre=wPre.next(n)
16
17    if dIn>0:
18        drawPost=drawExp
19    else:
20        dPost=drawUni
21
22    if dOut>0:
23        drawPre=drawExp
24    else:
25        drawPre=drawUni
26
27    maxC=numpy.floor(n*m*p)
```

Appendix A. Source Code for the Generation of Structured Weight Lists

```
25     w=weights.next(maxC)
26     d=delays.next(maxC)
27
28     tmpList=numpy.array([],[( 'pre ',int),('post ',int),('w',float),('d',numpy.
        ndarray)])
29     tmpList.resize(maxC)
30
31     connE=numpy.zeros((n,m))
32
33     for c in numpy.arange(0,maxC):
34         source=drawPre(dOut,n)
35         target=drawPost(dIn,m)
36         timeout=100
37         decCount=0
38         decisor=numpy.random.randint(2)
39         while connE[source,target]>0:
40             decCount+=1
41             if decisor:
42                 if decCount>timeout:
43                     target=drawPost(dIn,m)
44                     decCount=0
45             else:
46                 source=drawPre(dOut,n)
47         else:
48             if decCount>timeout:
49                 source=drawPre(dOut,n)
50                 decCount=0
51             else:
52                 target=drawPost(dIn,m)
53         wT=w[c]
54
55         if corrOut>0:
56             wT*=vPre[source]
57         if corrIn>0:
58             wT*=vPost[target]
59
60         tmpList[c]=((source),(target),wT,d[c])
61         connE[source,target]=1
62
63     return tmpList
```

Bibliography

Amit D, Brunel N (1997a) Dynamics of a recurrent network of spiking neurons before and following learning. *Network: Computation in Neural Systems* 8:373–404.

Amit D, Brunel N (1997b) Model of global spontaneous activity and local structured activity during delay periods in the cerebral cortex. *Cerebral Cortex* 7:237.

Aronoff R, Petersen C (2008) Layer, column and cell-type specific genetic manipulation in mouse barrel cortex. *Frontiers in Neuroscience* 2:64.

Avermann M, Tomm C, Mateo C, Gerstner W, Petersen CCH (2011) Microcircuits of excitatory and inhibitory neurons in layer 2/3 of mouse barrel cortex. *Submitted* .

Barabási A, Albert R (1999) Emergence of scaling in random networks. *Science* 286:509.

Bock D, Lee W, Kerlin A, Andermann M, Hood G, Wetzell A, Yurgenson S, Soucy E, Kim H, Reid R (2011) Network anatomy and in vivo physiology of visual cortical neurons. *Nature* 471:177–182.

Bonifazi P, Goldin M, Picardo M, Jorquera I, Cattani A, Bianconi G, Represa A, Ben-Ari Y, Cossart R (2009) Gabaergic hub neurons orchestrate synchrony in developing hippocampal networks. *Science* 326:1419.

Borst J, Helmchen F (1998) Calcium influx during an action potential. *Methods in Enzymology* 293:352–371.

Boucsein C, Nawrot M, Rotter S, Aertsen A, Heck D (2005) Controlling synaptic input patterns in vitro by dynamic photo stimulation. *Journal of neurophysiology* 94:2948–2958.

Bibliography

- Boyden E, Zhang F, Bamberg E, Nagel G, Deisseroth K (2005) Millisecond-timescale, genetically targeted optical control of neural activity. *Nature Neuroscience* 8:1263.
- Brette R, Gerstner W (2005) Adaptive exponential integrate-and-fire model as an effective description of neuronal activity. *Journal of Neurophysiology* 94:3637.
- Brette R, Rudolph M, Carnevale T, Hines M, Beeman D, Bower J, Diesmann M, Morrison A, Goodman P, Harris F et al. (2007) Simulation of networks of spiking neurons: A review of tools and strategies. *Journal of Computational Neuroscience* 23:349–398.
- Brunel N (2000) Dynamics of sparsely connected networks of excitatory and inhibitory spiking neurons. *Journal of Computational Neuroscience* 8:183–208.
- Brunel N, Hakim V (1999) Fast global oscillations in networks of integrate-and-fire neurons with low firing rates. *Neural Computation* 11:1621–1671.
- Butz M, Wörgötter F, van Ooyen A (2009) Activity-dependent structural plasticity. *Brain Research Reviews* 60:287–305.
- Callaway E, Katz L (1993) Photostimulation using caged glutamate reveals functional circuitry in living brain slices. *Proceedings of the National Academy of Sciences* 90:7661.
- Daidsen J, Ebel H, Bornholdt S (2002) Emergence of a small world from local interactions: Modeling acquaintance networks. *Physical Review Letters* 88:128701.
- Davison AP, Brüderle D, Eppler JM, Kremkow J, Müller E, Pecevski D, Perrinet L, Yger P (2009) Pynn: a common interface for neuronal network simulators. *Frontiers in Neuroinformatics* 2.
- Feldmeyer D, Egger V, Lübke J, Sakmann B (1999) Reliable synaptic connections between pairs of excitatory layer 4 neurones within a single 'barrel' of developing rat somatosensory cortex. *The Journal of Physiology* 521:169.
- Feldmeyer D, Lübke J, Sakmann B (2006) Efficacy and connectivity of intracolumnar pairs of layer 2/3 pyramidal cells in the barrel cortex of juvenile rats. *The Journal of Physiology* 575:583.

- Feldmeyer D, Lübke J, Silver R, Sakmann B (2002) Synaptic connections between layer 4 spiny neurone-layer 2/3 pyramidal cell pairs in juvenile rat barrel cortex: physiology and anatomy of interlaminar signalling within a cortical column. *The Journal of Physiology* 538:803–822.
- Feldt S, Bonifazi P, Cossart R (2011) Dissecting functional connectivity of neuronal microcircuits: experimental and theoretical insights. *Trends in Neurosciences* 34:225–236.
- Ferezou I, Bolea S, Petersen C (2006) Visualizing the cortical representation of whisker touch: voltage-sensitive dye imaging in freely moving mice. *Neuron* 50:617–629.
- Fino E, Yuste R (2011) Dense inhibitory connectivity in neocortex. *Neuron* 69:1188–1203.
- Gentet LJ, Avermann M, Matyas F, Staiger JF, Petersen CCH (2010) Membrane potential dynamics of gabaergic neurons in the barrel cortex of behaving mice. *Neuron* 65:422–435.
- Gerhard F, Pipa G, Lima B, Neuenschwander S, Gerstner W (2011) Extraction of network topology from multi-electrode recordings: is there a small-world effect? *Frontiers in Computational Neuroscience* 5.
- Gerstner W, Brette R (2009) Adaptive exponential integrate-and-fire model. *Scholarpedia* 4:8427.
- Gerstner W, Kistler W (2002) *Spiking neuron models: Single neurons, populations, plasticity* Cambridge Univ Pr.
- Gerstner W, Sjöström J (2010) Spike-timing dependent plasticity. *Scholarpedia* 5:1362.
- Gewaltig M, Diesmann M (2007) Nest (neural simulation tool). *Scholarpedia* 2:1430.
- Grewe B, Langer D, Kasper H, Kampa B, Helmchen F (2010) High-speed in vivo calcium imaging reveals neuronal network activity with near-millisecond precision. *Nature Methods* 7:399–405.
- Grinvald A, Anglister L, Freeman J, Hildesheim R, Manker A (1984) Real-time optical imaging of naturally evoked electrical activity in intact frog brain. *Nature* 308:848–850.

Bibliography

Grinvald A, Lieke E, Frostig R, Gilbert C, Wiesel T (1986) Functional architecture of cortex revealed by optical imaging of intrinsic signals. *Nature* 324:361–364.

Helmstaedter M, Sakmann B, Feldmeyer D (2009) L2/3 interneuron groups defined by multiparameter analysis of axonal projection, dendritic geometry, and electrical excitability. *Cerebral Cortex* 19:951.

Helmstaedter M, Staiger J, Sakmann B, Feldmeyer D (2008) Efficient recruitment of layer 2/3 interneurons by layer 4 input in single columns of rat somatosensory cortex. *The Journal of Neuroscience* 28:8273.

Hertz J (2010) Cross-correlations in high-conductance states of a model cortical network. *Neural Computation* 22:427–447.

Holmgren C, Harkany T, Svennenfors B, Zilberter Y (2003) Pyramidal cell communication within local networks in layer 2/3 of rat neocortex. *The Journal of Physiology* 551:139.

Humphries M, Gurney K (2008) Network 'small-world-ness': a quantitative method for determining canonical network equivalence. *PLoS One* 3:e0002051.

Janssen M, Jager W (2001) Fashions, habits and changing preferences: Simulation of psychological factors affecting market dynamics. *Journal of Economic Psychology* 22:745–772.

Jeffress L (1948) A place theory of sound localization. *Journal of Comparative and Physiological Psychology* 41:35.

Keeling M, Eames K (2005) Networks and epidemic models. *Journal of the Royal Society Interface* 2:295.

Kennedy J, Eberhart R (1995) Particle swarm optimization In *Neural Networks, 1995. Proceedings., IEEE International Conference on*, Vol. 4, pp. 1942–1948. IEEE.

Knott G, Quairiaux C, Genoud C, Welker E (2002) Formation of dendritic spines with gabaergic synapses induced by whisker stimulation in adult mice. *Neuron* 34:265–273.

- Koulakov A, Hromadka T, Zador A (2009) Correlated connectivity and the distribution of firing rates in the neocortex. *Journal of Neuroscience* 29:3685.
- LeBlanc J, Ward M, Wittels N (1990) Exploring n-dimensional databases In *Proceedings of the 1st conference on Visualization'90*, p. 237. IEEE Computer Society Press.
- Lefort S, Tomm C, Sarria JCF, Petersen CCH (2009) The excitatory neuronal network of the c2 barrel column in mouse primary somatosensory cortex. *Neuron* 61:301–316.
- Lütcke H, Murayama M, Hahn T, Margolis D, Astori S, zum Alten Borgloh S, Göbel W, Yang Y, Tang W, Kügler S et al. (2010) Optical recording of neuronal activity with a genetically-encoded calcium indicator in anesthetized and freely moving mice. *Frontiers in Neural Circuits* 4.
- Mao T, Kusefoglou D, Hooks B, Huber D, Petreanu L, Svoboda K (2011) Long-range neuronal circuits underlying the interaction between sensory and motor cortex. *Neuron* 72:111–123.
- Markram H, Lübke J, Frotscher M, Roth A, Sakmann B (1997) Physiology and anatomy of synaptic connections between thick tufted pyramidal neurones in the developing rat neocortex. *The Journal of Physiology* 500:409.
- Mateo C, Avermann M, Gentet L, Zhang F, Deisseroth K, Petersen C (2011) In vivo optogenetic stimulation of neocortical excitatory neurons drives brain-state-dependent inhibition. *Current Biology* 21:1593–1602.
- Mensi S, Naud R, Pozzorini C, Avermann M, Petersen CCH, Gerstner W (2011) Parameter extraction and classification of three cortical neuron types reveals two distinct adaptation mechanisms. *Submitted*.
- Milo R, Shen-Orr S, Itzkovitz S, Kashtan N, Chklovskii D, Alon U (2002) Network motifs: simple building blocks of complex networks. *Science* 298:824.
- Morrison A, Aertsen A, Diesmann M (2007) Spike-timing-dependent plasticity in balanced random networks. *Neural Computation* 19:1437–1467.

Bibliography

- Mutoh H, Perron A, Akemann W, Iwamoto Y, Knöpfel T (2011) Optogenetic monitoring of membrane potentials. *Experimental Physiology* 96:13.
- Nagel G, Ollig D, Fuhrmann M, Kateriya S, Musti A, Bamberg E, Hegemann P (2002) Channelrhodopsin-1: a light-gated proton channel in green algae. *Science* 296:2395.
- Nagel G, Szellas T, Huhn W, Kateriya S, Adeishvili N, Berthold P, Ollig D, Hegemann P, Bamberg E (2003) Channelrhodopsin-2, a directly light-gated cation-selective membrane channel. *Proceedings of the National Academy of Sciences* 100:13940.
- Naud R, Marcille N, Clopath C, Gerstner W (2008) Firing patterns in the adaptive exponential integrate-and-fire model. *Biological Cybernetics* 99:335–347.
- Nikolenko V, Poskanzer K, Yuste R (2007) Two-photon photostimulation and imaging of neural circuits. *Nature Methods* 4:943–950.
- Packer A, Yuste R (2011) Dense, unspecific connectivity of neocortical parvalbumin-positive interneurons: A canonical microcircuit for inhibition? *The Journal of Neuroscience* 31:13260–13271.
- Peng W (2005) Clutter-based dimension reordering in multi-dimensional data visualization Master's thesis, Worcester MA: Worcester Polytechnic Institute.
- Perin R, Berger T, Markram H (2011) A synaptic organizing principle for cortical neuronal groups. *Proceedings of the National Academy of Sciences* 108:5419.
- Pernice V, Staude B, Cardanobile S, Rotter S (2011) How structure determines correlations in neuronal networks. *PLoS Computational Biology* 7:e1002059.
- Peterka D, Takahashi H, Yuste R (2011) Imaging voltage in neurons. *Neuron* 69:9–21.
- Peterlin Z, Kozloski J, Mao B, Tsiola A, Yuste R (2000) Optical probing of neuronal circuits with calcium indicators. *Proceedings of the National Academy of Sciences* 97:3619.
- Petersen C (2007) The functional organization of the barrel cortex. *Neuron* 56:339–355.

- Petersen C, Hahn T, Mehta M, Grinvald A, Sakmann B (2003) Interaction of sensory responses with spontaneous depolarization in layer 2/3 barrel cortex. *Proceedings of the National Academy of Sciences* 100:13638.
- Pillow J, Shlens J, Paninski L, Sher A, Litke A, Chichilnisky E, Simoncelli E (2008) Spatio-temporal correlations and visual signalling in a complete neuronal population. *Nature* 454:995–999.
- Prettejohn B, Berryman M, McDonnell M (2011) Methods for generating complex networks with selected structural properties for simulations: A review and tutorial for neuroscientists. *Frontiers in Computational Neuroscience* 5.
- Renart A, De la Rocha J, Bartho P, Hollender L, Parga N, Reyes A, Harris K (2010) The asynchronous state in cortical circuits. *Science* 327:587.
- Roxin A, Hakim V, Brunel N (2008) The statistics of repeating patterns of cortical activity can be reproduced by a model network of stochastic binary neurons. *The Journal of Neuroscience* 28:10734.
- Roxin A (2011) The role of degree distribution in shaping the dynamics in networks of sparsely connected spiking neurons. *Frontiers in Computational Neuroscience* 5.
- Shimegi S, Akasaki T, Ichikawa T, Sato H (2000) Physiological and anatomical organization of multiwhisker response interactions in the barrel cortex of rats. *The Journal of Neuroscience* 20:6241.
- Shoham D, Glaser D, Arieli A, Kenet T, Wijnbergen C, Toledo Y, Hildesheim R, Grinvald A (1999) Imaging cortical dynamics at high spatial and temporal resolution with novel blue voltage-sensitive dyes. *Neuron* 24:791–802.
- Smetters D, Majewska A, Yuste R (1999) Detecting action potentials in neuronal populations with calcium imaging. *Methods* 18:215–221.
- Song S, Sjöström P, Reigl M, Nelson S, Chklovskii D (2005) Highly nonrandom features of synaptic connectivity in local cortical circuits. *PLoS Biology* 3:e68.

Bibliography

Taylor A, Hickey T, Prinz A, Marder E (2006) Structure and visualization of high-dimensional conductance spaces. *Journal of Neurophysiology* 96:891.

Thomson A, Lamy C (2007) Functional maps of neocortical local circuitry. *Frontiers in Neuroscience* 1:19.

van Rossum M, van der Meer M, Xiao D, Oram M (2008) Adaptive integration in the visual cortex by depressing recurrent cortical circuits. *Neural Computation* 20:1847–1872.

Van Vreeswijk C, Sompolinsky H (1996) Chaos in neuronal networks with balanced excitatory and inhibitory activity. *Science* 274:1724.

Vazquez A, Pastor-Satorras R, Vespignani A (2002) Internet topology at the router and autonomous system level. *Arxiv preprint cond-mat/0206084*.

Vogels T, Abbott L (2005) Signal propagation and logic gating in networks of integrate-and-fire neurons. *The Journal of Neuroscience* 25:10786.

Vogels T, Abbott L (2009) Gating multiple signals through detailed balance of excitation and inhibition in spiking networks. *Nature Neuroscience* 12:483–491.

Vogels T, Rajan K, Abbott L (2005) Neural network dynamics. *Annual Review of Neuroscience* 28:357–376.

Voges N, Schuz A, Aertsen A, Rotter S (2010) A modeler's view on the spatial structure of intrinsic horizontal connectivity in the neocortex. *Progress in Neurobiology* 92:277–292.

Voorneveld M (2003) Characterization of pareto dominance. *Operations Research Letters* 31:7–11.

Wang H, Peca J, Matsuzaki M, Matsuzaki K, Noguchi J, Qiu L, Wang D, Zhang F, Boyden E, Deisseroth K et al. (2007) High-speed mapping of synaptic connectivity using photostimulation in channelrhodopsin-2 transgenic mice. *Proceedings of the National Academy of Sciences* 104:8143.

- Wang X, Chen G (2003) Complex networks: small-world, scale-free and beyond. *Circuits and Systems Magazine, IEEE* 3:6–20.
- Watts D, Strogatz S (1998) Collective dynamics of 'small-world' networks. *Nature* 393:440–442.
- Wickersham I, Lyon D, Barnard R, Mori T, Finke S, Conzelmann K, Young J, Callaway E (2007) Monosynaptic restriction of transsynaptic tracing from single, genetically targeted neurons. *Neuron* 53:639–647.
- Wilson S, Bednar J, Prescott T, Mitchinson B (2011) Neural computation via neural geometry: A place code for inter-whisker timing in the barrel cortex? *PLoS Computational Biology* 7:e1002188.
- Yoshimura Y, Callaway E (2005) Fine-scale specificity of cortical networks depends on inhibitory cell type and connectivity. *Nature Neuroscience* 8:1552–1559.
- Yoshimura Y, Dantzker J, Callaway E (2005) Excitatory cortical neurons form fine-scale functional networks. *Nature* 433:868–873.
- Zhang F, Wang L, Boyden E, Deisseroth K (2006) Channelrhodopsin-2 and optical control of excitable cells. *Nature Methods* 3:785.
- Zitzler E, Laumanns M, Thiele L et al. (2001) Spea2: Improving the strength pareto evolutionary algorithm. *EUROGEN* 3242:1–21.
- Zitzler E, Thiele L (1999) Multiobjective evolutionary algorithms: A comparative case study and the strength pareto approach. *Evolutionary Computation, IEEE Transactions on* 3:257–271.

curriculum vitae

Christian Tomm

Adress: Chemin de la Chiesaz 7
1024 Ecublens VD

Phone: +41 21 634 06 33

E-Mail: ctomm@gmx.de

born: 10. July 1981

family status: married, one child

nationality: german

Education

2007 – 2012 PhD student in the Laboratory of Computational Neuroscience (Prof. Wulfram Gerstner), BMI, EPFL

March 2007 Diplom Computer Science

2002 – 2007 Studies in Computer Science (Diplom) at Ulm University

22.06.2001 German Abitur

Professional experience

2007 – 2011 Tutor for undergraduate teaching, EPFL

2005 – 2007 Tutor for undergraduate teaching, Uni Ulm

2001 Webdesign for Cheng Shin Rubber GmbH

1999 – 2001 Assistant in Innovationszentrum Itzehoe (IZET)

foreign languages

excellent english skills.

good french skills.

basic danish skills.

programming skills

excellent skills in Java and Python programming (>5 years).

very good skills in C/C++ and Matlab programming (>3 years).

further skills in php programming.